
Genotype-Phenotype Correlation in Noonan Syndrome – Focus on LZTR1 and its Substrates

Dissertation

for the award of the degree

“Doctor rerum naturalium”

of the Georg-August-Universität Göttingen

within the doctoral program

International Max Planck Research School for Genome Science (IMPRS-GS)

of the Georg-August University School of Science (GAUSS)

submitted by

Alexandra Viktoria Busley

born in Frankfurt am Main, Germany

I. Thesis Committee Members

Dr. Lukas Cyganek (Supervisor and 1st Referee)

Stem Cell Unit (SCU)
University Medical Center Göttingen
Robert-Koch-Straße 40
37075 Göttingen

Prof. Dr. med. Wolfram-Hubertus Zimmermann (2nd Referee)

Institute of Pharmacology and Toxicology
University Medical Center Göttingen
Robert-Koch-Straße 40
37075 Göttingen

Prof. Dr. med. Bernd Wollnik (3rd Referee)

Institute of Human Genetics
Georg-August-University Göttingen
Heinrich-Düker-Weg 12
37073 Göttingen

Members of the examination board

Prof. Dr. Argyris Papantonis

Institute of Pathology
University Medical Center Göttingen
Robert-Koch-Straße 40
37075 Göttingen

Prof. Dr. Ralf Dressel

Institute for Cellular and Molecular Immunology
Heinrich-Düker-Weg 12
37075 Göttingen

Prof. Dr. Rüdiger Behr

Institute for Stem Cell Biology
German Primate Center Leibniz Institute for Primate Research
Kellnerweg 4
37077 Göttingen

Date of oral examination: 09.05.2023

II. Affidavit

Here I declare that my doctoral thesis entitled '**Genotype-Phenotype Correlation in Noonan Syndrome – Focus on LZTR1 and its Substrates**' has been written independently with no other sources and aids than quoted.

Göttingen, 28.03.2023

Alexandra Viktoria Busley

III. Acknowledgments

First of all, I would like to thank Dr Lukas Cyganek for giving me the opportunity to work on many exciting projects during my time in the Stem Cell Unit. After completing my Master's thesis in your research group, you fortunately offered me to stay for my PhD, and I decided to stay because I have never had a more open boss as well as an amazing team before. So, I would like to thank you again for always having your door open and for listening to unqualified but mostly reasonable questions and long discussions about science. I learned a lot not only personally but also scientifically and I still remember all the things you taught me. I also really liked that you were always extremely curious and open to suggestions and new methods, so I could always try out new things. Thank you for the last years and in particular, the energy you put into shaping me as a scientist.

I want to further thank Prof. Dr. med. Wolfram-Hubertus Zimmermann and Prof. Dr. med. Bernd Wollnik for being part of my Thesis Advisory Committee and especially for guiding my project throughout the last years during our meetings. I am very thankful for your scientific advice and support.

I would like to thank the Extended Thesis Committee Prof. Dr. Argyris Papantonis, Prof. Dr. Ralf Dressel and Prof. Dr. Rüdiger Behr for their time to review this work.

I want to also thank Dr. Elke Hammer and Anja Wiechert for introducing me to the world of proteomics during my stay in the institute for genetics and functional genomics in Greifswald. It was a pleasure to get to know you and, the whole research group. I really appreciate your patience while teaching me different methods.

A big thank you also goes to Dr. Henriette Irmer and Frauke Bergmann for making the IMPRS-GS graduate program a wonderful platform for interactions and scientific exchange. Thank you again for solving all the questions and concerns a PhD student could have.

I also want to thank Dr. Heike Conrad and all the members of the Hertha Sponer College and the MBExC community for the exciting retreats, interesting scientific discussions, great workshops, and the endless motivation to help each other. I am pleased to be part of this awesome community where I could also make new friends!

I would also like to express my gratitude to the whole Stem Cell Unit team. It was a real pleasure to work with all of you including past and current members. I would like to especially thank Laura Cyganek, Lisa Schreiber, Nadine Gotzmann, Yvonne Wedekind, Yvonne Hintz, Jakob Fell, Carolin Knauer, Fabian Koitka, Óscar Gutiérrez-Gutiérrez, Mario Pavez-Giani, Robin Hindmarsh and Mandy Kleinsorge. I found with you a second family and you all made this experience every day worth it and

enjoyable. A big thank also goes to all the wonderful students I could work with; it was always a lot of fun and very productive.

I also really appreciate the support of my family, my great friends in Göttingen and outside, and Jörn, who always believed in me more than I did. I am glad to have you all in my life!

Table of Contents

Table of Contents	5
List of Figures.....	7
List of Tables.....	8
List of Abbreviations.....	1
Abstract	1
1 General Introduction.....	3
1.1 Noonan syndrome – a rather new kid on the block ‘LZTR1’	3
1.2 Human induced pluripotent stem cells as a disease model for Noonan Syndrome.....	7
1.3 Genotype-phenotype correlation of Noonan syndrome patients.....	9
1.4 Current therapeutic strategies for the treatment of Noonan syndrome	10
2 Aims of the thesis.....	14
2.1 Chapter 1: LZTR1 polymerization provokes cardiac pathology in recessive Noonan syndrome	14
2.2 Chapter 2: Generation of a genetically-modified induced pluripotent stem cell line harboring a Noonan syndrome-associated gene variant MRAS p.G23V	15
2.3 Chapter 3: Generation of a genetically-modified induced pluripotent stem cell line harboring an oncogenic gene variant KRAS p.G12V	15
3 Author contributions.....	16
4 Chapter 1: LZTR1 polymerization provokes cardiac pathology in recessive Noonan syndrome	19
4.1 Abstract.....	19
4.2 Introduction	20
4.3 Results.....	21
4.4 Discussion.....	27
4.5 Materials and methods	31
4.6 Acknowledgements.....	37
4.7 Author contributions.....	37
4.8 Figure Legends	38

5	Generation of a genetically-modified induced pluripotent stem cell line harboring a Noonan syndrome-associated gene variant MRAS p.G23V.....	54
5.1	Abstract.....	54
5.2	Resource utility.....	56
5.3	Resource Details.....	56
5.4	Materials and Methods.....	57
5.5	Acknowledgements.....	59
6	Generation of a genetically-modified induced pluripotent stem cell line harboring an oncogenic gene variant KRAS p.G12V.....	66
6.1	Abstract.....	66
6.2	Resource utility.....	68
6.3	Resource Details.....	68
6.4	Materials and Methods.....	69
6.5	Acknowledgements.....	71
7	General discussion.....	78
7.1	Noonan syndrome – focus on LZTR1.....	79
7.2	Recessive LZTR1 mutation and its role in cardiac pathology.....	80
7.3	MRAS-just one LZTR1 interaction partner or is it one of the key players in cardiac hypertrophy? 83	
7.4	<i>KRAS</i> ^{G12V} -induced effect on RAS/MAPK signalling.....	84
8	Conclusion & Outlook.....	86
9	References.....	88

List of Figures

Figure 1: Noonan syndrome- (NS) associated symptoms.	4
Figure 2: Structural model of Leucine Zipper-like Transcriptional Regulator 1 (LZTR1).	5
Figure 3: Dysregulated RAS/MAPK signalling pathway upon <i>LZTR1</i> missense mutations.	6
Figure 4: Human induced pluripotent stem cells (iPSCs) are a versatile disease model.	8
Figure 5: CRISPR/Cas9 mode of action and the cell's internal repair mechanisms.....	12
Figure 6: Generation of patient-specific and CRISPR-corrected iPSCs for disease modeling of recessive NS.	38
Figure 7: Homozygous <i>LZTR1</i> ^{L580P} causes accumulation of RAS GTPases.....	40
Figure 8: Homozygous <i>LZTR1</i> ^{L580P} provokes cardiomyocyte hypertrophy.	42
Figure 9: Homozygous <i>LZTR1</i> ^{L580P} does not compromise contractile function.	43
Figure 10: Homozygous <i>LZTR1</i> ^{L580P} induces polymerization of LZTR1-cullin 3 ubiquitin ligase complexes.	44
Figure 11: Homozygous <i>LZTR1</i> ^{L580P} alters binding affinities of dimerization domains.....	46
Figure 12: Off-target screening in CRISPR/Cas9-edited iPSCs. (Supplementary figure).....	47
Figure 13: Homozygous <i>LZTR1</i> ^{L580P} showed no upregulation of RAS GTPases at transcriptional level. (Supplementary figure)	48
Figure 14: Unique <i>LZTR1</i> ^{L580P} -induced polymerization of LZTR1 complexes. (Supplementary figure)..	49
Figure 15: Computational prediction for LZTR1 interactions via ColabFold. (Supplementary figure)..	50
Figure 16: Generation of a CRISPR-edited <i>MRAS</i> ^{G23V} iPSC line.....	60
Figure 17: Generation of a CRISPR-edited <i>KRAS</i> ^{G12V} iPSC line.	72
Figure 18: Genotype-phenotype correlation of Noonan syndrome patients.	87

List of Tables

Table 1: Antibodies used for Western blot, immunocytochemistry and flow cytometry. (Supplementary table).	51
Table 2: Primer sequences used for PCR and real-time PCR. (Supplementary table).....	52
Table 3: Plasmids used for ectopic expression studies. (Supplementary table)	53
Table 4: Ressource Table	55
Table 5: Characterization and validation of <i>MRAS</i> ^{G23V} iPSC line.	62
Table 6: Reagents details.....	64
Table 7: Resource Table	66
Table 8: Characterization and validation of <i>KRAS</i> ^{G12V} iPSC line.....	74
Table 9: Reagents details.....	76

List of Abbreviations

ATTR.....	<i>Transthyretin-amyloidosis</i>
BTB/POZ	<i>BR-C, ttk and bab/Pox virus and Zinc finger</i>
cDNA.....	<i>complementary DNA</i>
CRISPR/Cas9 .	<i>Clustered Regularly Interspaced Short Palindromic Repeats/CRISPR-associated protein 9</i>
crRNA.....	<i>CRISPR-RNA</i>
CUL3	<i>cullin 3 ubiquitin ligase</i>
DSB	<i>Double-strand break</i>
GAPs	<i>GTPase activating proteins</i>
HCM.....	<i>Hypertrophic cardiomyopathy</i>
HDR.....	<i>Homology-directed repair</i>
iPSC-EHM.....	<i>iPSC-engineered human myocardium</i>
iPSCs	<i>Induced pluripotent stem cells</i>
LZTR1	<i>Leucine Zipper like Transcription Regulator 1</i>
MEKi.....	<i>MEK1/2 inhibitor</i>
NF1	<i>Neurofibromatose Type 1</i>
NHEJ.....	<i>Non-homologous end joining</i>
NS	<i>Noonan syndrome</i>
RAS/MAPK	<i>RAS/mitogen-activated protein kinase pathway</i>
R-HCM	<i>Rasopathy-associated HCM</i>
RTKs	<i>Receptor tyrosine kinases</i>
RT-PCR	<i>Reverse-Transcriptase PCR</i>
SNVs.....	<i>Single nucleotide variants</i>
tracrRNA	<i>trans-activating RNA</i>
WES.....	<i>Whole exome sequencing, Whole exome sequencing</i>
WT	<i>wild-type</i>

Abstract

Noonan syndrome (NS) is a multisystemic disorder that is known as one of the most common monogenetic diseases associated with early-onset congenital heart defects, such as hypertrophic cardiomyopathy (HCM). Infants diagnosed with NS and HCM have a worse late survival and are more likely to develop heart failure than non-syndromic HCM patients harboring classical mutations in sarcomeric genes (e.g. β -myosin heavy chain, *MYH7*). In recent years, many germline mutations affecting different components of the RAS/mitogen-activated protein kinase (RAS/MAPK) pathway (including LZTR1, which negatively regulates signalling activity) have been identified as responsible for the development of NS and NS-associated diseases. Indeed, RASopathies result from of a signalling hyperactivation of the RAS/MAPK signalling and further cross-linked signalling pathways. However, based on clinical genotype-phenotype data as well as *in vitro* and *in vivo* studies, it has been suggested that the underlying, potentially overlapping pathomechanisms might be dependent on the cell type and the specific disease-causing variant. Patient-specific induced pluripotent stem cell-derived cardiomyocytes (iPSC-CMs) from different NS patients are a powerful tool to study a genotype-phenotype correlation by investigating their molecular and functional properties in physiological relevant cells and tissues. In this work, a novel gene variant p.L580P in Leucine Zipper like Transcription Regulator 1 (LZTR1) has been identified as causative for recessive NS. Patient-derived as well as CRISPR-corrected induced pluripotent stem cells (iPSCs) were differentiated into ventricular-like iPSC-CMs and characterized on the molecular and functional level. Upon recapitulation of the patient's phenotype by showing increased cell diameters as a characteristic of HCM and a hyperactivation of the RAS/MAPK pathway, we could reveal a novel gene variant-specific pathomechanism by which mutated *LZTR1* shows dysfunction in ubiquitinating active RAS proteins. We could also prove that, besides the classical RAS GTPases (HRAS, NRAS and KRAS), MRAS was one of the main interaction partners of LZTR1 in the heart. Importantly, CRISPR/Cas9 based correction of this specific gene variant was able to rescue the disease phenotype *in vitro*. As gene variants in *MRAS* are also linked to NS and NS-associated HCM, the NS-associated mutation MRAS p.G23V was introduced into wild-type (WT) iPSCs to study its impact on cardiac physiology. Furthermore, we generated an iPSC line harboring a cancer-associated mutation KRAS p.G12V, known to cause severe signalling hyperactivity. Future work will proceed in uncovering the MRAS- and KRAS-specific phenotypes on the molecular and functional levels. In addition, the established iPSC models will be used to test new personalized treatment strategies based on pharmacological interventions and CRISPR/Cas9 gene therapy.

To summarize, we successfully showed that the application of patient-derived iPSCs is a suitable model system to recapitulate the patients' cardiac phenotypes *in vitro* and to perform deeper investigations to understand the gene-specific molecular pathomechanisms of NS-associated HCM.

1 General Introduction

RASopathies are a group of pleomorphic multisystem disorders with overlapping symptoms but variable clinical phenotypes and different severities. What they have in common is that the disease-causing germline mutations are linked to the RAS/RAS/MAPK signalling pathway. The most prominent disorder is Noonan syndrome (NS) followed by associated diseases such as cardiofaciocutaneous syndrome, Legius syndrome, Costello syndrome, and NS with multiple lentiginos.^{1,2} Several studies have shown that many RAS patients diagnosed with structural heart defects, such as pulmonary valve stenosis, have better survival than NS patients suffering from a severe form of HCM, who have even worse survival compared to patients with idiopathic or familial HCM in childhood.^{3,4} Upon diagnosis, the current standard therapy approaches for NS patients with HCM are beta-blockers⁵, surgery including myomectomy⁶, and, since very recently, off-label application of cancer-proven drugs inhibiting RAS/MAPK signalling like MEK inhibitors (MEKi).⁷ For most of the HCM patients, heart transplantation, which comes with a high mortality of 33%, is inevitable.⁶ Due to the immense heterogeneity of RASopathy mutations resulting in different phenotypes, a better understanding of the molecular and functional correlation between the genotypes and phenotypes is a prerequisite to develop novel therapies tailored to the individual genotype of each patient

1.1 Noonan syndrome – a rather new kid on the block ‘LZTR1’

Noonan syndrome, first described in 1968 by Jacqueline Noonan⁷ is a developmental multisystem disorder with an approximate prevalence of 1 in 1,000 to 2,000 live births.⁸ Commonly observed symptoms are facial abnormalities like hypertelorism, low-set ears, short stature, and chest deformation as pectus excavatum. Other features apart from severe heart defects are neurodevelopmental disabilities, lymphedema, and bleeding disorders.^{9,10} NS is further known to be the most common monogenetic disease being associated with early-onset HCM¹¹ (Figure 1). Based on a clinical registry, around 18% of children diagnosed with HCM are RASopathy patients. In patients younger than 1 year, RASopathy-affected patients account for 42% of all HCM cases.¹² This patient group (<1 year) is more prone to develop heart failure compared patients with non-syndromic HCM.¹³ Further, one can distinguish between Rasopathy-associated HCM (R-HCM) and sarcomeric HCM. Both are represented by a severe phenotype. Whereas R-HCM has an increased prevalence of left ventricular outflow tract obstruction and a higher risk for hospitalization due to a heart failure risk and inevitable septal myectomy already during childhood.^{14–17}

Noonan syndrome (NS)

Common symptoms

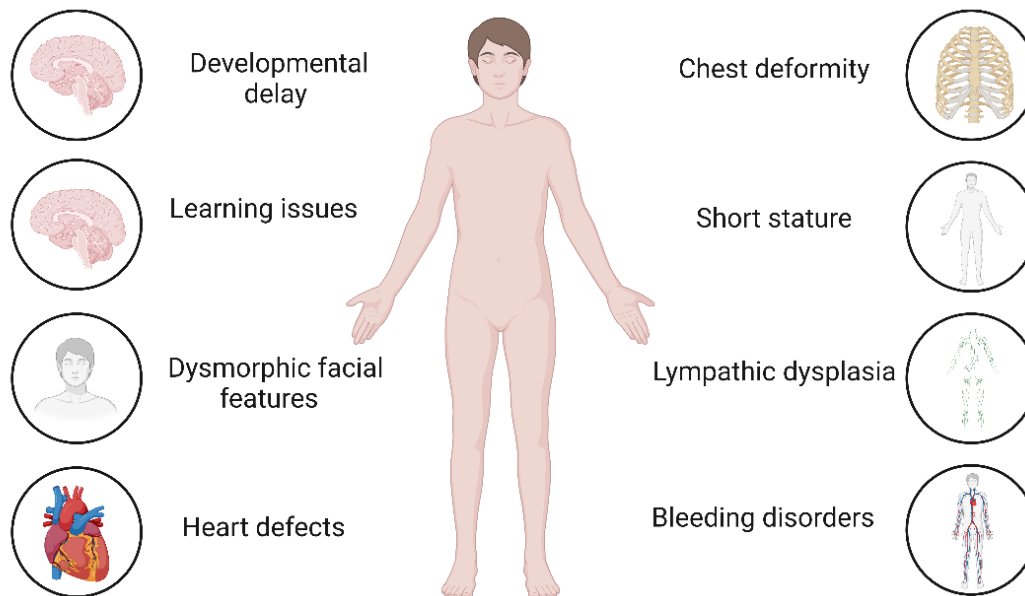


Figure 1: Noonan syndrome- (NS) associated symptoms.

Due to the large heterogeneity of NS-causing mutations, the phenotypes are quite diverse. As a result, diagnosis is sometimes difficult or patients are not diagnosed until adulthood. Here the major symptoms are summarised associated with NS. Not only symptoms are quite variable and depend on the underlying mutation, but also the severity and onset vary from patient to patient. The lowest survival rate is associated with congenital heart defects, such as hypertrophic cardiomyopathy (HCM), which is the life-limiting factor in these patients. Image created with BioRender.com.

Similar to RASopathy-associated diseases, NS is induced by germline mutations affecting various RAS/MAPK-candidates leading to overall enhanced signalling transduction. The most frequently affected genes in NS are *PTPN11*, *SOS1*, *SOS2*, *NRAS*, *KRAS*, *MRAS*, *RRAS2*, *RIT1*, *LZTR1*, *RAF1* and *MAP2K1*.^{18–24} Deciphering a genotype-phenotype correlation on the molecular level is still the focus of current research, although a correlation between mutated genes and the corresponding clinical phenotype has already been established. *PTPN11* is more likely to induce pulmonary stenosis (PS) whereas mutated *RAF1*, *MRAS* and *RIT1* are highly associated with the development of HCM.^{25–31} Common mutations mainly induce hyperactivity either based on increased signalling through the upregulated activity of RAS proteins (*KRAS*, *HRAS*, *NRAS*, *MRAS*, *RRAS*, *RRAS2*, *RIT1*) by downstream proteins that promote signalling transduction (*SHOC2*, *PPP1CB*) or by an elevated function of upstream transducers and regulators controlling RAS function (*SHP2*, *SOS1*, *SOS2*). Additionally, mutated proteins like *NF1*, *CBL*, *LZTR1*, *SPRED1*, and *SPRED2* evoke dysregulation of the pathway by interrupting the feed-back mechanism tightly controlling RAS.³² Due to improvements in sequencing techniques

such as whole exome sequencing (WES), many more disease-causing mutations are uncovered. One of these genes is *LZTR1* encoding for the Leucine Zipper-like Transcriptional Regulator 1 that was first identified in a patient with an adult-onset tumour predisposition called schwannomatosis.²⁴

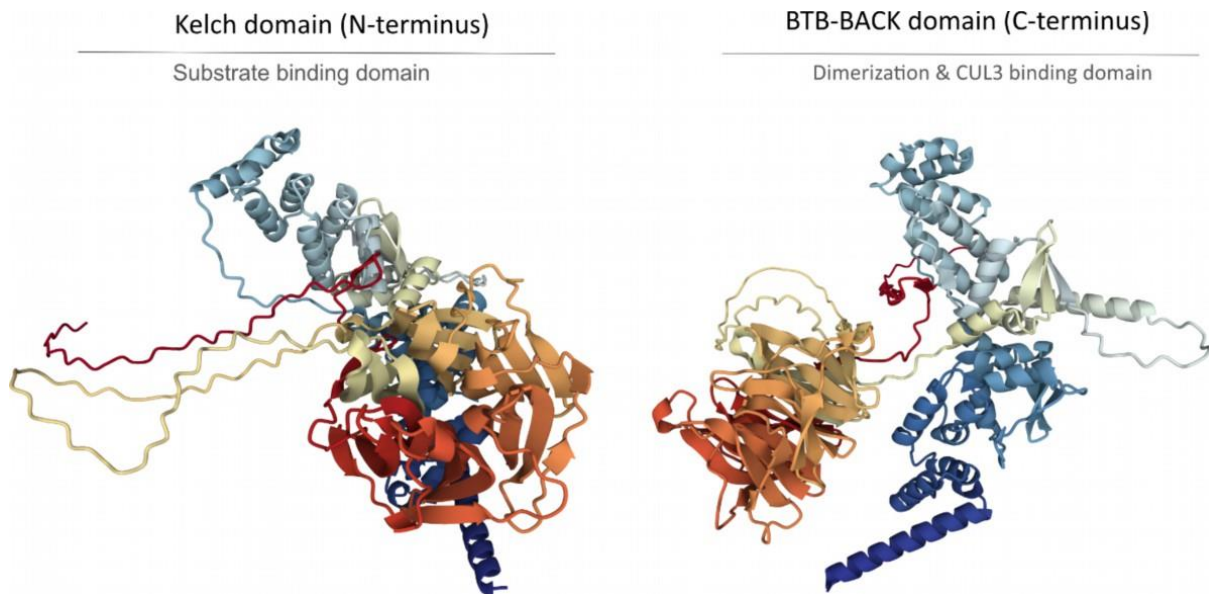


Figure 2: Structural model of Leucine Zipper-like Transcriptional Regulator 1 (LZTR1).

Structural model of the adaptor protein LZTR1 showing its N-terminal Kelch domain and the C-terminal BTB-BACK domain. Based on previous observations, Kelch motifs are responsible for proper substrate binding. Many dominant LZTR1 mutations are located within the Kelch domain and prevent proper substrate binding resulting in an active substrate accumulation. So far, LZTR1 substrates are known to be RAS protein family members (KRAS, NRAS, HRAS, MRAS and RIT1). The C-terminal BTB-BACK domain is further known to be important for protein dimerization and the binding of CUL3. Modelling was performed with AlphaFold2.³³ Figure modified from Dr. Lukas Cyganek (unpublished).

In 2018, LZTR1 was found to be mutated in a biallelic manner causing NS.³⁴ Followed by, two publications a year later that presented NS patients harboring an *LZTR1* mutation in a dominant and recessive form.^{35,36} Considering its protein structure, LZTR1 consists of six tandemly arranged Kelch motifs at the N-terminus, and two C-terminal BR-C, ttk and bab/Pox virus and Zinc finger (BTB/POZ) domains. Its cellular function was long time believed to be involved in transcriptional regulation as a tumour suppressor. However, recent studies have shown that LZTR1 functions as an adaptor protein that binds cullin 3 ubiquitin ligase (CUL3) via its C-terminus and ligand proteins via its N-terminal domain^{37,38} (Figure 2). Additionally, BTB family proteins are known to build hetero- or homodimers.³⁹ LZTR1 has been shown to build BTB-BTB homodimers that are then able to bind their substrates.³⁹ Several studies uncovered the role of LZTR1 within the RAS/MAPK signalling pathway acting as a negative regulator of active RAS proteins by promoting their ubiquitination and subsequent

proteasomal degradation^{39–44} (Figure 3). However, open questions still exist concerning the number of LZTR1-specific substrates that are targeted for subsequent degradation processes.³² To elucidate these open questions related to protein function, disease-specific pathomechanisms, and potential therapeutics, the use of human iPSCs has already been shown to be a suitable and promising model.^{45,46}

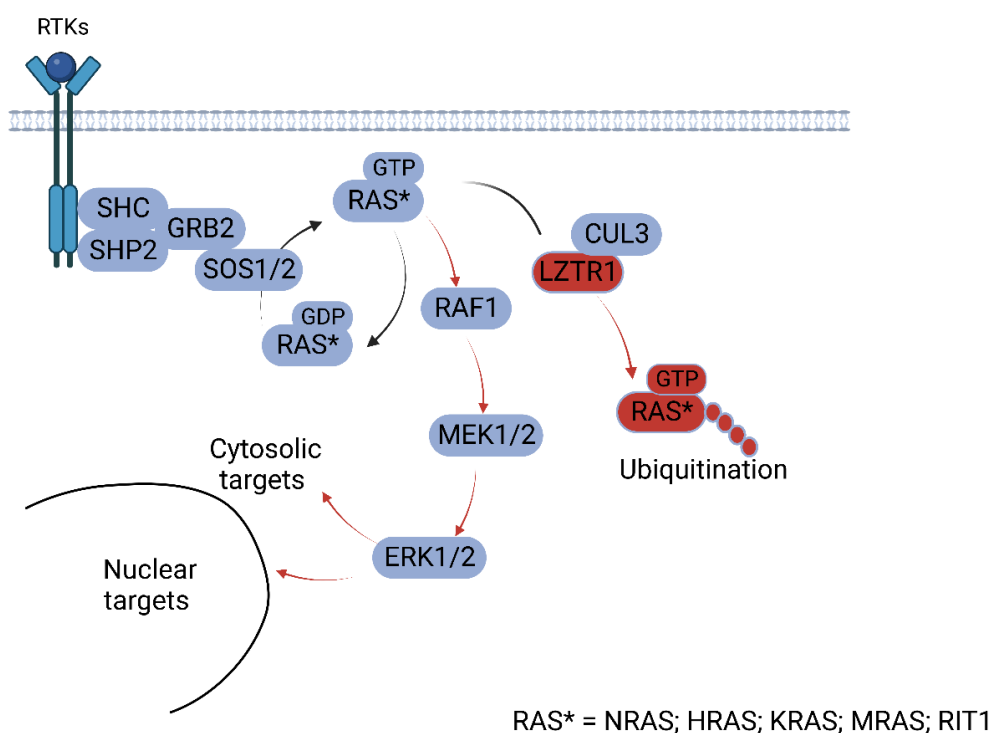


Figure 3: Dysregulated RAS/MAPK signalling pathway upon LZTR1 missense mutations.

Receptor tyrosine kinases (RTKs) bind various growth factors and dimerize upon binding. Phosphorylated RTKs bind GRB2, SHC, and SHP2 which form a complex and recruit SOS1/2. This protein then acts as a guanine nucleotide exchange factor and induce a RAS-GDP switch to its active RAS-GTP form. Active RAS transmits an activating signal through RAF1, MEK1/2, and ERK1/2 based on a fine-tuned phosphorylation cascade. Activated ERK1/2 translocates into the nucleus to initiate the transcription of nuclear targets but to also further activate cytosolic substrates. GTPase activating proteins (GAPs) catalyze the switch from GTP to GDP via hydrolysis to terminate RAS activity. Leucine transcriptional regulator 1 (LZTR1) was known to be a tumor suppressor being responsible for the ubiquitination and subsequent degradation of active RAS proteins, by serving as an adaptor that binds active RAS and cullin 3 ubiquitin ligase. Missense variants within the LZTR1 protein (red) can cause an accumulation of active RAS proteins (red) due to absent ubiquitination causing a pathological signalling hyperactivation indicated by red arrows. Image created with BioRender.com.

1.2 Human induced pluripotent stem cells as a disease model for Noonan Syndrome

The goal of studying diseases in human-like models was finally achieved with the revolutionary innovation of Yamanaka et al. who obtained iPSCs by transducing human fibroblasts with four defined factors. (*Oct3/4*, *Sox2*, *Klf4*, and *c-Myc*).⁴⁷ Since then, researchers apply this reprogramming technology to robustly generate iPSC from somatic cells isolated from e.g., (patient) skin biopsies or blood samples. As most current research is based on animal models, one of the biggest advantages of iPSCs is that they are derived from human cell material meaning they have the identical genome to the donor, including all single nucleotide variants (SNVs) and genetic defects.⁴⁸ Human iPSCs possess the ability to differentiate into almost any kind of cell type like cardiomyocytes or cardiac fibroblasts ending up with large amount of homogenous populations of disease-relevant cells.^{49,50} Studying human-derived cells provide a solid basis for extensive *in vitro* studies to better understand molecular human cell physiology in healthy and diseased state. However, it should be noted that iPSC-CMs are more similar to fetal cardiomyocytes in terms of their molecular, functional and structural properties.⁵¹ Therefore, several developments have been made to promote the maturation of these cells. One option is to use iPSC-derived engineered heart muscles (iPSC-EHM) as a complementary three-dimensional model, consisting of iPSC-CMs in combination with fibroblasts embedded in a collagen matrix. Upon deeper phenotyping, they resemble a more native state of the human heart muscle similar to an infant's myocardium compared to two-dimensional iPSC-CM cultures^{51,52} (Figure 4).

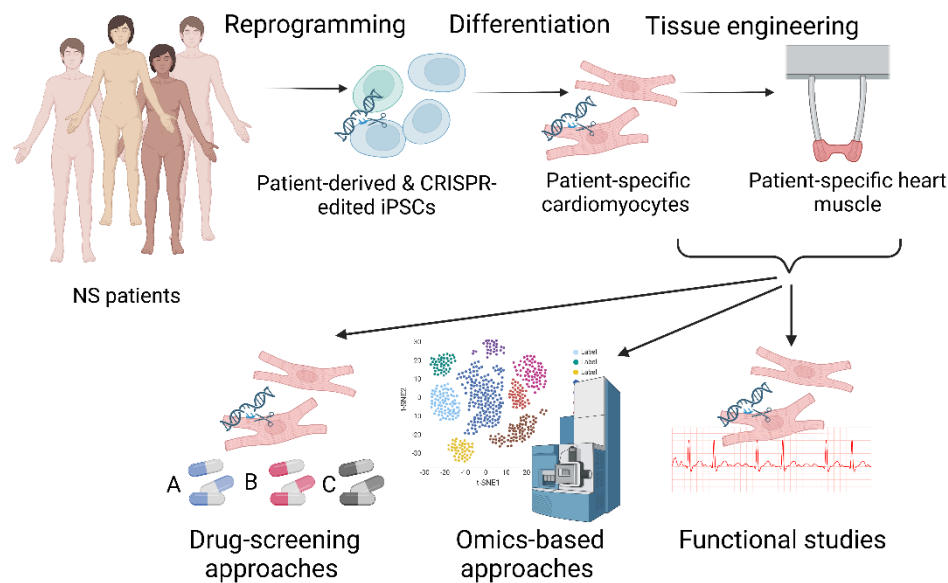


Figure 4: Human induced pluripotent stem cells (iPSCs) are a versatile disease model.

Noonan syndrome (NS) patients' biopsies derived mainly from skin fibroblasts are reprogrammed into patient-specific iPSCs and differentiated into iPSC-derived cardiomyocytes to study cardiac pathologies and the underlying molecular pathomechanism in detail. To obtain more mature cells and to study mutation effects in a more complex tissue-like environment, iPSC-CMs can be used to generate engineered heart muscles (EHM). Both iPSC-CM and EHM can be further used for functional studies, high-throughput drug screening approaches or to obtain a more global overview about disease signatures using omics-based approaches. Image created with BioRender.com.

Several studies could prove that iPSC-CMs are a powerful tool to model diseases including RASopathies and sarcomeric cardiomyopathies by recapitulating the patient's phenotype and by enabling further investigation of the cellular pathology in a dish.^{45,46,53} Upon identification of key pathomechanism, new therapeutic strategies can be tested, due to an unlimited source of cells that were previously limited by the number of heart biopsies available. Therefore iPSC-CM, iPSC-cardiac fibroblasts and other cells can be applied for *in vitro* preclinical testing, before performing safety, efficacy and toxicity tests in a high-throughput manner in small and large animal models. It is further considered that they might allow a more precise prediction of drug responses and cardiotoxicity in patients' cardiac tissue based on their human origin.^{54,55}

The current standards for RASopathy-related therapies are limited and not adapted to specific genetic variants. Standard treatments upon NS-related HCM diagnosis are common beta- or calcium channel blockers. In patients with elevated risk for developing heart failure, surgical interventions such as septal myectomy are necessary.⁵⁶ In order to improve the patients' lives and to prevent surgical interventions, a more personalized therapeutic strategy would be highly beneficial in tailoring

individual genotypes, especially for the heterogeneous group of RASopathy patients.⁵⁷ Understanding each NS-causing mutation and the associated pathophysiological changes is a prerequisite for establishing more personalized medicine, in order to ultimately treat HCM as the life-limiting factor in these patients.

1.3 Genotype-phenotype correlation of Noonan syndrome patients

The development of more precise and personalized therapies should be based on an accurate genotype-phenotype correlation study that reveals the molecular pathomechanisms behind individual mutations. One recent study correlated 116 RASopathy patients and the respective genotypes to their clinical presentation while focusing on the cardiac defects and the course of the treatments.⁵⁸ They could observe that patients harboring a *PTPN11* mutation are more affected by pulmonary valve stenosis and pulmonary valve dysplasia whereas *SOS1* mutations more often induce valvular defects. While other mutations such as *RIT1* caused HCM, *SOS2* was associated with septal defects and *SHOC2* caused septal and valve abnormalities. This study and others have shown that there is a specific correlation between cardiac defects and the disease-causing mutation, but the molecular mechanism behind many of them remains unknown.^{58,59} However, for some NS-causing mutations, there were studies in which the mechanism of how a single mutation caused a severe heart defect have been uncovered in an iPSC-CMs model. One of these, published in 2019 by Jaffré et al., utilized patient-derived iPSCs from a *RAF1* patient. 73% of *RAF1*-NS patients present a severe and lethal form of HCM.⁶⁰ By differentiating patient-derived iPSC into cardiomyocytes and applying CRISPR/Cas9 genome editing strategies, they could uncover a novel *RAF1*-induced pathomechanism. On the one hand, deeper phenotyping of the diseased iPSC-CM and their isogenic control showed hyperactive MEK1/2 and ERK1/2 signalling causing myofibrillar disarray. On the other hand, cardiomyocyte enlargement was induced by an elevated ERK5 signalling. A pathway previously not associated with NS or HCM development.⁴⁶ Another example uncovering the pathomechanism behind *LZTR1* mutation, a so far rare NS-causing variant, was published by our group in 2020.⁴⁵ Here, iPSC-CMs from two patients with truncating *LZTR1* variants have been successfully applied to recapitulate the patient's phenotype in 2D by showing RAS/MAPK signalling dysfunction and cellular hypertrophy. This was by then the first description of a causal connection between induced RAS/MAPK hyperactivation due to a *LZTR1* dysfunction in autosomal recessive NS patients with a severe form of HCM. Furthermore, in this study, the standard therapeutic options such as calcium channel blockers and MEKis were tested and did not reveal significant effects on cellular hypertrophy indicating a low beneficial effect for NS patients at least on a cellular basis. In addition to the drug treatment, preclinical testing of translatable intronic CRISPR repair was conducted and revealed a beneficial rescue of cellular hypertrophy.⁴⁵ Due to the immense heterogeneity of RASopathies and NS patients in particular, clustering of patients would

facilitate the development of novel treatments for patients with similar pathologies and disease outcomes. One promising approach is to repurpose already existing drugs depending on common disease signatures of NS patients.

In conclusion, a genotype-phenotype study focusing on the molecular level is needed to uncover the pathologies of different NS patients. Once these pathomechanisms are identified, drug repurposing might be a fast and efficient way to improve patients' lives. However, long-term use of drugs is associated with unknown side effects, as patients with severe phenotypes need to be treated within the first few months and over years. A future treatment option would be to use precise gene therapy approaches, such as CRISPR-based therapies, to target the affected heart and - to improve the lives of patients with NS.

1.4 Current therapeutic strategies for the treatment of Noonan syndrome

Little progress has been made in the development of optimized and adapted treatment options for RASopathies and for NS patients in particular, whereas significant progress has been made in the treatment of cancer patients who suffer from gain-of-function mutations within the RAS/MAPK pathway.¹ RAS genes are one of the most frequently mutated genes in cancer patients, accounting for approximately 19% of cases, with others having a mutation in the *BRAF* gene (8%) or mutations affecting the further canonical RAS/MAPK pathway-associated proteins.^{61,62} To prevent or inhibit RAS hyperactivation, several components of this well-studied pathway may serve as potential therapeutic targets. Novel compounds can be clustered into three classes: direct RAS inhibitors, inhibitors of RAS activation, or MAPK inhibitors.⁶³ One of the most commonly tested RAS/MAPK compounds targets MEK1/2, as it is the mediating protein within the phosphorylation cascade and thus transmits the activating signal. As a result, many MEKis have been developed and are currently on the market for oncological indications, but some have shown limited beneficial effects and have had to be used in combination with other anti-cancer therapies.^{63–68} Studies showing the effect of MEKis suggest that their limited efficacy is due to disruption of the negative feedback loop of RAF proteins. However, as MEK inhibition has been successfully used as a prenatal preventive therapy in several animal models, further research is essential to understand their pharmacological mode of action as well as their patient-specific effects. In two NS mouse models harboring *Sos1*^{E846K}, *Kras*^{V14I}, and a CFC (*Braf*^{Q241R}) mutation, prenatal or postnatal treatment could prevent the development of a RASopathy phenotype.^{69,70} MEKis could also rescue the phenotype of *PTPN11* and *NRAS*-associated NS in zebrafish.^{71,72} In some studies, MEK inhibition was not efficient, as shown in a heterozygous *Lztr1* mouse model, in spite of the treatment being started prenatally.⁴¹ As several examples have shown, the timing of the treatment, but more importantly the genetic background of the patient, is essential to reverse the phenotype upon efficient MEKi treatment. One promising example is the use of the MEK

inhibitor trametinib, which showed significant clinical improvement by reducing HCM-associated heart failure in NS patients having a pathogenic variant in the *RIT1* gene.⁷³ In addition to the study by Andelfinger et al., another MEK inhibitor, selumetinib, has been approved by the US Food and Drug Administration for the use in Neurofibromatose Typ 1 (NF1) patients.⁷⁴ In general, before repurposing therapeutic strategies, some differences between cancer and RASopathy patients should be considered. First, while cancer patients show somatic gain-of-function mutations, RASopathy patients are presented with germline gain-of-function mutations causing different levels of RAS/MAPK activity in a tissue-and cell-dependent manner. Second, MEKi treatment in cancer patients would be typically administered during adulthood while RASopathy patients have to be treated during the early months of life and for the long term in lower doses. Consequently, not only the predicted and observed side-effects but also the efficacy might vary in RASopathy patients.¹ In addition to the already complex genetic variability, RAS/MAPK hyperactivity can also further affect other signalling pathways such as PI3K/AKT signalling. Hence, some studies also suggest inhibitors for mTOR to alleviate cardiac symptoms in patients suffering from HCM.⁷⁵ Active RAS/MAPK has also been shown to communicate with other pathways such as the Hippo pathway, the hypertrophy-related calcineurin-NFAT, and NFκB pathway, and these pathways could consequently become promising targets for pharmacological interventions based on individual genetic backgrounds.^{76–78} Based on this highly interconnected pathway network, blocking one pathway might cause an adaptation or resistance due to a compensatory mechanism. Studies showed that metastatic melanoma caused by *MAP2K1* and *MAP2K2* mutations, were resistant to RAF and MEK inhibition.⁷⁹ According to more studies claiming a resistance development, a dual-inhibition might be necessary, especially considering the required long-term treatment in NS patients. Dual-inhibition was successful in KRAS colon and pancreatic cancer patients, by blocking RAS/MAPK and PI3K/AKT via trametinib and borussertib application.⁸⁰

In summary, the current treatment options for NS are symptomatic and none of them are curative. Novel and personalized treatments are therefore needed, especially for patients with monogenetic diseases such as NS, in which it is evident that genetic correction will reverse the disease phenotype in most cases. One promising approach is CRISPR/Cas9-mediated gene therapy. With this target-specific editing of the genome, it has become possible to modify or precisely correct disease-relevant loci.⁸¹ Similar to zinc finger nucleases and Transcription activator-like effector nucleases, a double-strand break (DSB) is induced by the Cas9 protein, which is guided to a specific genomic target site by a pre-designed CRISPR-RNA (crRNA) that is hybridized to a Cas9-specific trans-activating RNA (tracrRNA). Two major repair mechanisms are activated upon DNA damage due to the DSB: non-homologous end joining (NHEJ) and homology-directed repair (HDR). In the absence of a suitable repair template, NHEJ repairs the break by error-prone re-ligation, mainly producing insertions or deletions that can be useful

for generating gene knockouts.⁸² Because HDR uses a repair template to repair the DSB, a precise editing can occur at the specific target site. Repair templates can be single-stranded oligonucleotides or double-stranded DNA with homology arms (Figure 5). These editing strategies have been shown to be sufficient to correct specific genetic variants in proliferating cells.⁸³ However, as HDR is only active in dividing cells, this CRISPR approach will hardly find application in mature terminally differentiated cells such as cardiomyocytes.

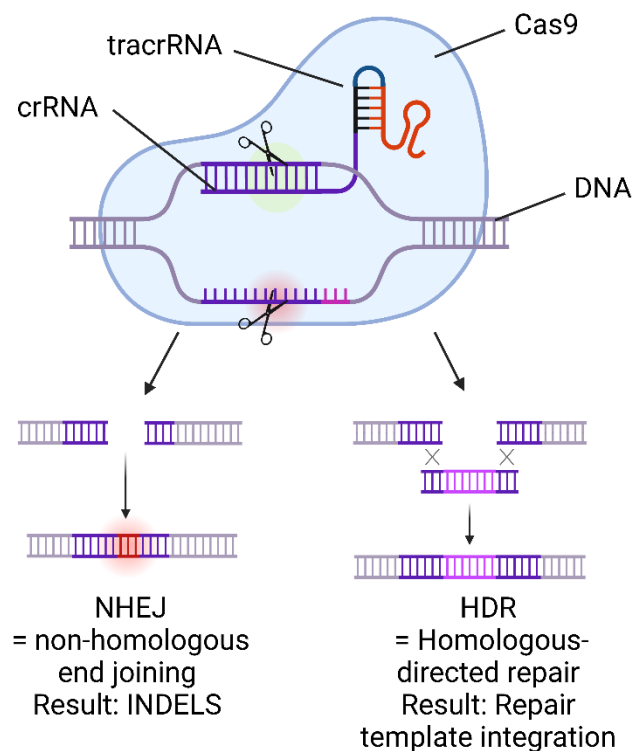


Figure 5: CRISPR/Cas9 mode of action and the cell's internal repair mechanisms.

CRISPR/Cas9 was discovered as a defence mechanism of bacteria against invading viruses. Nowadays researchers apply the same method by using Cas9 proteins purified from bacteria (e.g. SpyCas9 = *Streptococcus pyogenes*). Upon hybridizing Cas-specific tracrRNA with the target-specific crRNA, the complex is mixed with Cas9 protein in a defined ratio and introduced into the cell via nucleofection. The guideRNA complex (tracrRNA and crRNA) guides Cas9 to the target-site and the protein induces a DNA double-strand break. Subsequently, the two main DNA repair mechanisms are activated at least in dividing cells. Non-homologous end joining repairs the two strands via recombination that finally results in a high number of insertion/deletions (INDELS), which is in contrast to homology-directed repair where the DSB is repaired by integration of the repair template. Image created with Biorender.com.

During the last years, several promising studies were published, proving the successful application of modified CRISPR/Cas9 *in vivo*, and were further translated to clinical trials. For instance, targeting the genetic variant that causes a rare disease called Leber Congenital Amaurosis¹⁰ is already in phase II of clinical trials. The whole editing complexes are hereby packed into an Adeno-associated virus 5 vector that is subretinally delivered, thus only targeting the photoreceptor cells and giving rise to vision loss restoration.⁸⁴ Another study has been already translated to clinical trials treating a disease called Transthyretin-amyloidosis (ATTR). This disease is caused by an accumulation of the misfolded protein transthyretin in tissues such as nerves and the heart. Hereby, NTLA-2001 describes an *in vivo* gene-editing strategy, based on a messenger RNA CRISPR-based system packed into lipid-nanoparticles targeting *TTR* gene. Currently there is an ongoing clinical trial treating six patients with inherited ATTR.⁸⁵ Furthermore, Amoasii et al. proved great progress in translational preclinical testing by applying CRISPR/Cas9 to treat Duchenne Muscular Dystrophy in a canine model resulting in a robust Dystrophin restoration upon editing.⁸⁶

Although, several CRISPR editing strategies hold promise for developing personalized therapeutic alternatives, delivery and safety will be the biggest obstacles in the coming years.

2 Aims of the thesis

The overall aim of this work was to investigate the molecular and functional pathological effects of NS-specific mutations on cardiac function using patient-derived iPSC-CMs. First, the cardiac pathological role of a recessive LZTR1 p.L580P mutation was investigated at the molecular, cellular and functional level and compared with other *LZTR1* mutations. Secondly, as MRAS is one of the major interaction partners of LZTR1, a NS-associated gene variant in MRAS p.G23V was introduced into healthy WT iPSC to elucidate its role in HCM development. Furthermore, as RASopathies are strongly associated with increased RAS/MAPK signalling, a common cancer-associated KRAS p.G12V was introduced into WT iPSCs to study the gain of function effect of a constitutively active RAS pathway on cellular physiology. During the PhD, all the above cell lines were generated, characterised and differentiated, and CRISPR/Cas9 strategies were used to obtain LZTR1-corrected isogenic control lines. Furthermore, these iPSC models were successfully used to identify gene variant specific pathomechanisms in NS.

2.1 Chapter 1: LZTR1 polymerization provokes cardiac pathology in recessive Noonan syndrome

Mutations affecting the *LZTR1* gene are highly associated with the development of severe HCM in NS patients. To elucidate the cardiac pathology in a patient harboring a recessive *LZTR1* mutation (*LZTR1*^{L580P}) *in vitro*, patient-derived iPSCs were differentiated into ventricular cardiomyocytes. CRISPR/Cas9 technology was applied to correct the respective mutation to generate isogenic control lines. Both cell populations, as well as WT cells, were analyzed on a molecular and cellular level. Patients' iPSC-derived cardiomyocytes displayed an increased cell size that was normalized upon genetic correction. Proteomic analysis revealed increased levels of RAS/MAPK- and HCM-associated candidates, such as accumulation of LZTR1-associated interaction partners RIT1 and MRAS, indicating a non-functional degradation of these RAS isoforms by the LZTR1-CUL3 ubiquitin ligase complex. Overexpression studies of mutated LZTR1 in WT iPSC-CMs showed severe protein oligomerization, likely resulting in protein complex dysfunction and, thereby, in manifestation of disease symptoms. In summary, we could demonstrate that our Noonan syndrome patient-derived iPSC-CM model is suitable to recapitulate the patient's phenotype and can be used to uncover patient-specific disease pathomechanisms.

2.2 Chapter 2: Generation of a genetically-modified induced pluripotent stem cell line harboring a Noonan syndrome-associated gene variant MRAS p.G23V

MRAS has been identified as one of the key LZTR1 substrates for degradation. Further, gene variants in *MRAS* are linked to a severe NS-associated cardiac hypertrophy. In order to study the pathological effect of mutated MRAS in cardiac cells, we introduced a previously described NS-causing mutation MRAS p.G23V into a WT iPSC line. This cell line complements our iPSC panel of NS patients in which we aim to correlate NS mutations with the corresponding RAS/MAPK activity and the disease severity.

2.3 Chapter 3: Generation of a genetically-modified induced pluripotent stem cell line harboring an oncogenic gene variant KRAS p.G12V

Since RASopathies are mainly caused by elevated RAS/MAPK signalling activity, we were interested in an iPSC line showing a constant and aberrant RAS/MAPK hyperactivity. Therefore, we introduced the common cancer-associated mutation KRAS p.G12V into a WT iPSC line. This variant is known to induce a strong pathway hyperactivation in cancer cells. The newly generated iPSC line was characterized and revealed higher proliferative capacity and RAS/MAPK activity under basal conditions. This cell line will be used to serve as a positive control in comparison to the different NS patient cells to study the effect of constant hyperactivation of this pathway on cardiac physiology.

3 Author contributions

4. Chapter 1

Individual contribution(s) to published article

Applicant (Name): Alexandra Viktoria Busley (first author)

Individual contribution:

1. Figures and Supplementary Figures (actively performed experiments and/or analyzed data)

Main Figures: 6 A, B, C, D, E, F, G, H; 7 A, H, I, J, K; 8 A, B, C, D, E, F; 9 A, B, C, D, E, F, G, H; 10 A, C, D, E, F, G, H, I

Supplementary Figures: 12 A; 13 A, B, C, D, E, F, G, H, I; 14 A.

Figures were designed by Dr. Lukas Cyganek.

2. Written

Main Text: Abstract, experimental procedures, main figure legends, introduction, results, and discussion. Supplementary Text: Supplementary figure legends.

3. Intellectual contribution

a. Experimental design and performance in close interaction with Dr. Lukas Cyganek. Design of guide RNAs targeting *LZTR1* locus and the repair template was performed by Dr. Lukas Cyganek.

b. Phenotypical characterization of patient-and CRISPR-edited iPSC-CM.

c. EHM generation in collaboration with Óscar Gutiérrez-Gutiérrez and the help of Branimir Berečić.

d. CellProfiler was programmed by Dr. Henning Schroeder.

e. ColabFold was performed in collaboration with Dr. Martin Steinegger.

f. Wrote significant parts of the manuscript.

g. Corrected and edited the manuscript in close interaction with Dr. Lukas Cyganek. **Manuscript submitted (under revision):** *LZTR1* polymerization provokes cardiac pathology in recessive Noonan syndrome; Alexandra V. Busley, MSc; Óscar Gutiérrez-Gutiérrez, PhD; Elke Hammer, PhD; Martin Steinegger, PhD; Linda Böhmer, BSc; Henning Schroeder, PhD; Mandy Kleinsorge, PhD; Janine Altmüller, MD; Felix Marbach, MD; Gerd Hasenfuss, MD; Wolfram-Hubertus Zimmermann, MD; Bernd Wollnik, MD; Lukas Cyganek, PhD, Preprint available in bioRxiv: <https://doi.org/10.1101/2023.01.10.523203>

5. Chapter 2

Individual contribution(s) to published article

Applicant (Name): Alexandra Viktoria Busley (first author)

Individual contribution:

1. Figures and Supplementary Figures (actively performed experiments and/or analyzed data)

Main Figures: 1 A, B, C, D, E, F, G, H, I, J, K, L, M. Figures were designed by Dr. Lukas Cyganek.

2. Written

Main Text: Abstract, experimental procedures, main figure legends, introduction and results.

3. Intellectual contribution

- a. Experimental design and performance in close interaction with Dr. Lukas Cyganek. Design of the repair template was performed by Dr. Lukas Cyganek.
- b. Phenotypical characterization of MRAS-edited iPSC clones.
- c. Wrote significant parts of the manuscript together with Dr. Lukas Cyganek.
- d. Corrected and edited the manuscript together with Dr. Lukas Cyganek.

Manuscript submitted: *Generation of a genetically-modified induced pluripotent stem cell line harboring a Noonan syndrome-associated gene variant MRAS p.G23V*; **Alexandra V. Busley** MSc, Lukas Cyganek PhD

6. Chapter 3

Individual contribution(s) to published article

Applicant (Name): Alexandra Viktoria Busley (first author)

Individual contribution:

1. Figures and Supplementary Figures (actively performed experiments and/or analyzed data)

Main Figures: 1 A, B, C, D, E, F, G, H, I, J, K. Figures were designed by Dr. Lukas Cyganek.

2. Written

Main Text: Abstract, experimental procedures, main figure legends, part of introduction, results, and discussion.

3. Intellectual contribution

- a. Experimental design and performance in close interaction with Dr. Lukas Cyganek. Design of the guide RNA targeting *KRAS* locus and the repair template was performed by Dr. Mandy Kleinsorge.
- b. Phenotypical characterization of *KRAS*-edited iPSC clones.
- c. Wrote significant parts of the manuscript together with Dr. Lukas Cyganek.
- d. Corrected and edited the manuscript together with Dr. Lukas Cyganek.

Manuscript submitted: Generation of a genetically-modified induced pluripotent stem cell line harboring an oncogenic *gene variant KRAS p.G12V*; **Alexandra Viktoria Busley** MSc, Mandy Kleinsorge PhD, Lukas Cyganek PhD

4 Chapter 1: LZTR1 polymerization provokes cardiac pathology in recessive Noonan syndrome

LZTR1 polymerization provokes cardiac pathology in recessive Noonan syndrome

Alexandra Viktoria Busley, MSc^{1,2,3}, Óscar Gutiérrez-Gutiérrez, PhD^{1,2}, Elke Hammer, PhD^{2,4}, Martin Steinegger, PhD⁵, Linda Böhmer, BSc¹, Henning Schroeder, PhD⁶, Mandy Kleinsorge, PhD^{1,2}, Janine Altmüller, MD^{7,8}, Felix Marbach, MD^{9,10}, Gerd Hasenfuss, MD^{1,2,3}, Wolfram-Hubertus Zimmermann, MD^{2,3,11}, Bernd Wollnik, MD^{2,3,12}, Lukas Cyganek, PhD^{1,2,3*}

¹Stem Cell Unit, Clinic for Cardiology and Pneumology, University Medical Center Göttingen, Göttingen, Germany; ²DZHK (German Center for Cardiovascular Research), partner site Göttingen and Greifswald, Germany; ³Cluster of Excellence "Multiscale Bioimaging: from Molecular Machines to Networks of Excitable Cells" (MBExC), University of Göttingen, Göttingen, Germany; ⁴Interfaculty Institute of Genetics and Functional Genomics, University Medicine Greifswald, Greifswald, Germany; ⁵School of Biological Sciences, Seoul National University, Seoul, South Korea; ⁶NMR Signal Enhancement Group, Max Planck Institute for Multidisciplinary Sciences, Göttingen, Germany; ⁷Cologne Center for Genomics, University of Cologne, Faculty of Medicine and University Hospital Cologne, Cologne, Germany; ⁸Genomics Platform, Berlin Institute for Medical Systems Biology, Max-Delbrück-Center for Molecular Medicine Berlin, Berlin, Germany; ⁹Institute of Human Genetics, University Hospital Cologne, Cologne, Germany; ¹⁰Institute of Human Genetics, Heidelberg University, Heidelberg, Germany; ¹¹Institute of Pharmacology and Toxicology, University Medical Center Göttingen, Göttingen, Germany; ¹²Institute of Human Genetics, University Medical Center Göttingen, Göttingen, Germany.

*Corresponding author: lukas.cyganek@gwdg.de

4.1 Abstract

Noonan syndrome patients harboring causative variants in *LZTR1* are particularly at risk to develop severe and early-onset hypertrophic cardiomyopathy. However, the underlying disease mechanisms of *LZTR1* missense variants driving the cardiac pathology are poorly understood. Hence, therapeutic options for Noonan syndrome patients are limited. In this study, we investigated the mechanistic consequences of a novel homozygous causative variant *LZTR1*^{L580P} by using patient-specific and CRISPR/Cas9-corrected iPSC-cardiomyocytes. Molecular, cellular, and functional phenotyping in combination with *in silico* prediction of protein complexes uncovered a unique *LZTR1*^{L580P}-specific disease mechanism provoking the cardiac hypertrophy. The homozygous variant was predicted to alter the binding affinity of the dimerization domains facilitating the formation of linear LZTR1 polymer chains. The altered polymerization resulted in dysfunction of the LZTR1-cullin 3 ubiquitin ligase complexes and subsequently, in accumulation of RAS GTPases, thereby provoking global pathological changes of the proteomic landscape ultimately leading to cellular hypertrophy. Importantly, uni- or biallelic genetic correction of the *LZTR1*^{L580P} missense variant rescued the molecular and cellular disease-associated phenotype, providing proof-of-concept for CRISPR-based gene therapies.

4.2 Introduction

Noonan syndrome (NS) is a multi-systemic developmental disorder with a broad spectrum of symptoms and varying degrees of disease severity. Common clinical symptoms range from intellectual disability, facial dysmorphisms, webbed neck, skeletal deformities, short stature, and in many cases congenital heart disease.¹⁰ With a prevalence of approximately 1 in 1,000 – 2,500 live births, NS is considered the most common monogenic disease associated with congenital heart defects and early-onset hypertrophic cardiomyopathy (HCM).² Young NS patients diagnosed with HCM are more prone to develop heart failure accompanied by a poor late survival in contrast to patients suffering from non-syndromic HCM.^{3,4} Like other phenotypically overlapping syndromes classified as RASopathies, NS is caused by variants in RAS-mitogen-activated protein kinase (MAPK)-associated genes, all typically leading to an increase in signalling transduction.⁸⁷ Within the RASopathy spectrum, patients harboring causative gene variants in *RAF1*, *HRAS*, *RIT1* and *LZTR1* are particularly at risk to develop severe and early-onset HCM.^{34,58}

Recent studies from others and our group revealed the functional role of *LZTR1* within the RAS/MAPK signalling cascade as a negative regulator of signalling activity. *LZTR1* encodes an adapter protein of the cullin 3 ubiquitin ligase complex by selectively targeting RAS proteins as substrates for degradation. *LZTR1* deficiency – caused by truncating or missense variants – results in an accumulation of the RAS protein pool and, as a consequence, in RAS/MAPK signalling hyperactivity.^{42,43,45} Whereas dominant *LZTR1* variants generally cluster in the Kelch motif perturbing RAS binding to the ubiquitination complex,⁴⁰ the mechanistic consequences of recessive *LZTR1* missense variants, which are distributed over the entire protein, are not understood.

Human induced pluripotent stem cell-derived cardiomyocytes (iPSC-CMs) generated from patients with inherited forms of cardiomyopathies offer a unique platform to study the disease mechanisms in physiologically relevant cells and tissues.^{54,88} A few RASopathy-linked iPSC-CM models had been described, including for variants in *PTPN11*, *RAF1*, *BRAF*, and *MRAS*.^{46,53,89,90} In line, we had recently added novel information as to the role of *LZTR1*-truncating variants in NS pathophysiology.⁴⁵ In the present study, we aimed to investigate the molecular, cellular, and functional consequences of a specific recessive missense variant *LZTR1*^{L580P} by utilizing patient-derived and CRISPR-corrected iPSC-CMs. We could show that *LZTR1*^{L580P} in homozygous state results in aberrant polymerization causing *LZTR1* dysfunction, marked increase of RAS GTPase levels, and cellular hypertrophy. Further, uni- and bi-allelic genetic correction of the missense variant by CRISPR/Cas9 technology rescued the cellular phenotype, indicating that correction of one allele is sufficient to restore the cardiac pathophysiology, thereby providing proof-of-concept for future personalized CRISPR-based gene therapies.

4.3 Results

LZTR1^{L580P} is causative for recessive Noonan syndrome

A 17-year old male patient presenting a HCM, stress-induced cardiac arrhythmias, pectus excavatum and facial anomalies was referred to our clinic and based on the combination of symptoms the clinical diagnosis of Noonan syndrome was given (Figure 6A). The patient was born to a consanguineous couple and both parents showed neither apparent clinical symptoms nor distinctive NS-specific features. Whole exome sequencing followed by detailed variant analysis detected one highly interesting, homozygous variant in *LZTR1*. Both parents were heterozygous carriers and the variant was not present in any current database of human genetic variations including the >250,000 alleles of gnomAD database. The homozygous missense variant, c.1739T>C, was located in exon 15 of the *LZTR1* gene and leads to the substitution of an evolutionary conserved leucine at the amino acid position 580 by proline (p. Leu580Pro, p.^{L580P}). The variant was predicted as likely causative by computational predictions.

To elucidate the molecular and functional consequences of the *LZTR1^{L580P}* missense variant, we generated iPSCs from the patient's skin fibroblasts using integration-free reprogramming methods and subsequently utilized CRISPR/Cas9 genome editing to engineer gene variant-corrected iPSC lines (Figure 6B). For genetic correction of the patient-specific iPSCs, the CRISPR guide RNA was designed to specifically target the mutated sequence in exon 15 of the *LZTR1* gene. Further, the ribonucleoprotein-based CRISPR/Cas9 complex was combined with a single-stranded oligonucleotide serving as template for homology-directed repair (Figure 6C). Upon transfection, cells were singularized and individual clones were screened for successful editing to identify heterozygously corrected as well as homozygously corrected iPSC clones, *LZTR1^{corr-het}* and *LZTR1^{corr-hom}*, respectively (Figure 6D). Molecular karyotyping of the edited iPSC clones confirmed chromosomal stability after genome editing and passaging (Figure 6E). As expected for individuals born to consanguineous parents, patient-specific as well as CRISPR-corrected iPSCs demonstrated a noticeable reduction of the overall heterozygosity using SNP-based genome-wide arrays, with around 30% of segments of the genome being assigned to regions of heterozygosity. Further, sequencing revealed no obvious off-target modifications by genome editing (Figure 12 in the supplement). Subsequently, patient-derived and CRISPR-corrected iPSCs were verified for pluripotency (Figure 6F-H). In addition to the patient-derived iPSC lines, iPSC lines from two unrelated healthy male donors, namely WT1 and WT11, were used as wild type (WT) controls in this study.

Homozygous LZTR1^{L580P} causes accumulation of RAS GTPases

At first, we aimed to investigate the impact of the identified homozygous *LZTR1^{L580P}* missense variant on the molecular mechanisms contributing to left ventricular hypertrophy in the patient. Patient-specific, heterozygously and homozygously corrected, as well as two individual WT iPSC lines were differentiated into functional ventricular-like iPSC-CMs in feeder-free culture conditions,⁴⁹ and on day 60 of differentiation subjected to unbiased proteome analyses (Figure 7A). We identified more than 4,700 proteins in the samples from the individual groups. All samples showed a comparably high abundance of prominent cardiac markers including myosin heavy chain β (*MHY7*), cardiac troponin T (*TNNT2*), α -actinin (*ACTN2*), titin (*TTN*), and ventricular-specific myosin light chain 2 (*MYL2*), indicating equal cardiomyocyte content in the different cultures (Figure 7B). By comparing the proteome profiles of *LZTR1^{L580P}* and WT iPSC-CMs, we identified enhanced abundance of the RAS isoforms muscle RAS oncogene homolog (MRAS) and RIT1 in the patient's iPSC-CMs (Figure 7C). This finding is in agreement with our previous observation in *LZTR1*-truncating variant carriers⁴⁵ and confirms the pivotal role of *LZTR1* in targeting various RAS isoforms for *LZTR1*-cullin 3 ubiquitin ligase complex-mediated ubiquitination, and degradation.^{42,43} Further, it highlights that *LZTR1^{L580P}* results in protein loss-of-function, causing an accumulation of RAS proteins in the cells, providing molecular evidence for the causative nature of the missense variant. Strikingly, protein levels of the different RAS isoforms were normalized in both the heterozygously as well as the homozygously corrected iPSC-CMs, confirming that only one functional *LZTR1* allele is sufficient to regulate the protein pool of RAS GTPases in cardiomyocytes (Figure 7D-E). As anticipated, transcriptome analyses showed similar mRNA expression levels of the different RAS isoforms in the patient's and CRISPR-corrected iPSC lines, indicating a post-translational cause for the higher abundance of RAS proteins in *LZTR1^{L580P}* cultures (Figure S2 in the supplement). In contrast, the significantly elevated protein levels of the protein quality control-associated heat shock-related 70 kDa protein 2 (*HSPA2*) in the patient's cells in comparison to the WT and CRISPR-corrected cells were related to upregulation of gene expression, suggesting that *HSPA2* is not directly targeted by *LZTR1* for degradation.

To assess the correlation of the different proteomic profiles with respect to the disease-specific proteome signatures upon *LZTR1* deficiency, we performed a comparison analysis of the data sets from (1) *LZTR1^{L580P}* versus WT, (2) *LZTR1^{corr-het}* versus *LZTR1^{L580P}*, and (3) *LZTR1^{corr-hom}* versus *LZTR1^{L580P}*. We found 78 proteins being differentially regulated in all three data sets (Figure 7F). Here, a profound subset of proteins of the overlapping profile that was significantly higher abundant in the patient's cells, such as the MAPK-activated protein kinase RPS6KA3, was normalized after heterozygous and homozygous CRISPR-correction of the pathological *LZTR1* variant. Vice versa, numerous downregulated proteins in the patient samples were found to be elevated in the gene-edited iPSC-

CMs. Further, we performed a Reactome pathway enrichment analysis to uncover dysregulated pathways and/or biological processes associated to *LZTR1*^{L580P}. The analysis indicated that differentially abundant proteins in patient-derived samples were enriched in critical cardiac-related biological processes, such as muscle contraction and extracellular matrix organization, as well as in cellular routes associated to metabolism (Figure 7G).

In agreement with the proteomic data, Western blot analysis confirmed the strong accumulation of MRAS, RIT1, and the classical RAS isoforms (HRAS, KRAS, and NRAS; detected by pan-RAS) in the *LZTR1*^{L580P} cultures, and further confirmed a normalization of RAS levels in the CRISPR-corrected isogenic iPSC-CMs to WT control levels (Figure 7H-K).

Collectively, these data demonstrate that the missense variant *LZTR1*^{L580P} in homozygosity resulted in protein loss-of-function causing an accumulation of RAS GTPases as the critical underlying disease mechanism in cardiomyocytes from the NS patient. In line, correction of the homozygous missense variant on at least one allele normalized the molecular pathology.

Homozygous LZTR1^{L580P} provokes cardiomyocyte hypertrophy

To elucidate the consequences of dysregulated RAS/MAPK signalling on the cellular characteristics of cardiomyocytes, we investigated the sarcomere homogeneity, the overall myofibril organization, and the cell size of the patient-derived iPSC-CMs, the CRISPR-corrected cells, as well as the WT controls at day 60 of differentiation (Figure 8A). Immunocytochemical staining of cardiac subtype-specific proteins revealed that all iPSC lines exhibit a well-organized sarcomeric organization with a pronounced striated expression of α -actinin and ventricular-specific MLC2V (Figure 8B). In order to analyze the homogeneity of sarcomeres in detail, we measured the distances between the sarcomeric Z-disks along individual myofibrils (Figure 8C). In agreement with the sarcomere length previously observed in neonatal and adult human hearts,⁹¹ *LZTR1*-deficient as well as corrected and WT cells revealed a typical sarcomere length ranging from 1.7 to 2.2 μm with an average of approximately 1.9 μm across all iPSC lines (Figure 8D). As sarcomeric disarray has been frequently reported in other iPSC-CM models of both NS-associated and non-syndromic HCM,^{46,92} we examined the myofibril organization in the individual iPSC-CMs stained for α -actinin by Fast Fourier Transform. The quantitative analysis did neither reveal any decrease of sarcomere regularity nor any pathological myofibril organization in *LZTR1*^{L580P} cultures (Figure 8E). On the contrary, *LZTR1*^{L580P} and CRISPR-corrected iPSC-CMs even demonstrated a slightly higher myofibril regularity compared to unrelated controls, indicating that the pathological gene variant has no severe impact on sarcomere structures.

As cardiomyocyte hypertrophy is a major hallmark of HCM, we further investigated the medium cell size of iPSC-CMs from all cell lines by utilizing our previously established assay to determine the cell size of iPSC-CMs in suspension.⁴⁵ Here, the patient's iPSC-CMs displayed a significant cellular enlargement compared to WT iPSC-CMs (Figure 8F). Strikingly, the hypertrophic phenotype was normalized in the CRISPR-corrected cells from both the *LZTR1*^{corr-het} and the *LZTR1*^{corr-hom} isogenic cultures. Moreover, and in line with the molecular observations, heterozygous correction of the pathological variant was sufficient to significantly reduce cellular hypertrophy.

In summary, the patient's iPSC-CMs harboring the homozygous missense variant *LZTR1*^{L580P} recapitulated the cardiomyocyte hypertrophy *in vitro*. Importantly, CRISPR-correction of the pathological variant was able to normalize the hypertrophic phenotype.

Homozygous LZTR1^{L580P} does not compromise contractile function

NS-associated HCM as well as inherited forms of non-syndromic HCM are frequently associated with contractile dysfunction and these patients are at risk for developing arrhythmias.^{93,94} Hence, we generated engineered heart muscles (EHMs) from diseased, CRISPR-corrected, and WT iPSC-CMs enabling us to investigate the functional characteristics in a three-dimensional environment closer resembling the native conditions of the human heart muscle (Figure 9A).^{51,95} Microscopically, all iPSC lines formed homogenous cardiac tissues without showing apparent cell line-dependent differences after six weeks of cultivation and maturation (Figure 9B). Optical measurements were performed to study beating rate, force of contraction, and contraction kinetics in spontaneously contracting EHMs (Figure 9C). In comparison to WT EHMs, a slightly increased spontaneous beat frequency was detected in the *LZTR1*^{L580P} EHMs (Figure 9D). Interestingly, all tissues reflected a robust beat rhythm and a very low beat-to-beat variability over the entire recording time, indicating that the diseased tissues do not provoke development of arrhythmic events (Figure 9E). Furthermore, no significant differences in force of contraction were identified (Figure 9F). In accordance with higher beat frequencies, significantly shorter contraction times, and relaxation times were observed in *LZTR1*^{L580P}-, *LZTR1*^{corr-het}- and the *LZTR1*^{corr-hom}-derived EHMs (Figure 9G,H). However, since the altered kinetics were noticed in both diseased and CRISPR-corrected tissues, this rather suggested a mutation-independent effect.

Taken together, this functional data indicates that the missense variant *LZTR1*^{L580P} does not significantly impact the contractile function and rhythmogenesis of cardiomyocytes.

Homozygous LZTR1^{L580P} induces polymerization of LZTR1-cullin 3 ubiquitin ligase complexes

Considering the severe consequence of *LZTR1^{L580P}* on the molecular and cellular pathophysiology in cardiomyocytes, we aimed to determine the specific effect of this variant on protein structure, complex formation, as well as its subcellular localization. We were not able to visualize endogenous LZTR1 in our cell model, neither by testing of multiple commercial antibodies nor by n-terminal or c-terminal genetic tagging of the *LZTR1* gene locus. In order to circumvent these obstacles, we established ectopic expression of tagged *LZTR1* in WT iPSC-CMs at around day 60 of differentiation by lipofectamine-based plasmid transfection (Figure 10A). Besides *LZTR1^{WT}* and *LZTR1^{L580P}*, we screened the NS patient database⁹⁶ for additional missense variants classified as likely pathogenic or variant of uncertain significance and located in close proximity to *LZTR1^{L580P}* (within the BACK1 domain), and included these in our screening panel (Figure 10B). Of note, except for *LZTR1^{L580P}* and *LZTR1^{E563Q}*,³⁴ none of the other variants had been reported to be present in homozygosity in *LZTR1*-associated NS. In addition, we also included a truncating variant *LZTR1^{ΔBTB2-BACK2}*, lacking the entire BTB2-BACK2 domain, that mimicked the genotype of the two siblings described in our previous study.⁴⁵

As previously observed in other cell types (such as HeLa⁴² and HEK293³⁹), *LZTR1^{WT}* presented as dotted pattern equally distributed throughout the cell (Figure 10C, Figure 14A in the supplement). A similar dotted appearance was observed for the variants *LZTR1^{E563Q}*, *LZTR1^{I570T}*, *LZTR1^{V579M}*, *LZTR1^{E584K}*, and *LZTR1^{R619H}*. As expected, the truncating variant *LZTR1^{ΔBTB2-BACK2}* showed a mislocalized homogeneous cytoplasmic distribution. Surprisingly, missense variant *LZTR1^{L580P}* formed large filaments within the cytoplasm (Figure 10C, Figure 14A in the supplement). To verify this initial finding, we co-expressed two differentially tagged *LZTR1* constructs and evaluated their overlap within the cells. In accordance, *LZTR1^{L580P}* appeared as large protein polymers, whereas *LZTR1^{WT}* remained speckle-like (Figure 10D). As *LZTR1^{L580P}* in heterozygous state did not induce a disease phenotype based on our clinical and our experimental evidence, we hypothesized that co-expression of *LZTR1^{L580P}* and *LZTR1^{WT}* might resolve the polymer chains. Strikingly, the *LZTR1^{L580P}*-induced filaments dispersed when co-expressed with the WT variant, implicating that the LZTR1 complexes exclusively assembled to large protein polymers when the specific *LZTR1^{L580P}* missense variant is present on both alleles (Figure 10E). To quantitatively analyze these observations, we established an automated image-based speckle/filament recognition and computation (Figure 14B in the supplement). Whereas *LZTR1^{WT}* displayed a mean speckle size of 0.9 μm, the mean filament length per cell in *LZTR1^{L580P}* amounted to 7.9 μm (Figure 10F). In line, co-expression of mutant and WT constructs, and vice versa, normalized the speckle size to 1.2 μm and 1.3 μm, respectively.

Next, we asked whether LZTR1 polymerization might potentially interfere with proper targeting of degradation substrate MRAS or binding of ubiquitin ligase cullin 3. Thus, we evaluated co-localization of WT and mutant *LZTR1* with MRAS and cullin 3 in WT iPSC-CMs after co-transfection (Figure 10G). Whereas, MRAS and cullin 3 displayed a homogeneous cytoplasmic distribution when expressed alone, both *LZTR1*^{WT} and *LZTR1*^{L580P} led to recruitment of MRAS and cullin 3 to the speckles and protein polymers, respectively (Figure 10H,I).

In summary, our data provides evidence that the missense variant *LZTR1*^{L580P} induces a unique polymerization of the LZTR1-cullin 3 ubiquitin ligase complexes. Furthermore, although binding of cullin 3 and degradation targets is not severely impaired by the mutation, it indicates that polymerization compromises the proper function of the LZTR1 ubiquitination complexes.

Homozygous LZTR1^{L580P} alters binding affinities of dimerization domains

Based on previous studies, proteins from the BTB-BACK-Kelch domain family including LZTR1 are predicted to assemble in homo-dimers.^{39,43,97} However, our current knowledge regarding the exact domains responsible for LZTR1 dimerization is limited. In order to identify a plausible explanation for the *LZTR1*^{L580P}-induced polymerization, we utilized ColabFold – an AlphaFold-based platform for the prediction of protein structures and homo- and heteromer complexes.⁹⁸ We used a homo-trimer configuration of the experimentally employed *LZTR1* variants (all within the BACK1 domain) and AlphaFold-multimer predicted five high-quality models each with an average predicted local distance difference test (a per-residue confidence metric) between 64.1 and 76.0. For all variants, we inspected the interaction between the chains through the predicted alignment error (PAE) generated by AlphaFold-multimer (Figure 15 in the supplement). Here, a low PAE indicates that the relative position and orientation of the positions x and y was correctly predicted – a measure indicating if interfacing residues were correctly predicted across chains. Based on these predictions, we compared the top-ranked models of each variant according to the predicted template modeling score, which corresponded to overall topological accuracy (Figure 11A). The top-ranked model for *LZTR1*^{WT} showed interaction as a homo-dimer via the BACK2-BACK2 domain, whereas the third LZTR1 protein remained monomeric (Figure 11A,B). We also observed the identical dimerization via the BACK2 domains for all other variants, except for *LZTR1*^{L580P}. In contrast, the top-ranked model for *LZTR1*^{L580P} predicted an interaction between all three chains, on the one hand via the BACK2-BACK2 domain and on the other hand via the BACK1-BACK1 domain (Figure 11A,B). Collectively, these *in silico* predictions suggest that LZTR1 typically forms homo-dimers via the BACK2 domains, and that the missense variant *LZTR1*^{L580P} alters the binding affinities of the BACK1 domain enabling formation of linear LZTR1 polymer chains

via both dimerization domains, thereby providing a rationale for the molecular and cellular impairments in NS (Figure 11C).

4.4 Discussion

Both autosomal dominant and autosomal recessive forms of *LZTR1*-associated NS have been described presenting with a broad clinical spectrum and various phenotypic expression of symptoms. However, the mechanistic consequences of numerous of these mutations, mostly classified as variants of uncertain significance, are still under debate. In previous studies, we and others elucidated the role of *LZTR1* as a critical negative regulator of the RAS/MAPK pathway by controlling the pool of RAS GTPases.^{39,42–45} By using patient-derived iPSC-CMs from NS patients with biallelic truncating *LZTR1* variants, we could show that *LZTR1* deficiency results in accumulation of RAS levels, signalling hyperactivity, and cardiomyocyte hypertrophy.⁴⁵ Further, by genetically correcting one of the two affected alleles, we could show that one functional *LZTR1* allele is sufficient to maintain normal RAS/MAPK activity in cardiac cells. In contrast to the truncating variants, dominant *LZTR1* missense variants generally cluster in the Kelch motif. Based on heterologous expression systems, these dominant variants are considered to perturb recognition or binding of RAS substrates to the *LZTR1* ubiquitination complex.^{40,42–44} Much less is known about the functional relevance of recessive *LZTR1* missense variants, which are distributed over the entire protein. Detailed insights in the underlying molecular and functional mechanisms of selective variants causing the severe cardiac phenotype in NS enable to gain insights into specific structure-function relations of *LZTR1* and are crucial to facilitate the development of patient-specific therapies.

In this study, we diagnosed a patient with NS, who presented typical clinical features of NS including an early-onset HCM and confirmed this diagnosis on genetic level by the identification of the homozygous, causative variant c.1739T>C/p.L580P in *LZTR1* by whole exome sequencing. The variant is novel and was not described before in patients with NS and we classified *LZTR1*^{L580P} as likely causative based on its absence in gnomAD and our computational prediction. Besides this *LZTR1* variant, no additional variants were detected in other NS-associated genes or novel RAS-associated candidate genes. By combining *in vitro* disease modeling using patient-specific and CRISPR/Cas9-corrected iPSC-CMs, with molecular and cellular phenotyping, as well as *in silico* structural modeling, we uncovered a unique *LZTR1*^{L580P}-specific disease mechanism provoking the cardiac pathology of NS. In detail, we found that a) *LZTR1*^{L580P} is predicted to alter the binding affinity of the BACK1 dimerization domain facilitating the formation of linear *LZTR1* protein chains; b) homozygous *LZTR1*^{L580P} fosters the assembly of large polymers of *LZTR1*-cullin 3 ubiquitin ligase complexes; c) pathological polymerization results in *LZTR1* complex dysfunction, accumulation of RAS GTPases and RAS/MAPK signalling hyperactivity;

and d) increased signalling activity induces global changes of the proteomic landscape ultimately causing cellular hypertrophy. Importantly, correction of one allele – in line with co-expression of WT and mutant *LZTR1* transcripts – is sufficient to normalize the cardiac disease phenotype both on molecular and cellular level.

Based on recent publications, there is a broad consensus about the role of LZTR1 as an adaptor protein for the cullin 3 ubiquitin ligase complex targeting RAS proteins for ubiquitination and subsequent protein degradation.^{39,40,42–45} In line with observations in other NS-associated genes and mutations, LZTR1 dysfunction and concomitant accumulation of RAS GTPases results in hyperactivation of RAS/MAPK signalling. However, it remains controversial, whether LZTR1 is able to recognize all members of the RAS GTPase family for degradation or whether there is a selective affinity towards particular isoforms. By using heterologous expression systems, LZTR1 interaction with the main highly conserved RAS isoforms HRAS, KRAS and NRAS was observed.^{39,42,44} On the contrary, Castel and colleagues observed a selective binding of LZTR1 with RIT1 and MRAS, but not with HRAS, KRAS or NRAS.⁴³ Moreover, in homozygous *Lztr1* knockout mice elevated RIT1 protein levels were detected across different organs including brain, liver, and heart, whereas HRAS, KRAS, and NRAS levels (recognized by pan-RAS) remained unchanged.⁹⁹ By using global proteomics, we now provide further evidence that LZTR1 dysfunction in cardiomyocytes in particular causes severe accumulation of MRAS and RIT1 and, to a lower extent, upregulation of the other isoforms HRAS, KRAS and NRAS, although all isoforms are robustly expressed in this cell type. We conclude that based on gene expression data and overall protein levels, MRAS seems to be the most prominent RAS candidate in cardiomyocytes driving the signalling hyperactivity in these cells. These observations suggest that under endogenous expression levels, LZTR1 possesses a certain selectivity towards MRAS and RIT1, and a lower affinity to the main isoforms HRAS, KRAS and NRAS. However, we cannot exclude that there might be potential cell type-specific differences in LZTR1-RAS binding affinities.

Besides accumulation of RAS members, HSPA2 was strongly upregulated in *LZTR1*-deficient iPSC-CMs both on transcriptional as well as on protein level, suggesting that HSPA2 is not a direct substrate of LZTR1. In line, severely increased HSPA2 levels had been observed by us in NS iPSC-CMs with *LZTR1*-truncating variants,⁴⁵ in a *RAF1*-related NS iPSC-CM model,⁴⁶ as well as in iPSC-CMs from Fabry disease patients, a lysosomal storage disorder associated with cardiac involvement such as HCM and arrhythmias.¹⁰⁰ Moreover, a significant cardiomyocyte-specific elevation of HSPA2 was also observed in HCM tissue from patients.^{101,102} A heat shock protein 70-based therapy has been shown to reverse lysosomal pathology,¹⁰³ whereas deletion of these gene members was assumed to induce cardiac dysfunction and development of cardiac hypertrophy.¹⁰⁴ As a member of the large group of chaperones, HSPA2 is known to have a dual function in cells: to mediate disaggregation and refolding

of misfolded proteins as well as to assist in protein degradation via the ubiquitin-proteasome system or the lysosome-mediated autophagy.^{105,106} This suggests that HSPA2 upregulation might be a cardio-protective adaptive response of the hypertrophic cardiomyocytes to cope with *LZTR1*^{L580P}-induced RAS accumulation (and potentially also with *LZTR1* polymerization), by regulating the quality control mechanisms for protein degradation.

Major hallmarks of pathological cardiac hypertrophy include impaired cardiac function, changes in extracellular matrix composition, and fibrosis, as well as metabolic reprogramming and mitochondrial dysfunction.¹⁰⁷ In accordance, the proteomic disease signature of patient-derived iPSC-CM cultures revealed impairments in muscle contraction, extracellular matrix organization, and metabolism, all crucial for proper cardiomyocyte function. Furthermore, *LZTR1*^{L580P}-derived iPSC-CMs recapitulated the patient's hypertrophic phenotype reflected by cellular enlargement. Strikingly, both the molecular profile as well as cellular hypertrophy were resolved upon CRISPR-correction of the missense variant. Interestingly, no myofibrillar disarray was observed in our cell model. However, the presence of myofibril disarray in NS remains controversial: whereas structural defects were described in *RAF1*-associated iPSC models,^{46,108} we and others did not observe any impact on sarcomere structures or myofibril organization in *LZTR1*-related, *PTPN11*-related, and *BRAF*-related iPSC-CMs,^{45,89,90} implying potential genotype-dependent differences in the manifestation of myofibril disassembly in NS.

Missense variants in *LZTR1* located within the Kelch domain are predicted to affect substrate recognition, whereas missense variants in the BTB-BACK domain are assumed to impair either binding of cullin 3, proper homo-dimerization, or correct subcellular localization. Several studies could provide proof that dominantly acting Kelch domain variants perturb recognition of RAS substrates, but do not affect *LZTR1* complex stability or subcellular localization.^{40,42-44,109} Vice versa, BTB-BACK missense variants showed no influence on RIT1 binding.^{43,109} However, variants located in the BTB1 or the BTB2 domain, such as *LZTR1*^{V456G}, *LZTR1*^{R466Q}, *LZTR1*^{P520L}, and *LZTR1*^{R688C}, caused a subcellular mislocalization from defined speckles to a diffuse cytoplasmic distribution, similar to the findings obtained from truncating *LZTR1* variants.^{42,44} In addition to these distinct pathological consequences from different variants analyzed so far, we now provide evidence for an alternative disease mechanism unique to BACK1 domain-located *LZTR1*^{L580P}: ectopic expression of *LZTR1*^{L580P} in iPSC-CMs caused a pathological polymerization of *LZTR1* ubiquitination complexes. Moreover, it triggered a re-localization of MRAS and cullin 3 to the polymer chains, hence, binding probabilities to substrates and interaction partners were not significantly affected by the mutation. This remarkable phenotype was not observed for any other variant within the BACK1 domain. Notably, ectopic co-expression of *LZTR1*^{L580P} and *LZTR1*^{WT} alleviated the polymerization, indicating that the assembly of *LZTR1* polymer chains exclusively occurs if the mutated proteins are present at homozygous state. Strikingly, an oligomerization of another BTB-

BACK family member had been reported previously: Marzahn and colleagues revealed that dimers from the cullin 3 ubiquitin ligase substrate adaptor SPOP (harboring only one BTB-BACK domain) self-associate into linear higher-order oligomers via BACK domain dimerization.¹¹⁰ These SPOP oligomers assembled in membrane-less cellular bodies, visualized as nuclear speckles, and it was proposed that the speckles might be important hotspots of ubiquitination. Based on these findings and our data, we propose that LZTR1 complexes concentrate in cellular speckles (either as dimers or as oligomers) to form subcellular clusters for efficient ubiquitination and degradation of RAS proteins. However, *LZTR1*^{L580P}-induced polymerization of these complexes compromises regular function, leading to accumulation of substrates.

Our knowledge about the particular domains responsible for LZTR1 homo-dimerization is still incomplete. Whereas Castel and colleagues proposed that the BTB1 and the BACK1 domain are required for dimerization,⁴³ Steklov et al. observed impaired assembly in a BACK2 domain mutated *LZTR1* variant.⁴⁴ Based on *in silico* modeling, we now propose that LZTR1 can dimerize either via the BACK2-BACK2 domains or via the BACK1-BACK1 domains. Although in *LZTR1*^{WT} the BACK2-BACK2 dimerization might be primarily utilized, changes in binding affinities of the BACK1 domain as a consequence of *LZTR1*^{L580P} facilitated tandem self-association of dimers to linear multimers. Strikingly, the *in silico* models for complex assembly of the different variants were consistent with the experimental data. However, this analysis must be taken with caution as the PAE signal across chains is overall weak and AlphaFold-multimer was not trained with single point variants in mind. Of note, dimer + monomer as well as trimer interactions (in diverse combinations, such as via BACK2-BACK2 and BACK1-BACK1 or via BACK2-BACK2-BACK2) had also been predicted for the other BACK1 variants as well as for WT in the lower-ranked models (Figure S4 in the supplement). As a next step, it would be interesting to see, if the trend stays consistent for complexes with more chains. However, due to technical prerequisites, we were currently not able to predict more than three chains.

So far, the relevance of certain *LZTR1* missense variants on the molecular and cellular processes had been investigated in heterologous expression systems, failing to faithfully represent human cardiac physiology. Our study demonstrates the potential of patient-specific iPSCs to model human diseases and to uncover variant-specific pathomechanisms, which might facilitate the development for early and more precise therapies. Despite the great advantages of this model system over other cellular models, iPSC-CMs possess certain limitations. As summarized by several reports, iPSC-CMs are considered to be developmentally immature characterized by molecular and functional properties similar to fetal CMs.^{51,111,112} Although we complemented our study by utilizing three-dimensional EHM, these *in vitro* models are currently not able to entirely resemble the disease phenotype at organ level. Nevertheless, our investigations at single cell and tissue level proved to be a valuable platform

for uncovering disease-relevant signalling pathways, identifying novel therapeutic targets and studying the disease progression during cardiogenesis.

Taken together, this study uncovered a novel mechanism causing recessive NS, which is initiated by *LZTR1*^{L580P}-driven polymerization of LZTR1 ubiquitination complexes, provoking molecular and cellular impairments associated with cardiac hypertrophy. Moreover, CRISPR-correction of the missense variant on one allele was sufficient to rescue the phenotype, thereby providing proof-of-concept for a sustainable therapeutic approach.

4.5 Materials and methods

Ethical approval

The study was approved by the Ethics Committee of the University Medical Center Göttingen (approval number: 10/9/15) and carried out in accordance with the approved guidelines. Written informed consent was obtained from all participants or their legal representatives prior to the participation in the study.

Whole exome sequencing

Whole exome sequencing on genomic DNA of the patient was performed using the SureSelect Human All Exon V6 kit (Agilent) on an Illumina HiSeq 4000 sequencer. The “Varbank 2.0” pipeline of the Cologne Center for Genomics (CCG) was used to analyze and interpret the exome data, as previously described.⁴⁵ Co-segregation analysis was performed in the family. Computational predictions for the pathogenicity of the variant were performed using MutationTaster (<https://www.mutationtaster.org/>), SIFT (<https://sift.bii.a-star.edu.sg/>), and PolyPhen-2 (<http://genetics.bwh.harvard.edu/pph2/>).

Generation and culture of human iPSCs

Human iPSC lines from two healthy donors, from an NS patient with a pathological missense variant in *LZTR1* (NM_006767.4: c.1739T>C/p.^{L580P}; ClinVar: RCV000677201.1), as well as heterozygous and homozygous CRISPR/Cas9-corrected iPSC lines were used in this study. Wild type iPSC lines UMGi014-C clone 14 (isWT1.14, here abbreviated as WT1) and UMGi130-A clone 8 (isWT11.8, here abbreviated as WT11) were generated from dermal fibroblasts and peripheral blood mononuclear cells from two male donors, respectively, using the integration-free Sendai virus and described previously.^{113,114} Patient-specific iPSC line UMGi137-A clone 2 (isNoonSf1.2, here abbreviated as *LZTR1*^{L580P}) was

generated from patient's dermal fibroblasts using the integration-free Sendai virus according manufacturer's instructions with modifications, as previously described.⁴⁵ Genetic correction of the pathological gene variant in the patient-derived iPSC line UMGi137-A clone 2 was performed using ribonucleoprotein-based CRISPR/Cas9 using crRNA/tracrRNA and Hifi SpCas9 (IDT DNA technologies) by targeting exon 15 of the *LZTR1* gene, as previously described.⁴⁵ The guide RNA target sequence was (PAM in bold): 5'-GCGGCACTCTCGCACACAAC **CGG**-3'. For homology-directed repair, a single-stranded oligonucleotide with 45-bp homology arms was used. After automated clonal singularization using the single cell dispenser CellenOne (Cellenion/Scienion) in StemFlex medium (Thermo Fisher Scientific), successful genome editing was identified by Sanger sequencing and the CRISPR-corrected isogenic iPSC lines UMGi137-A-1 clone D8 (isNoonSf1-corr.D8, here abbreviated as ^{L580P}corr-het) and UMGi137-A-1 clone D1 (isNoonSf1-corr.D1, here abbreviated as ^{L580P}corr-hom) were established. Newly generated iPSC lines were maintained on Matrigel-coated (growth factor reduced, BD Biosciences) plates, passaged every 4-6 days with Versene solution (Thermo Fisher Scientific) and cultured in StemMACS iPS-Brew XF medium (Miltenyi Biotec) supplemented with 2 μ M Thiazovivin (Merck Millipore) on the first day after passaging with daily medium change for at least ten passages before being used for molecular karyotyping, pluripotency characterization, and differentiation experiments. Pluripotency analysis via immunocytochemistry and flow cytometry was performed, as previously described.⁴⁵ For molecular karyotyping, genomic DNA of iPSC clones was sent for genome-wide analysis via Illumina BeadArray (Life&Brain, Germany). Digital karyotypes were analyzed in GenomeStudio v2.0 software (Illumina). For off-target screening, the top five predicted off-target regions for the respective guide RNA ranked by the CFD off-target score using CRISPOR¹¹⁵ were analyzed by Sanger sequencing. Human iPSCs and iPSC-derivatives were cultured in feeder-free and serum-free culture conditions in a humidified incubator at 37°C and 5% CO₂. All antibodies used for immunofluorescence and flow cytometry are listed in Table S1 in the supplement.

Cardiomyocyte differentiation of iPSCs and generation of engineered heart muscle

Human iPSC lines were differentiated into ventricular iPSC-CMs via WNT signalling modulation and subsequent metabolic selection, as previously described,⁴⁹ and cultivated in feeder-free and serum-free culture conditions until day 60 post-differentiation before being used for molecular and cellular experiments. Defined, serum-free EHMs were generated from iPSC-CMs around day 30 of differentiation and human foreskin fibroblasts (ATCC) at a 70:30 ratio according to previously published protocols.⁹⁵ Optical analysis of contractility and rhythm of spontaneously beating EHMs in a 48 well plate was performed between day 34 and day 42 of culture using a custom-built setup with a

high-speed camera by recording the movement of the two UV light-absorbing flexible poles. Contractility parameters of EHM recordings of at least 1 min recording time were analyzed via a custom-build script in MatLab (MathWorks). For each iPSC line, three individual differentiations were used for EHM casting.

Proteomics and Western blot analysis of iPSC-CMs

For proteomic analysis, iPSC-CMs were pelleted at day 60 of differentiation by scratching in RIPA buffer (Thermo Fisher Scientific) containing phosphatase and protease inhibitor (Thermo Fisher Scientific) and snap-frozen in liquid nitrogen. Cell pellets were reconstituted in 8 M urea/ 2 M thiourea solution (Sigma-Aldrich) and lysed by five freeze-thaw cycles at 30°C and 1.600 rpm. Protein containing supernatant was collected by centrifugation. Nucleic acid was degraded enzymatically with 0.125 U/μg benzonase (Sigma-Aldrich), and protein concentration was determined by Bradford assay (Bio-Rad). Five μg protein was processed for LC-MS/MS analysis, as previously described.¹¹⁶ Briefly, protein was reduced (2.5 mM dithiothreitol, Sigma-Aldrich; 30 min at 37°C) and alkylated (10 mM iodacetamide, Sigma-Aldrich; 15 min at 37°C) before proteolytic digestion with LysC (enzyme to protein ratio 1:100, Promega) for 3 h and with trypsin (1:25, Promega) for 16 h both at 37°C. The reaction was stopped with 1% acetic acid (Sigma-Aldrich), and the peptide mixtures were desalted on C-18 reverse phase material (ZipTip μ-C18, Millipore). Eluted peptides were concentrated by evaporation under vacuum and subsequently resolved in 0.1% acetic acid / 2% acetonitrile containing HRM/iRT peptides (Biognosys) according to manufacturer's recommendation. LC-MS/MS analysis was performed in data-independent acquisition (DIA) mode using an Ultimate 3000 UPLC system coupled to an Exploris 480 mass spectrometer (Thermo Scientific). Peptides were separated on a 25 cm Accucore column (75 μm inner diameter, 2.6 μm, 150 Å, C18) at a flow rate of 300 nl/min in a linear gradient for 60 min. Spectronaut software (Biognosys) was used for the analysis of mass spectrometric raw data. For peptide and protein identification, the Direct DIA approach based on UniProt database limited to human entries was applied. Carbamidomethylation at cysteine was set as static modification, oxidation at methionine and protein N-terminal acetylation were defined as variable modifications, and up to two missed cleavages were allowed. Ion values were parsed when at least 20% of the samples contained high quality measured values. Peptides were assigned to protein groups and protein inference was resolved by the automatic workflow implemented in Spectronaut. Statistical data analysis was conducted using an in-house developed R tool and based on median-normalized ion peak area intensities. Methionine oxidized peptides were removed before quantification. Differential abundant proteins (p -value ≤ 0.05) were identified by the algorithm ROPECA¹¹⁷ and application of the reproducibility-optimized peptide change averaging approach¹¹⁸ applied on peptide level. Only proteins quantified by at least two peptides were considered for further analysis. Reactome pathway

enrichment analysis was performed using the ClueGo plugin in Cytoscape. For each iPSC line, at least three individual differentiations were analyzed. For Western blot analysis, protein containing supernatant was collected by centrifugation. Protein concentration was determined by BCA assay (Thermo Fisher Scientific). Samples were denatured at 95°C for 5 min. 15 µg protein were loaded onto a 4-15% Mini-PROTEAN TGX Stain-Free precast gel (Bio-Rad). The protein was separated by sodium dodecyl sulfate-polyacrylamide gel electrophoresis (SDS-PAGE) by applying 200 V for 30 min. Post-running, TGX gels were activated via UV light application using the Trans-Blot Turbo transfer system (Bio-Rad). While blotting, proteins were transferred to a nitrocellulose membrane (25 V constant, 1.3 A for 7 min). Total protein amount was detected via the ChemiDoc XRS+ (Bio-Rad) system and used for protein normalization. After 1 h in blocking solution (5% milk in TBS-T, Sigma-Aldrich), membranes were incubated in primary antibody solution (1% milk in TBS-T) overnight. Membrane was washed three times with TBS-T before applying the secondary antibody (1:10,000 in 1% milk in TBS-T) at RT for 1 h. After washing, signals were detected upon application of SuperSignal West Femto Maximum Sensitivity Substrate (Thermo Fisher Scientific). Image acquisition was performed with the ChemiDoc XRS+ (Bio-Rad) at the high-resolution mode. For protein quantification, ImageLab (Bio-Rad) was used and protein levels were first normalized to total protein and second to the corresponding WT samples on each blot. For each iPSC line, 8 individual differentiations were analyzed. All antibodies used for Western blot are listed in Table S1 in the supplement.

Real-time PCR analysis of iPSC-CMs

Pellets of iPSC-CMs at day 60 of differentiation were snap-frozen in liquid nitrogen and stored at -80°C. Total RNA was isolated using the NucleoSpin RNA Mini kit (Macherey-Nagel) according to manufacturer's instructions. 200 ng RNA was used for the first-strand cDNA synthesis by using the MULV Reverse Transcriptase and Oligo d(T)16 (Thermo Fisher Scientific). For real-time PCR, cDNA was diluted 1:1 with nuclease-free water (Promega). Quantitative real-time PCR reactions were carried out using the SYBR Green PCR master mix and ROX Passive Reference Dye (Bio-Rad) with Micro-Amp Optical 384-well plates, and the 7900HT fast real-time PCR system (Applied Biosystems) according to the manufacturer's instructions with the following parameters: 95°C for 10 min, followed by 40 cycles at 95°C for 15 s and 60°C for 1 min. Analysis was conducted using the $\Delta\Delta\text{CT}$ method and values were normalized to *GAPDH* gene expression and to WT controls. Primer sequences are listed in Table S2 in the supplement.

Analysis of sarcomere length and myofibril organization of iPSC-CMs

To analyze the sarcomere length and myofibril organization, iPSC-CMs were cultured on Matrigel-coated coverslips and fixed at day 60 of differentiation in 4% Roti-Histofix (Carl Roth) at RT for 10 min and blocked with 1% Bovine Serum Albumin (BSA; Sigma-Aldrich) in PBS (Thermo Fisher Scientific) overnight at 4°C. Primary antibodies were applied in 1% BSA and 0.1% Triton-X100 (Carl Roth) in PBS at 37°C for 1 h or at 4°C overnight. Secondary antibodies with minimal cross reactivity were administered in 1% BSA in PBS (Thermo Fisher Scientific) at RT for 1 h. Nuclei were stained with 8.1 µM Hoechst 33342 (Thermo Fisher Scientific) at RT for 10 min. Samples were mounted in Fluoromount-G (Thermo Fisher Scientific). Images were collected using the Axio Imager M2 microscopy system (Carl Zeiss) and Zen 2.3 software. For analysis of the sarcomere length, images with α -actinin staining of iPSC-CMs were evaluated using the SarcOptiM plugin in ImageJ (National Institutes of Health).¹¹⁹ Here, three independent lines along different myofibrils within one cell were selected to calculate the mean sarcomere length per cell. For each iPSC line, three individual differentiations with 9-13 images per differentiation and two cells per image were analyzed. To analyze the myofibril organization, images with α -actinin staining of iPSC-CMs were processed using the Tubeness and Fast Fourier Transform plugins in ImageJ. Processed images were radially integrated using the Radial Profile Plot plugin in ImageJ and the relative amplitude of the first-order peak in the intensity profile as a measure of sarcomere and myofibril regularity was automatically analyzed using LabChart (ADIstruments). For each iPSC line, three individual differentiations with 7-11 images per differentiation were analyzed. All antibodies used for immunofluorescence are listed in Table S1 in the supplement.

Analysis of cell size of iPSC-CMs

To study cellular hypertrophy, iPSC-CMs at day 60 of differentiation were analyzed for cell size in suspension, as previously described.⁴⁵ In brief, iPSC-CMs at day 50 of differentiation were plated at a density of 2.5×10^5 cells per well on Matrigel-coated 12-well plates. At day 60 of differentiation, cells were singularized with StemPro Accutase Cell Dissociation Reagent (Thermo Fisher Scientific) and measured for cell diameter using the CASY cell counter system (OMNI Life Science). Each value represents a mean of 5×10^2 to 1.5×10^4 cells per measurement. To exclude cell debris and cell clusters, only values within a diameter range of 15-40 µm were selected. For each iPSC line, at least three individual differentiations with 3-5 replicates per differentiation were analyzed.

Ectopic expression of LZTR1 variants in iPSC-CMs

For ectopic expression studies, the human WT *LZTR1* coding sequence was synthesized (Genewiz/Azenta Life Sciences) and subcloned in *pcDNA3-HA-humanNEMO* (gift from Kunliang Guan, Addgene plasmid #13512) by exchanging the *NEMO* coding sequence. Additionally, the HA-tag was exchanged by a FLAG-tag by synthesis of the fragment and subcloning in *pcDNA3-HA-LZTR1-WT* (Genewiz/Azenta Life Sciences). Patient-specific mutations were introduced into *pcDNA3-HA-LZTR1-WT* and *pcDNA3-FLAG-LZTR1-WT* using mutagenesis PCR. The plasmids *pCMV6-MRAS-Myc-DDK* (Origene, #RC212259) and *pcDNA3-Myc-CUL3* (gift from Yue Xiong, Addgene plasmid #19893) were used for co-expression experiments. Plasmid DNA was isolated via the endotoxin-free NucleoBond Xtra Midi Plus EF kit (Macherey-Nagel). For transfection, WT1 iPSC-CMs cultured on Matrigel-coated 4-well chamber slides at a density of 7×10^4 cells per well were transfected at day 60 of differentiation with the respective plasmids using Lipofectamine Stem Transfection Reagent (Thermo Fisher Scientific) according to manufacturer's instructions with 700 ng per plasmid. After 24 h post-transfection, cells were fixed, stained, and imaged as described above. To quantitatively analyze speckle size and filament length, a custom-build pipeline in CellProfiler (BROAD institute) was applied. For each *LZTR1* variant, plasmid transfections were performed in at least three replicates. All antibodies used for immunofluorescence are listed in Table S1 in the supplement. All plasmids used are listed in Table S3 in the supplement.

In silico prediction of protein structures and multimer complexes

Homo-trimer configurations of the different *LZTR1* variants were predicted using ColabFold (version 02c53)⁹⁸ and AlphaFold-multimer v2³³ with 6 recycles and no templates on an A5000 GPU with 24 GBs of RAM and repeated twice. The five predicted models for each variant were ranked according to the predicted template modeling score and interactions between the chains were inspected through the predicted alignment error generated by AlphaFold-multimer.

Statistics

Data are presented as the mean \pm standard error of the mean, unless otherwise specified. Statistical comparisons were performed using the D'Agostino-Pearson normality test and the nonparametric Kruskal-Wallis test followed by Dunn correction in Prism 8 (GraphPad). Results were considered statistically significant when the p-value was ≤ 0.05 .

Data and biomaterial availability

The mass spectrometry proteomics data have been deposited to the ProteomeXchange Consortium via the PRIDE partner repository (<https://www.proteomexchange.org/>) with the identifiers PXD038425 and PXD038417. All human iPSC lines used in this study are deposited in the stem cell biobank of the University Medical Center Göttingen and are available for research use upon request.

4.6 Acknowledgements

We thank Laura Cyganek, Yvonne Hintz, Nadine Gotzmann, Lisa Schreiber, and Yvonne Wedekind (Stem Cell Unit, University Medical Center Göttingen), Branimir Berečić, Tim Meyer and Malte Tiburcy (Institute of Pharmacology and Toxicology, University Medical Center Göttingen), and Anja Wiechert and Manuela Gesell Salazar (Interfaculty Institute of Genetics and Functional Genomics, University Medicine Greifswald) for excellent technical assistance.

This work was supported by the German Research Foundation (DFG): project number 417880571 to L.C.; project number 501985000 to L.C.; project number 193793266, Collaborative Research Centre 1002, C04, D01, D02 and S01 to W.H.Z., G.H., B.W. and L.C.; project number 390729940, Germany's Excellence Strategy - EXC 2067/1 to A.V.B., G.H., W.H.Z., B.W. and L.C.; by the Else Kröner Fresenius Foundation: project number 2019_A75 to L.C.; by the German Federal Ministry of Education and Research (BMBF)/ German Center for Cardiovascular Research (DZHK) to E.H., G.H., W.H.Z., B.W. and L.C.; and by the Leducq Foundation: project number 20CVD04 to W.H.Z.

4.7 Author contributions

L.C. designed the study. L.C. and A.V.B. designed the experiments. A.V.B., O.G.G., E.H., M.S., L.B., H.S., M.K., J.A., F.M., and L.C. performed the experiments and analyzed the data. G.H., W.H.Z. and B.W. gave technical support and conceptual advice. L.C. and A.V.B. wrote and edited the manuscript.

Conflict of interest disclosures

The authors declare that they have no conflict of interest.

4.8 Figure Legends

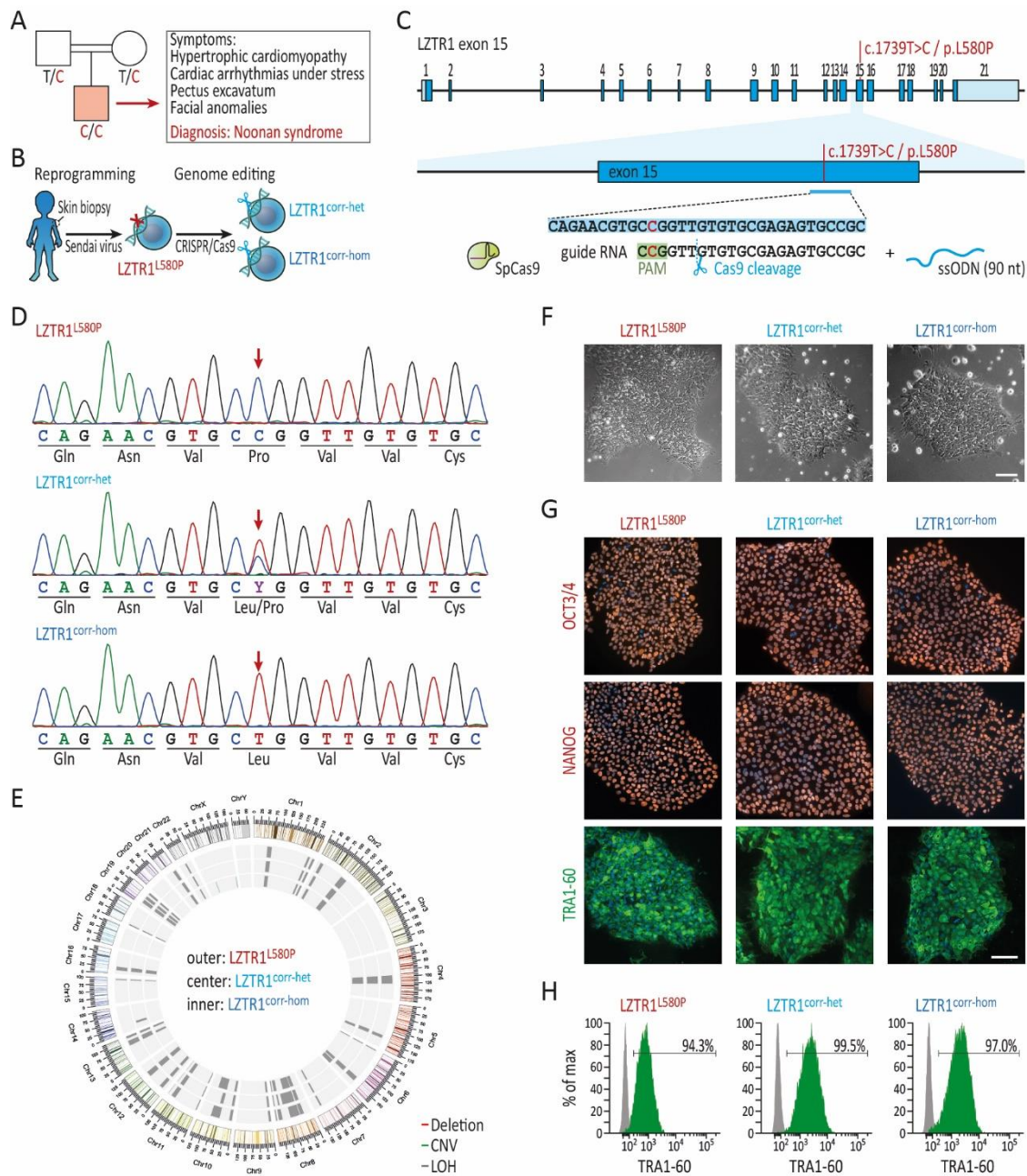


Figure 6: Generation of patient-specific and CRISPR-corrected iPSCs for disease modeling of recessive NS.

(A) Pedigree of the consanguineous family with healthy parents and the son affected by recessive NS harboring the *LZTR1* variant (c.1739T>C/p.L580P) in homozygosity. **(B)** Generation of patient-specific iPSCs by reprogramming of patient's skin fibroblasts via integration-free Sendai virus and genetic correction of the missense variant by CRISPR/Cas9. **(C)** Depiction of the genome editing approach for correction of the missense variant in *LZTR1* exon 15 by CRISPR/Cas9 and single-stranded oligonucleotide (ssODN) for homology-directed repair. **(D)** Sanger sequencing of the patient-derived iPSCs (*LZTR1*^{L580P}) with the *LZTR1* missense variant in homozygosity and the CRISPR/Cas9-edited heterozygously corrected (*LZTR1*^{corr-het}) and homozygously corrected (*LZTR1*^{corr-hom}) iPSCs. **(E)** Molecular karyotyping using a genome-wide microarray demonstrated a high percentage of loss of heterozygosity (LOH) because of consanguinity as well as chromosomal stability of iPSCs after genome

editing. **(F)** Patient-specific and CRISPR-corrected iPSCs showed a typical human stem cell-like morphology; scale bar: 100 μm . **(G)** Expression of key pluripotency markers OCT3/4, NANOG, and TRA-1-60 in the generated iPSC lines was assessed by immunocytochemistry; nuclei were counter-stained with Hoechst 33342 (blue); scale bar: 100 μm . **(H)** Flow cytometry analysis of pluripotency marker TRA-1-60 revealed homogeneous populations of pluripotent cells in generated iPSC lines. Gray peaks represent the negative controls.

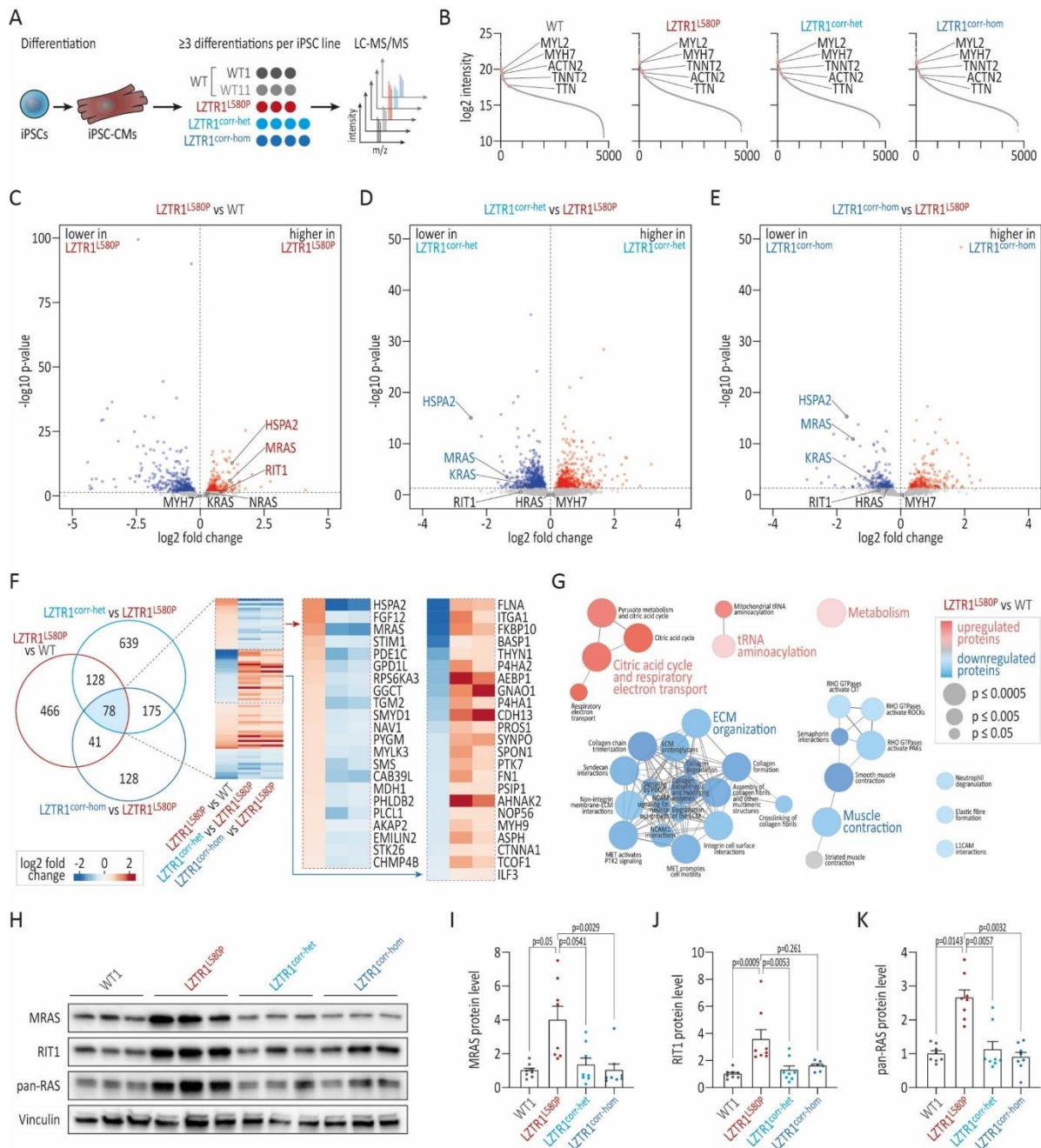


Figure 7: Homozygous LZTR1^{L580P} causes accumulation of RAS GTPases.

(A) Depiction of the experimental design: two individual WT, the patient-specific, and the two CRISPR-corrected iPSC lines were differentiated into ventricular iPSC-CMs and analyzed by quantitative global proteomics via LC-MS/MS at day 60 of differentiation; $n=3-4$ individual differentiations per iPSC line. (B) Over 4,700 proteins were present in the individual proteomic samples, all showing comparable high abundance of cardiac markers myosin heavy chain β (*MYH7*), cardiac troponin T (*TNNT2*), α -actinin (*ACTN2*), titin (*TTN*), and ventricular-specific MLC2V (*MYL2*). (C-E) Volcano plots representing relative protein abundances comparing patient's versus WT iPSC-CMs (C; LZTR1^{L580P} vs WT), heterozygously corrected versus non-corrected iPSC-CMs (D; LZTR1^{corr-het} vs LZTR1^{L580P}), and homozygously corrected versus non-corrected iPSC-CMs (E; LZTR1^{corr-hom} vs LZTR1^{L580P}) revealed high abundance of RAS GTPases in patient samples. (F) Comparison of differentially abundant proteins between the three datasets revealed an overlap of 78 proteins, many of which showed opposite abundance in patient's versus

CRISPR-corrected iPSC-CMs. **(G)** Reactome pathway enrichment analysis of differentially abundant proteins in *LZTR1*^{L580P} vs WT displayed dysregulation of cardiac-related pathways and biological processes. **(H)** Representative blots of RAS GTPase levels in WT, patient's, and CRISPR-corrected iPSC-CMs at day 60 of differentiation, assessed by Western blot; Vinculin served as loading control; n=3 individual differentiations per iPSC line. **(I-K)** Quantitative analysis of Western blots for MRAS (I), RIT1 (J), and pan-RAS recognizing HRAS, KRAS, and NRAS (K); data were normalized to total protein and to the corresponding WT samples on each membrane; n=8 independent differentiations per iPSC line. Data were analyzed by nonparametric Kruskal-Wallis test with Dunn correction and are presented as mean \pm SEM (I-K).

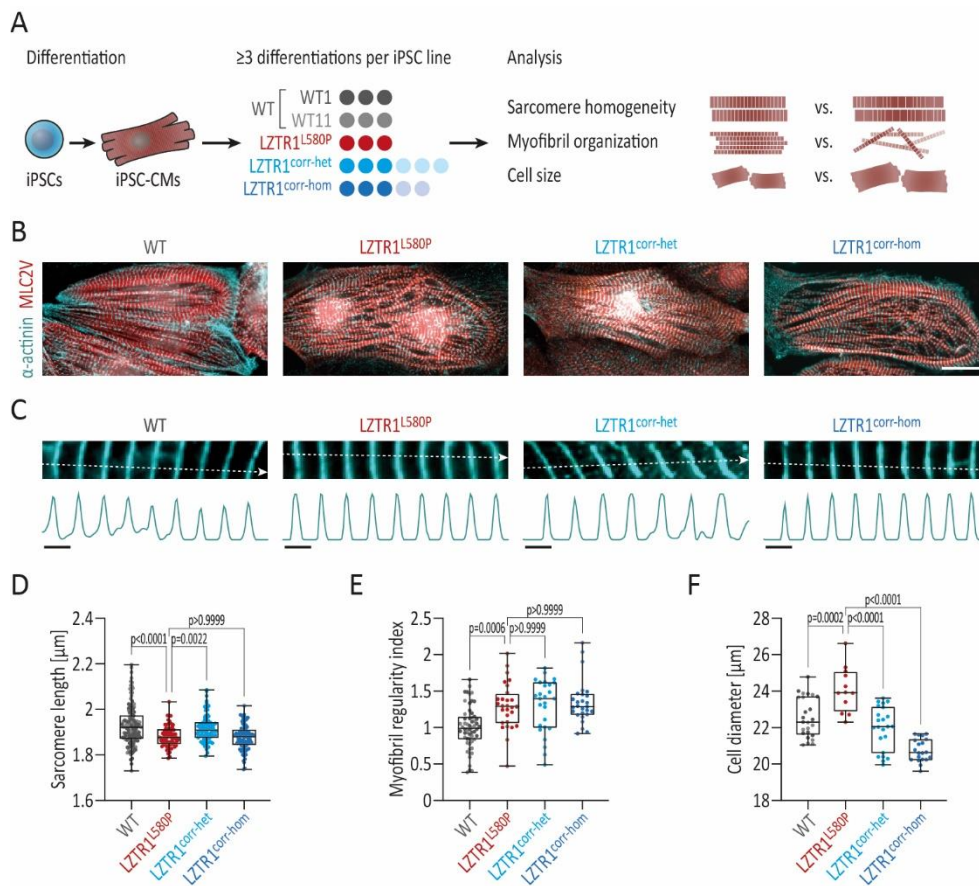


Figure 8: Homozygous *LZTR1*^{L580P} provokes cardiomyocyte hypertrophy.

(A) Depiction of the experimental design: two individual WT, the patient-specific, and the two CRISPR-corrected iPSC lines were differentiated into ventricular iPSC-CMs and analyzed for sarcomere length, myofibril organization, and cell size at day 60 of differentiation. **(B)** Representative images of iPSC-CMs stained for α-actinin and ventricular-specific MLC2V indicated a regular and well-organized sarcomeric assembly across all iPSC lines; scale bar: 20 μm. **(C)** Analysis of the mean sarcomere length per cell was based on measurement of multiple α-actinin-stained individual myofibrils; representative myofibrils and corresponding intensity plots are shown; scale bar: 2 μm. **(D)** Quantitative analysis displayed a typical sarcomere length in iPSC-CMs ranging from 1.7 to 2.2 μm across all iPSC lines; n=75-135 cells from 3 individual differentiations per iPSC line. **(E)** Quantitative analysis of the myofibril organization in α-actinin-stained iPSC-CMs, assessed by Fast Fourier Transform algorithm, demonstrated a high myofibril regularity across all iPSC lines; data were normalized to WT; n=27-58 images from 3 individual differentiations per iPSC line. **(F)** Quantitative analysis of the cell diameter in suspension in singularized iPSC-CMs, assessed by CASY cell counter, revealed a hypertrophic cell diameter in patient's cells, compared with WT and CRISPR-corrected iPSC-CMs; n=12-25 samples from 3-6 individual differentiations per iPSC line. Data were analyzed by nonparametric Kruskal-Wallis test with Dunn correction and are presented as mean ± SEM (D-F).

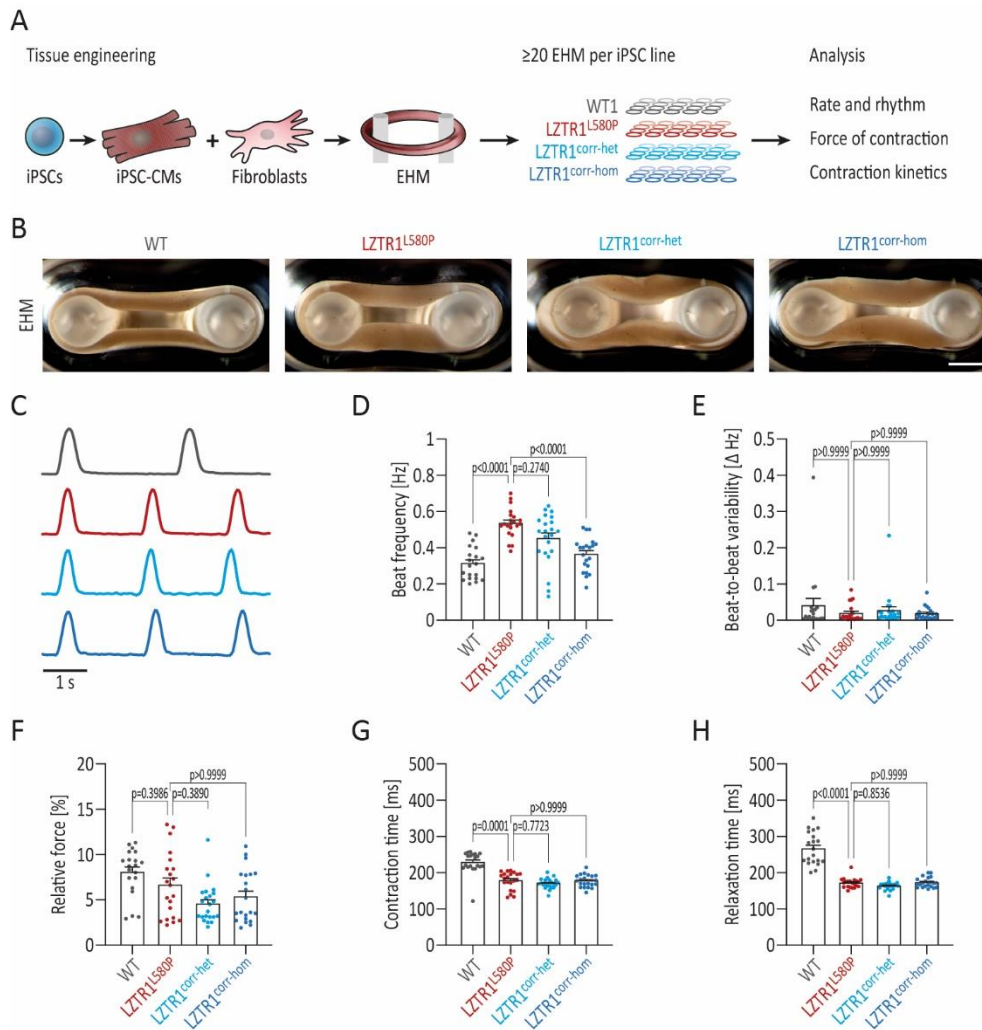


Figure 9: Homozygous *LZTR1*^{L580P} does not compromise contractile function.

(A) Depiction of the experimental design: the WT, the patient-specific, and the two CRISPR-corrected iPSC lines were differentiated into ventricular iPSC-CMs and casted at day 30 of differentiation together with fibroblasts in a collagen matrix for generation of EHMs. Tissues were analyzed for rhythmogenicity and contractile parameters by optical recordings at 5-6 weeks post-casting; n=20-22 EHMs from 3 individual differentiations per iPSC line. **(B)** Representative microscopic images of generated EHMs 6 weeks post-casting showing comparable tissue morphologies; scale bar: 1 mm. **(C)** Exemplary contraction traces from optical recordings of EHMs 6 weeks post-casting; peak amplitudes were normalized. **(D)** Quantitative analysis of the beating frequency of spontaneously contracting EHMs displayed minor differences in patient-derived tissues. **(E)** Quantitative measurement of the beat-to-beat variability of spontaneously contracting EHMs showed equal beating regularities across all tissues. **(F)** Quantitative analysis of the force of contraction, assessed by measuring the relative deflection of flexible poles, identified no significant differences across all iPSC lines. **(G-H)** Quantitative analysis of the contraction kinetics revealed longer contraction times (G) and relaxation times (H) in WT compared to patient's and CRISPR-corrected EHMs. Data were analyzed by nonparametric Kruskal-Wallis test with Dunn correction and are presented as mean \pm SEM (D-H).

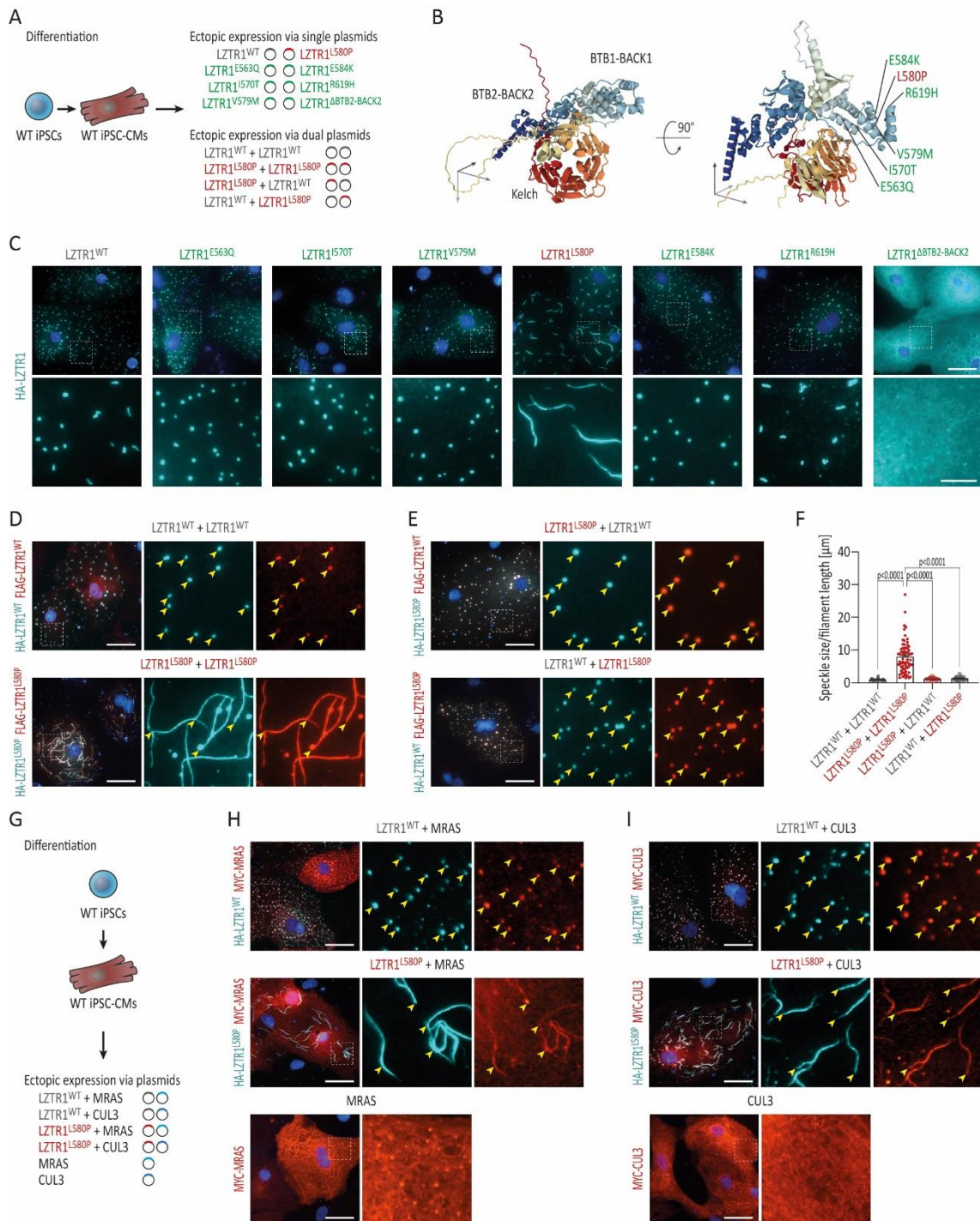


Figure 10: Homozygous *LZTR1*^{L580P} induces polymerization of LZTR1-cullin 3 ubiquitin ligase complexes.

(A) Depiction of the experimental design: the WT iPSC line was differentiated into ventricular iPSC-CMs, transfected at day 60 of differentiation with plasmids by lipofection for ectopic expression of *LZTR1* variants and analyzed 24 h post-transfection for subcellular localization LZTR1 complexes. (B) AlphaFold protein structure of monomeric *LZTR1* highlighting the location of LZ of selected variants within the BACK1 domain. (C) Representative images of iPSC-CMs after single plasmid transfection stained for HA-tagged *LZTR1* revealed that *LZTR1*^{WT} and most other variants present a speckle-like pattern equally distributed throughout the cytoplasm, whereas missense variant *LZTR1*^{L580P} forms large filaments; nuclei were counter-stained with Hoechst 33342 (blue); scale

bars: 20 μm in upper panel, 5 μm in lower panel. **(D-E)** Representative images of iPSC-CMs after dual plasmid transfection stained for HA-tagged and FLAG-tagged LZTR1 confirmed the filament formation of *LZTR1*^{L580P} (D), whereas co-expression of *LZTR1*^{WT} and *LZTR1*^{L580P} in different combinations resolved the polymer chains (E); nuclei were counter-stained with Hoechst 33342 (blue); scale bar: 20 μm . **(F)** Quantitative analysis of the mean speckle size and mean filament length per cell of HA-tagged LZTR1 in co-transfected iPSC-CMs, assessed by a customized CellProfiler pipeline, confirmed formation of *LZTR1*^{L580P}-induced filaments; n=34-74 cells per condition. **(G)** Experimental outline for co-localization studies: the WT iPSC line was differentiated into ventricular iPSC-CMs, transfected at day 60 of differentiation with plasmids by lipofection for ectopic expression of *LZTR1* variants and MRAS or cullin 3 (CUL3), and analyzed 24 h post-transfection. **(H-I)** Representative images of iPSC-CMs after dual plasmid transfection stained for HA-tagged LZTR1 and MYC-tagged MRAS (H) or MYC-tagged CUL3 (I) indicated recruitment of the interaction partners to speckles in *LZTR1*^{WT} or polymer chains in *LZTR1*^{L580P}; nuclei were counter-stained with Hoechst 33342 (blue); scale bar: 20 μm . Data were analyzed by nonparametric Kruskal-Wallis test with Dunn correction and are presented as mean \pm SEM (F).

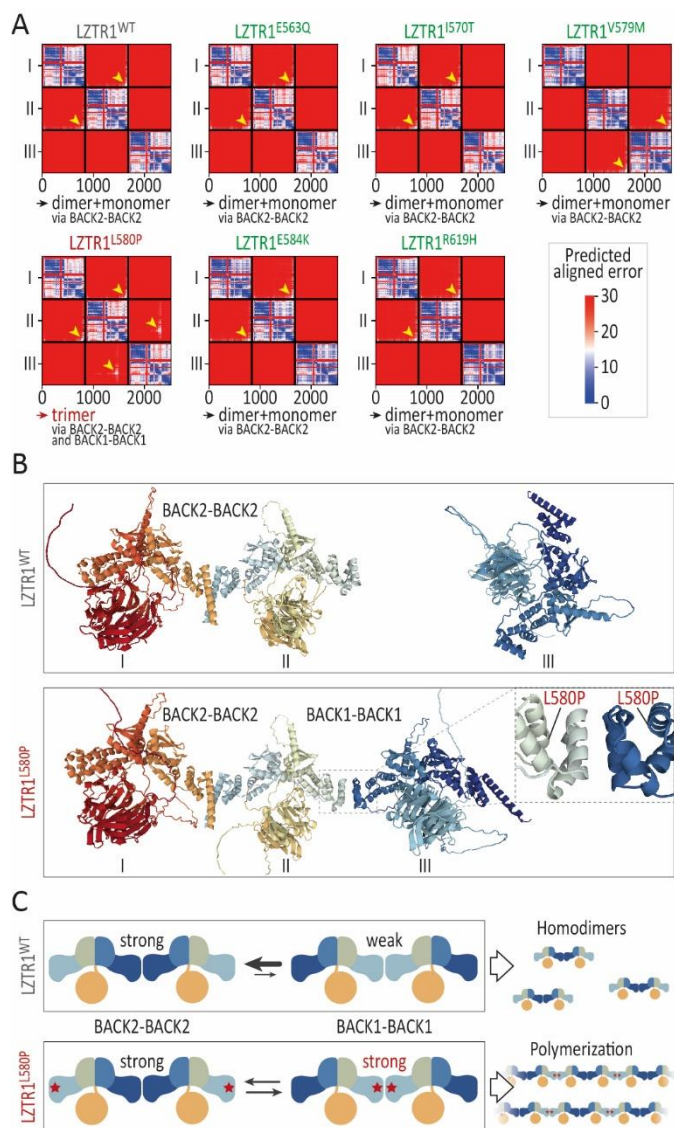


Figure 11: Homozygous *LZTR1*^{L580P} alters binding affinities of dimerization domains.

(A) Computational modeling of the top-ranked *LZTR1* homo-trimer interactions from selected variants within the BACK1 domain, assessed by the predicted alignment error generated by ColabFold, predicted a dimer plus monomer configuration via BACK2-BACK2 dimerization for *LZTR1*^{WT} and the other variants, whereas the top-ranked model for *LZTR1*^{L580P} was predicted to form linear trimers via BACK2-BACK2 and BACK1-BACK1 dimerization; yellow arrows highlight the predicted interaction domains between proteins. **(B)** Visualization of the top-ranked protein interaction models for *LZTR1*^{WT} assembling as dimer and monomer and for *LZTR1*^{L580P} forming linear trimers. **(C)** Hypothetical model for *LZTR1* complex formation: whereas *LZTR1*^{WT} assembles in homo-dimers via the BACK2-BACK2 dimerization domain, *LZTR1*^{L580P} might alter the binding affinity of the BACK1 domain, causing formation of linear *LZTR1* polymer chains via dimerization of both BACK2 and BACK1 domains.

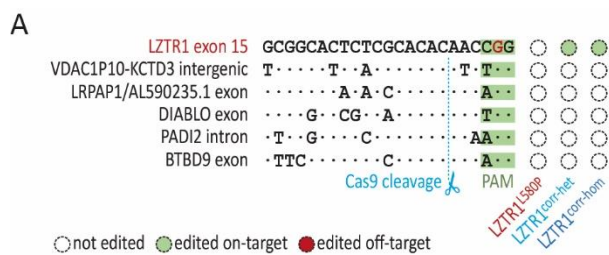


Figure 12: Off-target screening in CRISPR/Cas9-edited iPSCs. (Supplementary figure)

(A) Sanger sequencing of the top five predicted off-target regions, ranked by the CFD off-target score using CRISPOR, revealed no off-target editing of CRISPR/Cas9 in CRISPR-corrected iPSCs compared to the patient-derived cells.

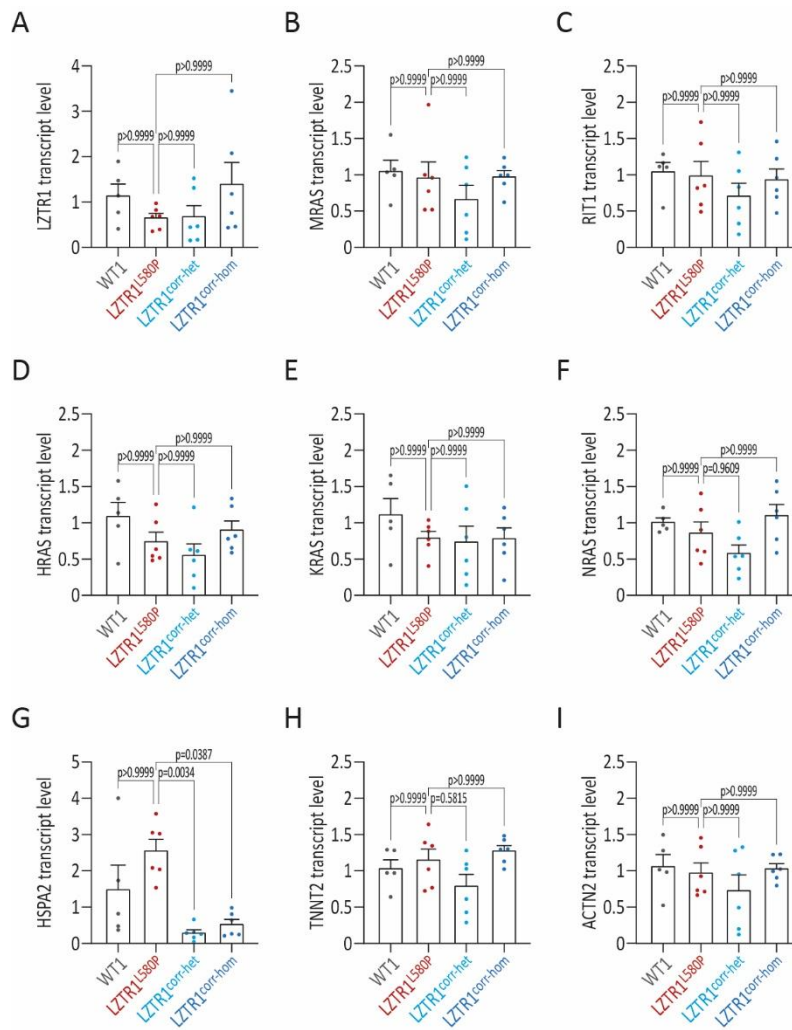


Figure 13: Homozygous *LZTR1*^{L580P} showed no upregulation of RAS GTPases at transcriptional level. (Supplementary figure)

(A-I) Quantitative gene expression analysis of *LZTR1* (A), of *LZTR1* substrates *MRAS* (B), *RIT1* (C), *HRAS* (D), *KRAS* (E), and *NRAS* (F), of *HSPA2* (G), and of cardiac-specific genes *TNNT2* (H), and *ACTN2* (I) in WT, the patient-specific, and the two CRISPR-corrected iPSC-CMs at day 60 of differentiation, assessed by real-time polymerase chain reaction, revealed no expression differences at transcriptional level across all iPSC lines; samples were analyzed in duplicates and data were normalized to *GAPDH* expression and WT controls; n=5-6 independent differentiations per iPSC line. Data were analyzed by nonparametric Kruskal-Wallis test with Dunn correction and are presented as mean \pm SEM (A-I).

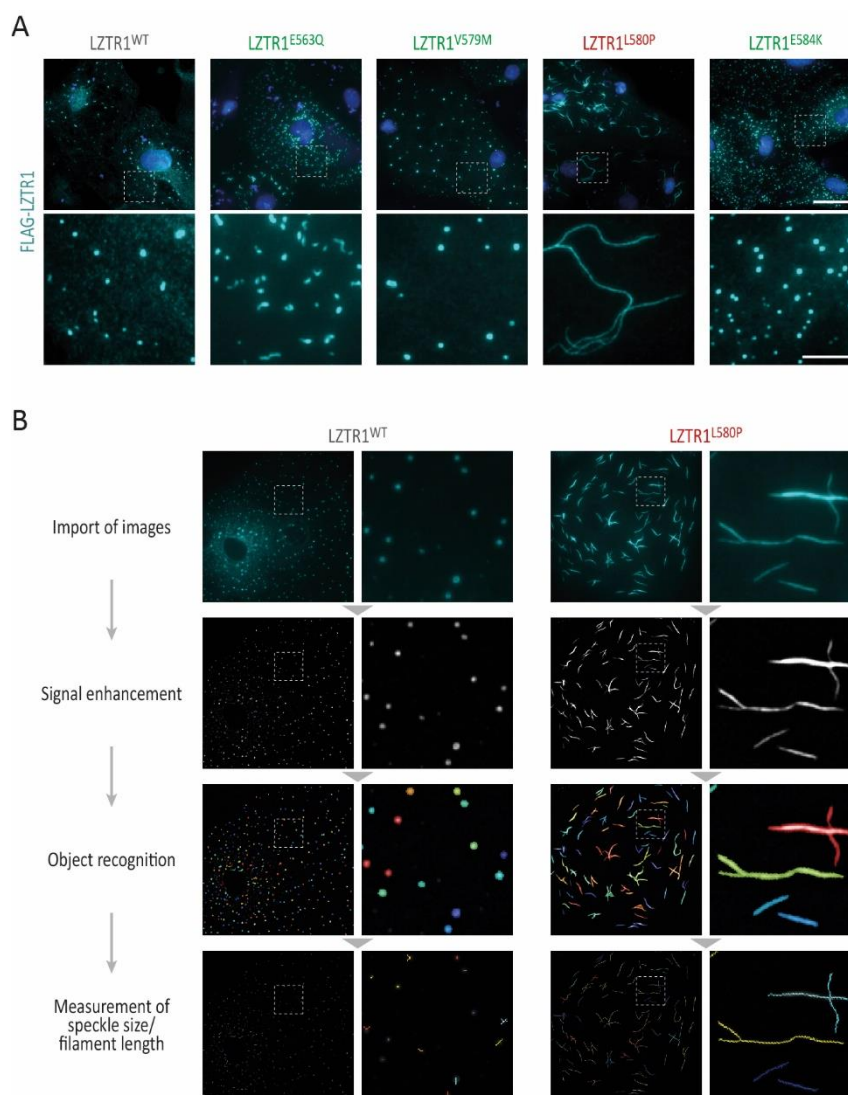


Figure 14: Unique *LZTR1*^{L580P}-induced polymerization of LZTR1 complexes. (Supplementary figure)

(A) Representative images of WT iPSC-CMs at day 60 of differentiation after single plasmid transfection stained for FLAG-tagged LZTR1 confirmed that only *LZTR1*^{L580P} forms large filaments, whereas *LZTR1*^{WT} and the other variants present a speckle-like pattern; nuclei were counter-stained with Hoechst 33342 (blue); scale bars: 20 μm in upper panel, 5 μm in lower panel. **(B)** Customized CellProfiler pipeline for recognition and quantification of speckle size and filament length in iPSC-CMs with ectopic expression of *LZTR1* variants.



Figure 15: Computational prediction for LZTR1 interactions via ColabFold. (Supplementary figure)

(A) The five predicted models for each *LZTR1* variant were ranked according to the predicted template modeling score and interactions between the chains were inspected through the predicted alignment error generated by AlphaFold-multimer.

Table 1: Antibodies used for Western blot, immunocytochemistry and flow cytometry. (Supplementary table).

Primary antibody	Supplier	Resource ID
α -actinin monoclonal mouse	Sigma-Aldrich	RRID:AB_476766
FLAG monoclonal mouse	Sigma-Aldrich	RRID:AB_262044
HA monoclonal rabbit	Cell Signalling	RRID:AB_1549585
MLC2V polyclonal rabbit	Proteintech	RRID:AB_2147453
MRAS polyclonal rabbit	Proteintech	RRID:AB_10950895
MYC monoclonal mouse	Cell Signalling	RRID:AB_331783
NANOG monoclonal mouse	Thermo Fisher Scientific	RRID:AB_2536677
OCT3/4-PE monoclonal human	Miltenyi Biotec	RRID:AB_2784442
pan-RAS monoclonal mouse	Merck Millipore	RRID:AB_2121151
RIT1 polyclonal rabbit	Abcam	RRID:AB_882379
Tra-1-60 monoclonal mouse	Abcam	RRID:AB_778563
TRA-1-60-Alexa488 monoclonal mouse	BD Biosciences	RRID:AB_1645379
Vinculin monoclonal mouse	Sigma-Aldrich	RRID:AB_477629
Secondary antibody	Supplier	Resource ID
Alexa488 polyclonal goat anti-rabbit	Thermo Fisher Scientific	RRID:AB_143165
Alexa555 polyclonal donkey anti-mouse	Thermo Fisher Scientific	RRID:AB_2536180
HRP polyclonal donkey anti-rabbit	Sigma-Aldrich	RRID:AB_2722659
HRP polyclonal donkey anti-mouse	Sigma-Aldrich	RRID:AB_772210

Table 2: Primer sequences used for PCR and real-time PCR. (Supplementary table)

Gene (gDNA)	Primer
LZTR1 Ex15	CGAGGCCTTG TTCCTACCTA / GAGGGGCTCACAGTGGTG
Off-target 1	GGTTCAGAAGCACTCATCTCC / AAGCCATCAACCCGAAACAA
Off-target 2	ATGGATCCTGACTGCAACCC / TCTGGGCAGTCTGTGTCTTT
Off-target 3	GATGCCACAATAACCGCTCC / TGAGGAGACGTGGAGAGGAG
Off-target 4	AGTAAGGCGTTTGAGTCCCA / AAGAGGCACATGGATGAGGG
Off-target 5	AACACACTGGGGAAGGAAGT / GAGCTGCTTCCTATCCCCTC
Gene (cDNA)	Primer
ACTN2	GCCAGAGAGAAGGATGCAATCAC/AAGCATGGGAACCTGGAATCAA
GAPDH	GGAGCGAGATCCCTCCAAAAT / GGCTGTTGTCATACTTCTCATGG
HRAS	ACGCACTGTGGAATCTCGGCAG / TCACGCACCAACGTGTAGAAGG
HSPA2	GACCAAGGACAATAACCTGCTGG/GGCGTCAATGTCTGAAGGTAACC
KRAS	AGTGCCTTGACGATACAG /GCATCATCAACACCCTGTCTT
LZTR1	GAGCCAACCTCAAGGAGCACT / CAATGTCCACTGGCTGGTCC
MRAS	CCACCATTGAAGACTCCTACCTG /ACGGAGTAGACGATGAGGAAGC
NRAS	GGCAATCCCATACAACCCTGAG / GAAACCTCAGCCAAGACCAGAC
RIT1	TTCATCAGCCACCGATTCCC / GCAGGCTCATCATCAATACGG
TNNT2	ACAGAGCGGAAAAGTGGGAAG / TCGTTGATCCTGTTTCGGAGA

Table 3: Plasmids used for ectopic expression studies. (Supplementary table)

Plasmid	Source
pcDNA3-HA-LZTR1-WT	modified from addgene plasmid #13512
pcDNA3-FLAG-LZTR1-WT	modified from pcDNA3-HA-LZTR1-WT
pcDNA3-HA-LZTR1-E563Q	modified from pcDNA3-HA-LZTR1-WT
pcDNA3-FLAG-LZTR1-E563Q	modified from pcDNA3-FLAG-LZTR1-WT
pcDNA3-HA-LZTR1-I570T	modified from pcDNA3-HA-LZTR1-WT
pcDNA3-HA-LZTR1-V579M	modified from pcDNA3-HA-LZTR1-WT
pcDNA3-FLAG-LZTR1-V579M	modified from pcDNA3-FLAG-LZTR1-WT
pcDNA3-HA-LZTR1 ^{-L580P}	modified from pcDNA3-HA-LZTR1-WT
pcDNA3-FLAG-LZTR1 ^{-L580P}	modified from pcDNA3-FLAG-LZTR1-WT
pcDNA3-HA-LZTR1-E584K	modified from pcDNA3-HA-LZTR1-WT
pcDNA3-FLAG-LZTR1-E584K	modified from pcDNA3-FLAG-LZTR1-WT
pcDNA3-HA-LZTR1-R619H	modified from pcDNA3-HA-LZTR1-WT
pcDNA3-HA-LZTR1- Δ BTB2-BACK2	modified from pcDNA3-HA-LZTR1-WT
pCMV6-MRAS-Myc-DDK	Origene plasmid #RC212259
pcDNA3-Myc-CUL3	Addgene plasmid #19893

5 Generation of a genetically-modified induced pluripotent stem cell line harboring a Noonan syndrome-associated gene variant MRAS p.G23V

Title:

Generation of a genetically-modified induced pluripotent stem cell line harboring a Noonan syndrome-associated gene variant MRAS p.G23V

Authors:

Alexandra Viktoria Busley^{1,2,3}, Lukas Cyganek^{1,2,3*}

Affiliations:

¹Stem Cell Unit, Clinic for Cardiology and Pneumology, University Medical Center Göttingen, Göttingen, Germany; ²DZHK (German Center for Cardiovascular Research), partner site Göttingen, Germany; ³Cluster of Excellence "Multiscale Bioimaging: from Molecular Machines to Networks of Excitable Cells" (MBExC), University of Göttingen, Germany & Hertha Sponer College;

5.1 Abstract

Patients harboring causative gene variants in RAS GTPase *MRAS* develop Noonan syndrome and early-onset hypertrophic cardiomyopathy. Here, we describe the generation of a human iPSC line harboring the Noonan syndrome-associated MRAS p.G23V variant by using CRISPR/Cas9 technology. The established *MRAS*^{G23V} iPSC line allows to study MRAS-specific pathomechanisms and to test novel therapeutic strategies in various disease-relevant cell types and tissues.

Table 4: Ressource Table

	UMGi014-C-17 clone G2
Unique stem cell line identifier	https://hpscereg.eu/cell-line/UMGi014-C-17
Alternative name(s) of stem cell line	isWT1-MRAS-G23V.G2
Institution	University Medical Center Göttingen, Germany
Contact information of the reported cell line distributor	Lukas Cyganek, lukas.cyganek@gwdg.de
Type of cell line	iPSC
Origin	human
Additional origin info <i>(applicable for human ESC or iPSC)</i>	Age: 31 Sex: male Ethnicity: Caucasian
Cell Source	Human iPSC line UMGi014-C clone 14 (isWT1.14) generated from skin fibroblasts of a healthy donor
Method of reprogramming	Non-integrating Sendai virus
Clonality	Clonal isolation was performed by automated single cell dispensation using CellenOne (Cellenion/Scienion)
Evidence of the reprogramming transgene loss (including genomic copy if applicable)	RT-PCR
The cell culture system used	Feeder-free and serum-free culture conditions with Matrigel (growth factor reduced, BD Biosciences) and StemMACS iPS-Brew XF medium (Miltenyi Biotec)
Type of the Genetic Modification	Induced mutation
Associated disease	Causative gene variant described in Noonan syndrome patients with severe disease progression and early-onset hypertrophic cardiomyopathy
Gene/locus	MRAS (NM_001085049.3): c.68G>T / p.Gly23Val (ClinVar: VCV000635781.3)
Method of modification / user-customisable nuclease (UCN) used, the resource used for design optimisation	CRISPR/Cas9
User-customisable nuclease (UCN) delivery method	Nucleofection of RNPs
All double-stranded DNA genetic material molecules introduced into the cells	N/A
Analysis of the nuclease-targeted allele status	Sanger sequencing of the targeted locus

Method of the off-target nuclease activity prediction and surveillance	Sanger sequencing of the top 5 predicted off-targets
Descriptive name of the transgene	N/A
Eukaryotic selective agent resistance cassettes (including inducible, gene/cell type-specific)	N/A
Inducible/constitutive expression system details	N/A
Date archived/stock creation date	30th September 2020
Cell line repository/bank	Biobank of the University Medical Center Göttingen
Ethical/GMO work approvals	Ethics Committee of the University Medical Center Göttingen, approval number: 10/9/15
Addgene/public access repository recombinant DNA sources' disclaimers (if applicable)	N/A

5.2 Resource utility

Causative gene variants in *MRAS* are known to cause Noonan syndrome with an associated early-onset form of hypertrophic cardiomyopathy.^{23,120} Human iPSCs harboring the common gene variant *MRAS*^{G23V} provide a powerful tool to study the *MRAS*-dependent pathomechanisms and to screen drug compounds in different iPSC-derived cell types and tissues.

5.3 Resource Details

To generate a human iPSC line harboring the Noonan syndrome-associated *MRAS*^{G23V} variant, we used CRISPR/Cas9 technology to introduce the mutation into a well-established wild type iPSC line previously generated by integration-free reprogramming of skin fibroblasts from a healthy donor (Figure 16A).¹¹³ The ribonucleoprotein-based CRISPR/Cas9 complex targeting exon 2 of the *MRAS* gene was combined with a single-stranded oligonucleotide homology-directed repair template containing the desired base pair exchange and introduced into iPSCs by nucleofection (Figure 16B). Following transfection, iPSCs were singularized and individual clones were screened for successful editing by Sanger sequencing. One iPSC line heterozygous for the *MRAS*^{G23V} variant was selected for further characterization (Figure 16C). Molecular karyotyping of the *MRAS*^{G23V} iPSCs confirmed chromosomal stability after genome editing and passaging (Figure 16D). Off-target analysis of the top five predicted off-targets demonstrated no genomic alterations after CRISPR/Cas9 application (Figure 16E). The generated iPSC line exhibited a typical human stem cell-like morphology (Figure 16F). Flow cytometric analysis for the pluripotency markers OCT3/4 and TRA-1-60 revealed a homogeneous population of pluripotent cells in *MRAS*^{G23V} iPSC cultures (Figure 16G). In addition, robust expression of the pluripotency markers OCT3/4, NANOG and TRA-1-60 was detected by immunocytochemistry (Figure

Generation of a genetically-modified induced pluripotent stem cell line harboring a Noonan syndrome-associated gene variant *MRAS* p.G23V (16H). To prove that the CRISPR-edited iPSCs were capable of differentiating into cells of all three germ layers, we performed embryoid body formation and assessed cell fate identity using immunocytochemistry. Differentiated cultures showed the presence of cells positive for endodermal-specific alpha fetoprotein, mesodermal-specific α -smooth muscle actin, and ectodermal-specific β -III-tubulin (Figure 16I).

Since *MRAS* is known to be predominantly expressed in cardiomyocytes, we differentiated the CRISPR-edited iPSCs into ventricular-like cardiomyocytes using an established protocol (Figure 16J).⁴⁹ The *MRAS*^{G23V} iPSC-cardiomyocytes at day 60 of differentiation displayed a regular myofibrillar organization, as visualized by the expression of α -actinin and ventricular-specific MLC2V (Figure 16K). Two alternatively spliced *MRAS* isoforms have been described: a long isoform 1 including exon 2 (which also includes the *MRAS*^{G23V} variant) and a shorter isoform 2 lacking exon 2. Interestingly, analysis of *MRAS* expression at the transcriptional level, assessed by reverse transcriptase PCR, revealed that both isoforms are expressed in the iPSC-cardiomyocytes (Figure 16L). Proteomic analysis by Western blot for *MRAS* (recognizing isoform 1) demonstrated that *MRAS*^{G23V} iPSC-cardiomyocytes expressed similar *MRAS* protein levels compared to wild type cardiomyocytes, indicating that the gene variant does not affect *MRAS* gene expression or *MRAS* degradation (Figure 16M).

In conclusion, the established *MRAS*^{G23V} iPSC line allows the study of *MRAS*-related Noonan syndrome pathology in various iPSC-derived cell types and tissues. In addition, this iPSC line and its iPSC-derivatives provide a unique opportunity to test therapeutics in physiologically relevant cells.

5.4 Materials and Methods

Genome editing and culture of human iPSCs

Wild type iPSC line UMGi014-C clone 14 (isWT1.14) was generated from dermal fibroblasts from a male donor using the integration-free Sendai virus and was described previously.¹¹³ Human iPSCs were cultured in feeder-free and serum-free culture conditions in StemMACS iPS-Brew XF medium (Miltenyi Biotec) or StemFlex medium (Thermo Fisher Scientific) on Matrigel-coated (growth factor reduced, BD Biosciences) plates in a humidified incubator at 37°C and 5% CO₂. Cells were passaged every 5-6 days with Versene solution (Thermo Fisher Scientific). For editing, the CRISPR/Cas9 ribonucleoprotein complex was assembled by mixing of the Alt-R CRISPR-Cas9 crRNA and the Alt-R CRISPR-Cas9 tracrRNA (preassembled in a 1:1 ratio) with the Alt-R Hifi SpCas9 Nuclease 3NLS (IDT DNA Technologies) at 1:3 molar ratio together with the single-stranded oligonucleotide for homology-directed repair in nucleofector solution. Nucleofection was performed with 2×10⁶ iPSCs using the 4D Amaxa

Generation of a genetically-modified induced pluripotent stem cell line harboring a Noonan syndrome-associated gene variant MRAS p.G23V

Nucleofector system (Lonza; program CA-137) and the P3 Primary Cell 4D-Nucleofector X Kit (Lonza) according to manufacturer's instructions. Following nucleofection, iPSCs were replated into a Matrigel-coated well of a 6-well plate containing StemFlex medium supplemented with 2 μ M Thiazovivin and 100 U/ml penicillin and 100 μ g/ml streptomycin (Thermo Fisher Scientific). After 3 days, transfected iPSCs were singularized using the single cell dispenser CellenOne (Cellenion/Scienion) in StemFlex medium on Matrigel-coated 96-well plates. Successful genome editing was identified by Sanger sequencing and the *MRAS*^{G23V} isogenic iPSC line UMGi014-C-17 clone G2 (isWT1-MRAS-G23V.G2) was expanded and maintained in StemMACS iPS-Brew XF medium on Matrigel-coated plates for at least five passages prior to molecular karyotyping, pluripotency characterization and differentiation experiments. *MRAS*^{G23V} and wild type iPSCs were differentiated into ventricular iPSC-cardiomyocytes via WNT signalling modulation and subsequent metabolic selection, as previously described,⁴⁹ and cultivated in feeder-free and serum-free culture conditions until day 60 post-differentiation.

Pluripotency characterization of human iPSCs

Pluripotency analysis was performed via immunocytochemistry and flow cytometry, as previously described.⁴⁵ For embryo body formation, 5×10^6 iPSCs were combined with 2.5×10^6 mouse embryonic fibroblasts and seeded into a 96-well U plate containing hES medium (DMEM-F12, 15% Knockout Serum Replacement, 1% MEM Non-Essential Amino Acids Solution, 1% β -Mercaptoethanol, 2 μ M Thiazovivin). After 24h, medium was exchanged to EB-Diff medium (IMDM with Glutamax, 20% fetal bovine serum, 1% MEM Non-Essential Amino Acids Solution, 450 μ M 1-thioglycerol). Eight days post-differentiation, embryo body were transferred to Matrigel-coated coverslips and cultured for 8 days. For molecular karyotyping, genomic DNA of iPSC clones was sent for genome-wide analysis via Illumina BeadArray (Life&Brain, Germany). Digital karyotypes were analyzed in GenomeStudio v2.0 (Illumina) with the CNV partition algorithm 3.2.0 (default settings). Copy number events were reported if larger than 3.5×10^5 bps and 1×10^6 bps for loss of heterozygosity. For off-target screening, the top 5 predicted off-target regions for the respective guide RNA ranked by the CFD off-target score using CRISPOR were analyzed by Sanger sequencing.

Western blot analysis of human iPSCs

For Western blot analysis, iPSC-cardiomyocytes were pelleted by scratching and collected in M-PER cell lysis buffer (Thermo Fisher Scientific), and snap-frozen in liquid nitrogen. Protein containing supernatant was collected by centrifugation and protein concentration was determined by BCA assay (Thermo Fisher Scientific). Protein separation was conducted by SDS-Page using nitrocellulose membranes (Bio-Rad). Membranes were blocked in 5 \times PVP solution (10 \times TBS, 10% PVP-30K, 15% PVP-

Generation of a genetically-modified induced pluripotent stem cell line harboring a Noonan syndrome-associated gene variant MRAS p.G23V (12K, 0.5% Tween-20, 1% Tween-80, 0.02% 1,1,1-Trichloro-2-methyl-2-propanol-hemihydrat) and incubated with primary and secondary HRP-coupled antibodies in 1x PVP solution. Signals were detected upon application of SuperSignal West Femto Maximum Sensitivity Substrate (Thermo Fisher Scientific). Image acquisition was performed with the ChemiDoc XRS+ (Bio-Rad) using the high-resolution mode.

5.5 Acknowledgements

We thank Laura Cyganek, Yvonne Hintz, Nadine Gotzmann, Lisa Schreiber, and Yvonne Wedekind (Stem Cell Unit, University Medical Center Göttingen) for excellent technical assistance. This work was supported by the German Research Foundation (DFG): project number 417880571 to L.C.; project number 501985000 to L.C.; project number 193793266, Collaborative Research Centre 1002, S01 to L.C.; project number 390729940, Germany's Excellence Strategy - EXC 2067/1 to A.V.B. and L.C.; by the Else Kröner Fresenius Foundation: project number 2019_A75 to L.C.; and by the German Federal Ministry of Education and Research (BMBF)/ German Center for Cardiovascular Research (DZHK) to L.C.

Generation of a genetically-modified induced pluripotent stem cell line harboring a Noonan syndrome-associated gene variant *MRAS* p.G23V

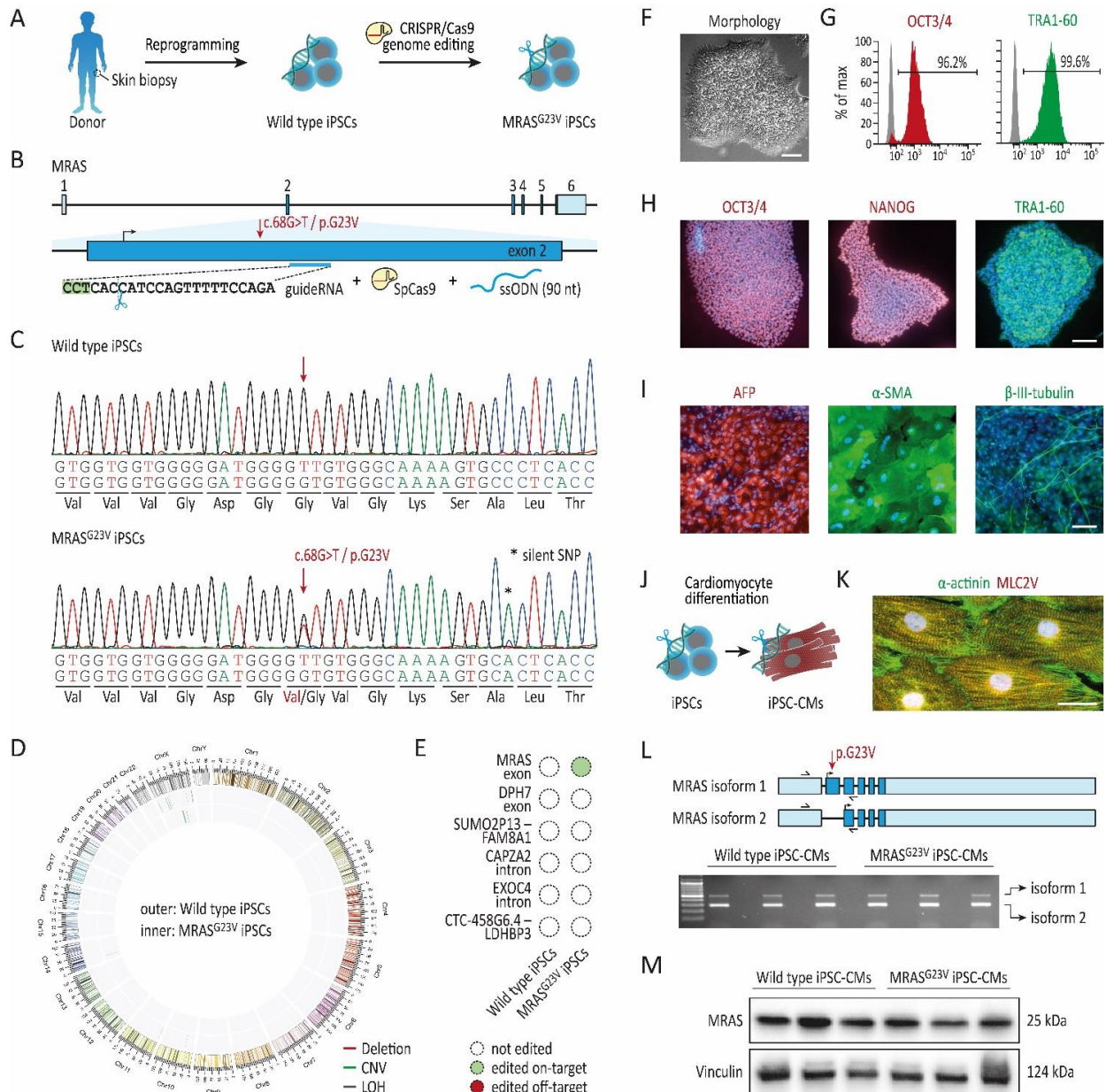


Figure 16: Generation of a CRISPR-edited *MRAS*^{G23V} iPSC line.

(A) Schematic demonstration of how somatic skin biopsies from a healthy donor are reprogrammed into iPSCs and further edited via CRISPR/Cas9 to introduce a pathogenic mutation. **(B)** Depiction of the CRISPR/Cas9 editing strategy to introduce the *MRAS*^{G23V} mutation (c.68G>T) using a target-specific guide RNA in combination with a SpyCas9. **(C)** Sanger Sequencing of the original WT and the CRISPR-edited iPSC line proving the heterozygous introduction of *MRAS*^{G23V} and one additional silent SNPs. **(D)** Molecular karyotyping using genome-wide microarray analysis revealed no chromosomal abnormalities and genome stability post-editing. **(E)** No editing was observed while screening the top five predicted off-target sites. **(F)** *MRAS*^{G23V} iPSC line showed typical stem-cell-like morphology. Scale bar: 100 μ m. **(G), (H)** Pluripotency was assessed via flow cytometry (OCT3/4 and TRA-1-60) and immunocytochemistry staining for defined markers like OCT3/4, NANOG, and TRA-1-60; nuclei were stained with Hoechst33342. Scale bar: 100 μ m. **(I)** Embryoid body formation proved that iPSCs retain their capacity to differentiate in all three germ layers: α -smooth muscle actin (mesoderm), α -fetoprotein (endoderm), and β -III-tubulin (ectoderm). **(J)** Directed differentiation of WT and *MRAS*^{G23V} iPSCs into functional ventricular-

Generation of a genetically-modified induced pluripotent stem cell line harboring a Noonan syndrome-associated gene variant *MRAS* p.G23V

like iPSC-CMs. **(K)** Sarcomere apparatus stained via α -actinin (green) and myosin light chain-2 (MLC2v) (red). Scale bar: 100 μ m. **(L)** RT-PCR using primer spanning exon 2 on transcript level was performed using cDNA from WT and *MRAS*^{G23V} iPSC-CM and revealed a second shorter *MRAS* isoform. **(M)** Western blot analysis showed similar *MRAS* protein levels in WT-and CRISPR-edited iPSC-CMs. Vinculin served as a loading control.

Table 5: Characterization and validation of MRAS^{G23V} iPSC line.

Classification (optional <i>italicized</i>)	Test	Result	Data
Morphology	Photography	The iPSC line displayed a typical human stem cell-like morphology	Figure 1 panel F
Pluripotency status evidence for the described cell line	Qualitative analysis (Immunocytochemistry)	The iPSC line showed robust expression of OCT3/4, NANOG and TRA-1-60	Figure 1 panel H
	Quantitative analysis (Flow cytometry)	The iPSC line showed >96% of positive cells for OCT3/4 and TRA-1-60 expression.	Figure 1 panel G
Karyotype	Karyotype, genome-wide analysis via Illumina BeadArray (Infinium Global Screening Array-24 Kit)	46XY, Resolution ~ 654,027 fixed markers	Figure 1 panel D
Genotyping for the desired genomic alteration/allelic status of the gene of interest	PCR across the edited site	The iPSC line showed a target-specific heterozygous insertion of the gene variant, assessed by Sanger sequencing	Figure 1 panel C
	Evaluation of the - (homo-/hetero-/hemi-) zygous status of introduced genomic alteration(s)	The iPSC line showed a target-specific heterozygous insertion of the gene variant, assessed by Sanger sequencing	Figure 1 panel C
	Transgene-specific PCR (when applicable)	N/A	N/A
Verification of the absence of random plasmid integration events	PCR/Southern	N/A	N/A
Parental and modified cell line genetic identity evidence	HLA typing	Identify of the iPSC line was verified by HLA typing.	Not shown but available with the author

Generation of a genetically-modified induced pluripotent stem cell line harboring a Noonan syndrome-associated gene variant MRAS p.G23V

Mutagenesis / genetic modification outcome analysis	Sequencing (genomic DNA PCR product)	The iPSC line showed a target-specific heterozygous insertion of the gene variant, assessed by Sanger sequencing	Figure 1 panel C
	PCR-based analyses	N/A	N/A
	Western blotting	The iPSC-cardiomyocytes showed robust expression of MRAS	Figure 1 panel M
Off-target nuclease activity analysis	PCR across top 5 predicted top likely off-target sites, Sanger sequencing	The iPSC line showed no off-target modifications in the top 5 predicted off-target regions	Figure 1 panel E, Sanger sequencing data available with the author
Specific pathogen-free status	Mycoplasma	The iPSC line was tested negative for the presence of Mycoplasma, assessed by MycoALERT PLUS Mycoplasma Detection Kit (Lonza)	Not shown but available with the author
Multilineage differentiation potential	Embryoid body formation	The iPSC line demonstrated an ability to differentiate into derivatives of all 3 germ layers	Figure 1 panel I
Donor screening (OPTIONAL)	HIV 1 + 2 Hepatitis B, Hepatitis C	Negative	Not shown but available with the author
Genotype - additional histocompatibility info (OPTIONAL)	Blood group genotyping	N/A	N/A
	HLA tissue typing	HLA typed Class I and Class II	Not shown but available with the author

Table 6: Reagents details

Antibodies and stains used for immunocytochemistry/flow-cytometry			
	Antibody	Dilution	Company Cat # and RRID
Pluripotency Markers	Human anti-OCT-3/4-PE	1:50	Miltenyi Biotec, RRID:AB_2784442
Pluripotency Markers	Mouse anti-OCT-3/4-PE	1:50	BD Biosciences, RRID: AB_1645318
Pluripotency Markers	Mouse anti-NANOG	1:100	Thermo Fisher Scientific, RRID:AB_2536677
Pluripotency Markers	Mouse anti-TRA-1-60	1:200	Abcam, RRID:AB_778563
Pluripotency Markers	Mouse anti-TRA-1-60-Alexa488	1:50	BD Biosciences, RRID:AB_1645379
Differentiation Markers	Rabbit anti-AFP	1:100	DAKO, RRID:AB_2650473
Differentiation Markers	Mouse anti- α -SMA	1:100	Sigma-Aldrich, RRID:AB_476701
Differentiation Markers	Rabbit anti-Tubulin-beta-3	1:2,000	Biolegend, RRID:AB_2728521
Differentiation Markers	Mouse anti- α -actinin	1:1,000	Sigma-Aldrich, RRID:AB_476766
Differentiation Markers	Rabbit anti-MLC2V	1:200	Proteintech, RRID:AB_2147453
Signalling Pathway	Rabbit anti-MRAS	1:1,000	Proteintech, RRID:AB_10950895
Signalling Pathway	Mouse anti-Vinculin	1:1,000	Sigma-Aldrich, RRID:AB_477629
Secondary antibodies	Alexa488 goat anti-rabbit	1:1,000	Thermo Fisher Scientific, RRID:AB_143165
Secondary antibodies	Alexa555 donkey anti-mouse	1:1,000	Thermo Fisher Scientific, RRID:AB_2536180
Secondary antibodies	HPR donkey anti-rabbit	1:8,000	Sigma Aldrich, RRID:AB_2722659
Secondary antibodies	HPR donkey anti-mouse	1:8,000	Sigma Aldrich, RRID:AB_772210
Nuclear stain	Hoechst33342	8.1 μ M	Thermo Fisher Scientific, # H3570
Site-specific nuclease			
Nuclease information	Hifi SpCas9	IDT SpCas9 Hi-Fi v.3	

Delivery method	Nucleofection	4D Amaxa Nucleofector system (Lonza, program CA-137), and P3 Primary Cell 4D-Nucleofector X Kit (Lonza)
Selection/enrichment strategy	N/A	N/A
Primers and Oligonucleotides used in this study		
	Target	Forward/Reverse primer (5'-3')
Genotyping	PCR specific for MRAS exon 2	ATTCCACATGTCTTGCTGCC/ TTCCTGATCCTCCCCATCT
RT-PCR	PCR specific for MRAS transcript exon 1 – exon 3	ATTCGAAGGGAATGCAGCTA/ TGACGGAGTAGACGATGAGG
gRNA oligonucleotide/crRNA sequence	MRAS exon 2	TCTGGAAAACTGGATGGTG
Genomic target sequence	Including PAM and other sequences likely to affect UCN activity	GRCh37 chr3:138091809-138091831
Bioinformatic gRNA on- and off-target binding prediction tool used, specific sequence/outputs link(s)	CRISPOR	http://crispor.tefor.net/crispor.py?batchId=UBsbumBMnW TcE9QneYEB
Primers for top off-target mutagenesis predicted site sequencing (for all CRISPR/Cas9, ZFN and TALENs)	OT1 - F&R OT2 - F&R OT3 - F&R OT4 - F&R OT5 - F&R	GGAGCCCTCTAGCCTGAAAA/ GCGGCTACTCCCTTTGATG AAGTCTACACACTCAGCCGA/ GGCCACCCCTAAAGATTCT ACCGGATCTGCTCTTGTAAG/ GGACTGAGCCTAAGTTCTCCA CCGATAACATTTAAGGCAAAGC/ TCTTCACGCAACCCTCTCTT ACAGTTCTGTCCCTAAGCCC/ TAAGACGACTGAGCTCCTGG
ODNs/ molecules used as templates for HDR-mediated site-directed mutagenesis.	no modifications	IDT-HDR T*A*CAAGCTGG TGGTGGTGGG GGATGGGGTT GTGGGCAAAA GTGCACTCAC CATCCAGTTT TTCCAGAAGA TCTTTGTGCC TGA CTATG*A*C

6 Generation of a genetically-modified induced pluripotent stem cell line harboring an oncogenic gene variant KRAS p.G12V

Title: Generation of a genetically-modified induced pluripotent stem cell line harboring an oncogenic gene variant KRAS p.G12V

Alexandra Viktoria Busley^{1,2,3}, Mandy Kleinsorge^{1,4}, Lukas Cyganek^{1,2, 3*}

¹Stem Cell Unit, Clinic for Cardiology and Pneumology, University Medical Center Göttingen, Göttingen, Germany; ²DZHK (German Center for Cardiovascular Research), partner site Göttingen, Germany; ³Cluster of Excellence "Multiscale Bioimaging: from Molecular Machines to Networks of Excitable Cells" (MBExC), University of Göttingen, Germany & Hertha Sponer College; ⁴Institute of Health in der Charité (BIH), Center of Biological Design, Berlin, Germany

6.1 Abstract

Activating *KRAS* codon 12 gene variants are known to cause severe RAS/MAPK and PI3K-AKT signalling pathway hyperactivity and are frequently involved in the development of various carcinomas. Here, we describe the generation of a human iPSC line harboring the common oncogenic *KRAS* p.G12V variant by using CRISPR/Cas9 technology. The established *KRAS*^{G12V} iPSC line allows the study of oncogenic *KRAS*-induced signalling dysregulation and its impact on cell physiology in various iPSC-derived cell types and tissues. Furthermore, it might serve as a powerful platform for drug and toxicity screenings to identify new chemotherapeutic drugs.

Table 7: Resource Table

Unique stem cell line identifier	UMGi014-C-2 clone 64 https://hpscereg.eu/cell-line/UMGi014-C-2
Alternative name(s) of stem cell line	isWT1-KRAS-G12V.64
Institution	University Medical Center Göttingen, Germany
Contact information of the reported cell line distributor	Lukas Cyganek, lukas.cyganek@gwdg.de
Type of cell line	iPSC
Origin	human
Additional origin info <i>(applicable for human ESC or iPSC)</i>	Age: 31 Sex: male Ethnicity: Caucasian
Cell Source	Human iPSC line UMGi014-C clone 14 (isWT1.14) generated from skin fibroblasts of a healthy donor
Method of reprogramming	Non-integrating Sendai virus

Clonality	Clonal isolation was performed by automated single cell dispensation using CellenOne (Cellenion/Scienion)
Evidence of the reprogramming transgene loss (including genomic copy if applicable)	RT-PCR
The cell culture system used	Feeder-free and serum-free culture conditions with Matrigel (growth factor reduced, BD Biosciences) and StemMACS iPS-Brew XF medium (Miltenyi Biotec)
Type of the Genetic Modification	Induced mutation
Associated disease	Oncogenic gene variant associated, among others, with lung carcinoma, pancreatic carcinoma, colorectal carcinoma, thyroid carcinoma, juvenile myelomonocytic leukemia, acute myeloid leukemia, neoplasm of the ovary and neoplasm of the large intestine
Gene/locus	KRAS (NM_004985.5): c.35G>T / p.Gly12Val (ClinVar: VCV000012583.18)
Method of modification / user-customisable nuclease (UCN) used, the resource used for design optimisation	CRISPR/Cas9
User-customisable nuclease (UCN) delivery method	Nucleofection of RNPs
All double-stranded DNA genetic material molecules introduced into the cells	N/A
Analysis of the nuclease-targeted allele status	Sanger sequencing of the targeted locus
Method of the off-target nuclease activity prediction and surveillance	Sanger sequencing of the top 5 predicted off-targets
Descriptive name of the transgene	N/A
Eukaryotic selective agent resistance cassettes (including inducible, gene/cell type-specific)	N/A
Inducible/constitutive expression system details	N/A
Date archived/stock creation date	28th February 2020
Cell line repository/bank	Biobank of the University Medical Center Göttingen
Ethical/GMO work approvals	Ethics Committee of the University Medical Center Göttingen, approval number: 10/9/15
Addgene/public access repository recombinant DNA sources' disclaimers (if applicable)	N/A

6.2 Resource utility

Activating *KRAS* codon 12 gene variants are known to cause severe RAS/MAPK and PI3K-AKT signalling pathway hyperactivity and are frequently involved in the development of various carcinomas.^{121,122} Human iPSCs harboring the oncogenic gene variant *KRAS*^{G12V} provide a powerful tool to study the *KRAS*-dependent pathophysiology in different cell types and tissues.

6.3 Resource Details

To establish a human iPSC line harboring the common oncogenic *KRAS*^{G12V} variant, we used CRISPR/Cas9 technology to insert the respective gene variant into a well-characterized wild type iPSC line,¹¹³ previously generated by integration-free reprogramming of skin fibroblasts from a healthy donor (Figure 17A). The ribonucleoprotein-based CRISPR/Cas9 complex targeting the *KRAS* exon 2 gene locus was combined with a single-stranded oligonucleotide harboring the base pair exchange (c.35G>T / p.G12V) and serving as a template for homology-directed repair (Figure 17B). In addition, three silent mutations were incorporated into the donor oligo to prevent re-cleavage by Cas9. After transfection, iPSCs were singularized and individual clones were screened for successful editing. Upon screening of 86 clones, we identified clones carrying the heterozygous *KRAS*^{G12V} gene variant (Figure 17C). Notably, no iPSC clones with a homozygous *KRAS*^{G12V} insertion were detected, suggesting that these clones may not be able to survive. Molecular karyotyping of the *KRAS*^{G12V} iPSCs confirmed chromosomal stability after genome editing and passaging (Figure 17D). Furthermore, sequencing of the top 5 predicted off-targets revealed no obvious off-target modifications by genome editing (Figure 17E). The generated *KRAS*^{G12V} iPSCs displayed a typical human stem cell-like morphology (Figure 17F). Flow cytometric analysis of the pluripotency marker OCT3/4 revealed a homogeneous population of pluripotent cells in *KRAS*^{G12V} iPSC cultures (Figure 17G). In addition, a robust expression of the key pluripotency markers OCT3/4, NANOG, and TRA-1-60 was detected in the CRISPR-edited iPSCs by immunocytochemistry (Figure 17H). To further demonstrate pluripotency, spontaneous differentiation of *KRAS*^{G12V} iPSCs into all three germ layers was performed by embryoid body formation and cell-fate identity was assessed by immunocytochemistry. Differentiated cultures expressed endodermal-specific alpha fetoprotein, mesodermal-specific α -smooth muscle actin, and ectodermal-specific β -III-tubulin (Figure 17I).

Since activating *KRAS* gene variants are associated with hyperactivity of the RAS/MAPK signalling pathway,¹²¹ we examined the pathway activity in wild type and *KRAS*^{G12V} iPSC cultures. Here, the *KRAS*^{G12V} iPSCs showed a trend toward increased levels of phosphorylated ERK compared to wild type cells, both in unstimulated culture conditions and upon stimulation with 20% fetal bovine serum

Generation of a genetically-modified induced pluripotent stem cell line harboring an oncogenic gene variant
KRAS p.G12V
(Figure 17J). In contrast, protein expression levels of RAS GTPases including KRAS (the pan-RAS antibody recognizes KRAS, HRAS, and NRAS) were unchanged between *KRAS*^{G12V} and wild type iPSCs, indicating that the gene variant does not affect protein stability or degradation. Consistent with signalling hyperactivity, *KRAS*^{G12V} has been associated with higher proliferation rates in multiple cell types.¹²² By examining the proliferation of iPSC cultures, we observed an increased proliferation rate of *KRAS*^{G12V} iPSCs compared to its isogenic wild type cells (Figure 17K).

In conclusion, the established *KRAS*^{G12V} iPSC line allows the study of oncogenic KRAS-induced RAS/MAPK signalling dysregulation and its impact on cell physiology in various iPSC-derived cell types and tissues. Furthermore, this iPSC line and its iPSC-derivatives offer a unique opportunity for high-throughput drug screening in physiologically relevant cells to assess drug efficacy and toxicity.

6.4 Materials and Methods

Genome editing and culture of human iPSCs

Wild type iPSC line UMGi014-C clone 14 (isWT1.14) was generated from dermal fibroblasts from a male donor using the integration-free Sendai virus and was described previously.¹¹³ Human iPSCs were cultured in feeder-free and serum-free culture conditions in StemMACS iPS-Brew XF medium (Miltenyi Biotec) or StemFlex medium (Thermo Fisher Scientific) on Matrigel-coated (growth factor reduced, BD Biosciences) plates in a humidified incubator at 37°C and 5% CO₂. Cells were passaged every 5-6 days with Versene solution (Thermo Fisher Scientific). For editing, the CRISPR/Cas9 ribonucleoprotein complex was assembled by mixing of the Alt-R CRISPR-Cas9 crRNA and the Alt-R CRISPR-Cas9 tracrRNA (preassembled in a 1:1 ratio) with the Alt-R Hifi SpCas9 Nuclease 3NLS (IDT DNA Technologies) at 1:3 molar ratio together with the single-stranded oligonucleotide for homology-directed repair in nucleofector solution. Nucleofection was performed with 2×10⁶ iPSCs using the 4D Amaxa Nucleofector system (Lonza; program CA-137) and the P3 Primary Cell 4D-Nucleofector X Kit (Lonza) according to manufacturer's instructions. Following nucleofection, iPSCs were replated into a Matrigel-coated well of a 6-well plate containing StemFlex medium supplemented with 2 μM Thiazovivin and 100 U/ml penicillin and 100 μg/ml streptomycin (Thermo Fisher Scientific). After 3 days, transfected iPSCs were singularized using the single cell dispenser CellenOne (Cellenion/Scienion) in StemFlex medium on Matrigel-coated 96-well plates. Successful genome editing was identified by Sanger sequencing and the *KRAS*^{G12V} isogenic iPSC line UMGi014-C-2 clone 64 (isWT1-KRAS-G12V.64) was expanded and maintained in StemMACS iPS-Brew XF medium on Matrigel-coated plates for at least five passages prior to molecular karyotyping, pluripotency characterization and differentiation

experiments. Proliferation was analyzed using the Incucyte S3 (Sartorius) and quantified using the Gompertz growth function in Prism 9 (GraphPad).

Pluripotency characterization of human iPSCs

Pluripotency analysis was performed via immunocytochemistry and flow cytometry, as previously described.⁴⁵ For embryoid body formation, 5×10^6 iPSCs were combined with 2.5×10^6 mouse embryonic fibroblasts and seeded into a 96-well U plate containing hES medium (DMEM-F12, 15% Knockout Serum Replacement, 1% MEM Non-Essential Amino Acids Solution, 1% β -Mercaptoethanol, 2 μ M Thiazovivin). After 24h, medium was exchanged to EB-Diff medium (IMDM with Glutamax, 20% fetal bovine serum, 1% MEM Non-Essential Amino Acids Solution, 450 μ M 1-thioglycerol). Eight days post-differentiation, embryoid body were transferred to Matrigel-coated coverslips and cultured for 8 days. For molecular karyotyping, genomic DNA of iPSC clones was sent for genome-wide analysis via Illumina BeadArray (Life&Brain, Germany). Digital karyotypes were analyzed in GenomeStudio v2.0 (Illumina) with the CNV partition algorithm 3.2.0 (default settings). Copy number events were reported if larger than 3.5×10^5 bps and 1×10^6 bps for loss of heterozygosity. For off-target screening, the top 5 predicted off-target regions for the respective guide RNA ranked by the CFD off-target score using CRISPOR were analyzed by Sanger sequencing.

Western blot analysis of human iPSCs

For analysis signalling activity, iPSCs were stimulated with 20% fetal bovine serum. After 15 minutes, cells were pelleted by scratching and collected in M-PER cell lysis buffer (Thermo Fisher Scientific), and snap-frozen in liquid nitrogen. Protein containing supernatant was collected by centrifugation and protein concentration was determined by BCA assay (Thermo Fisher Scientific). Protein separation was conducted by SDS-Page using nitrocellulose membranes (Bio-Rad). Membranes were blocked in 5 \times PVP solution (10 \times TBS, 10% PVP-30K, 15% PVP-12K, 0.5% Tween-20, 1% Tween-80, 0.02% 1,1,1-Trichloro-2-methyl-2-propanol-hemihydrat) and incubated with primary and secondary HRP-coupled antibodies in 1x PVP solution. Signals were detected upon application of SuperSignal West Femto Maximum Sensitivity Substrate (Thermo Fisher Scientific). Image acquisition was performed with the ChemiDoc XRS+ (Bio-Rad) using the high-resolution mode.

6.5 Acknowledgements

We thank Laura Cyganek, Yvonne Hintz, Nadine Gotzmann, Lisa Schreiber, and Yvonne Wedekind (Stem Cell Unit, University Medical Center Göttingen) for excellent technical assistance. This work was supported by the German Research Foundation (DFG): project number 417880571 to L.C.; project number 501985000 to L.C.; project number 193793266, Collaborative Research Centre 1002, S01 to L.C.; project number 390729940, Germany's Excellence Strategy - EXC 2067/1 to A.V.B. and L.C.; by the Else Kröner Fresenius Foundation: project number 2019_A75 to L.C.; and by the German Federal Ministry of Education and Research (BMBF)/ German Center for Cardiovascular Research (DZHK) to L.C.

Generation of a genetically-modified induced pluripotent stem cell line harboring an oncogenic gene variant
KRAS p.G12V

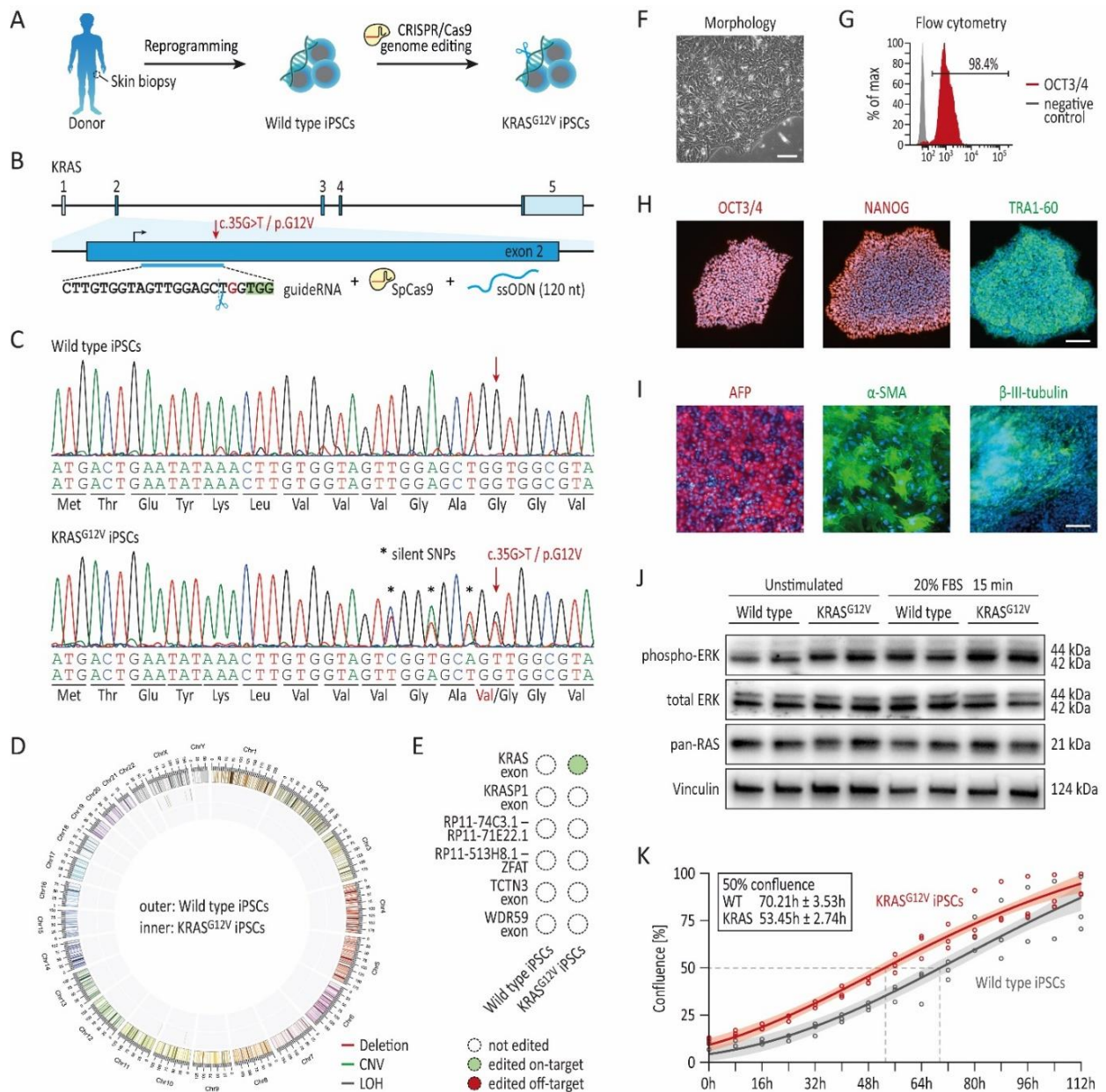


Figure 17: Generation of a CRISPR-edited *KRAS*^{G12V} iPSC line.

(A) Schematic demonstration of how somatic skin biopsies from a healthy donor are reprogrammed into iPSCs and edited via CRISPR/Cas9 to introduce a pathogenic mutation. **(B)** Depiction of the CRISPR/Cas9 editing strategy to introduce the *KRAS*^{G12V} mutation (c.35G>T) using a target-specific guide RNA in combination with a SpCas9. **(C)** Sanger Sequencing of the original WT and the CRISPR-edited iPSC line proving the heterozygous introduction of *KRAS*^{G12V} and three additional silent SNPs. **(D)** Molecular karyotyping using genome-wide microarray analysis revealed no chromosomal abnormalities and genome stability post-editing. **(E)** No editing was observed while screening the top five predicted off-target sites. **(F)** *KRAS*^{G12V} iPSC line showed typical stem-cell-like morphology. Scale bar: 100 μ m. **(G)**, **(H)** Pluripotency was assessed via flow cytometry (OCT3/4) and immunocytochemistry staining for defined markers like OCT3/4, NANOG, and TRA-1-60; nuclei were stained with Hoechst33342. Scale bar: 100 μ m. **(I)** Embryoid body formation proved iPSCs retain their capacity to differentiate in all three germ layers: α -smooth muscle actin (mesoderm), α -fetoprotein (endoderm), and β -III-tubulin (ectoderm). **(J)** Western blot analysis to study RAS/MAPK activity in *KRAS*^{G12V} iPSCs stimulated with 20% FBS for 15 min compared to WT iPSCs. Vinculin served as a loading control. **(K)** Proliferation assay of WT and *KRAS*^{G12V} iPSC was assessed for

Generation of a genetically-modified induced pluripotent stem cell line harboring an oncogenic gene variant
KRAS p.G12V
around 112 hours. Proliferation was recorded using the Incucyte S3 (Sartorius). Analysis was performed with
default settings using the Incucyte software.

Table 8: Characterization and validation of KRAS^{G12V} iPSC line.

Classification (optional <i>italicized</i>)	Test	Result	Data
Morphology	Photography	The iPSC line displayed a typical human stem cell-like morphology	Figure 1 panel F
Pluripotency status evidence for the described cell line	Qualitative analysis (Immunocytochemistry)	The iPSC line showed robust expression of OCT3/4, NANOG and Tra1-60	Figure 1 panel H
	Quantitative analysis (Flow cytometry)	The iPSC line showed >98% of positive cells for OCT3/4 expression.	Figure 1 panel G
Karyotype	Karyotype, genome-wide analysis via Illumina BeadArray (Infinium Global Screening Array-24 Kit)	46XY, Resolution ~ 654,027 fixed markers	Figure 1 panel D
Genotyping for the desired genomic alteration/allelic status of the gene of interest	PCR across the edited site	The iPSC line showed a target-specific heterozygous insertion of the gene variant, assessed by Sanger sequencing	Figure 1 panel C
	Evaluation of the - (homo-/hetero-/hemi-) zygous status of introduced genomic alteration(s)	The iPSC line showed a target-specific heterozygous insertion of the gene variant, assessed by Sanger sequencing	Figure 1 panel C
	Transgene-specific PCR (when applicable)	N/A	N/A
Verification of the absence of random plasmid integration events	PCR/Southern	N/A	N/A
Parental and modified cell line genetic identity evidence	HLA typing	Identity of the iPSC line was verified by HLA typing.	Not shown but available with the author

Mutagenesis / genetic modification outcome analysis	Sequencing (genomic DNA PCR product)	The iPSC line showed a target-specific heterozygous insertion of the gene variant, assessed by Sanger sequencing	Figure 1 panel C
	PCR-based analyses	N/A	N/A
	Western blotting	The iPSC line showed robust expression of KRAS, detected by pan-RAS	Figure 1 panel J
Off-target nuclease activity analysis	PCR across top 5 predicted top likely off-target sites, Sanger sequencing	The iPSC line showed no off-target modifications in the top 5 predicted off-target regions	Figure 1 panel E, Sanger sequencing data available with the author
Specific pathogen-free status	Mycoplasma	The iPSC line was tested negative for the presence of Mycoplasma, assessed by MycoALERT PLUS Mycoplasma Detection Kit (Lonza)	Not shown but available with the author
Multilineage differentiation potential	Embryoid body formation	The iPSC line demonstrated an ability to differentiate into derivatives of all 3 germ layers.	Figure 1 panel I
Donor screening (OPTIONAL)	HIV 1 + 2 Hepatitis B, Hepatitis C	Negative	Not shown but available with the author
Genotype - additional histocompatibility info (OPTIONAL)	Blood group genotyping	N/A	N/A
	HLA tissue typing	HLA typed Class I and Class II	Not shown but available with the author

Table 9: Reagents details

Antibodies and stains used for immunocytochemistry/flow-cytometry			
	Antibody	Dilution	Company Cat # and RRID
Pluripotency Markers	Human anti-OCT-3/4-PE	1:50	Miltenyi Biotec, RRID:AB_2784442
Pluripotency Markers	Human anti-OCT-3/4-PE	1:50	BD Biosciences, RRID: AB_1645318
Pluripotency Markers	Mouse anti-NANOG	1:100	Thermo Fisher Scientific, RRID:AB_2536677
Pluripotency Markers	Mouse anti-TRA-1-60	1:200	Abcam, RRID:AB_778563
Differentiation Markers	Rabbit anti-AFP	e.g. 1:100	DAKO, RRID:AB_2650473
Differentiation Markers	Mouse anti- α -SMA	e.g. 1:100	Sigma-Aldrich, RRID:AB_476701
Differentiation Markers	Rabbit anti-Tubulin-beta-3	e.g. 1:2,000	Biolegend, RRID:AB_2728521
Signalling Pathway	Rabbit anti-phospho-ERK	1:1,000	Cell signalling, RRID:AB_331646
Signalling Pathway	Rabbit anti-ERK	1:1,000	Cell signalling, RRID:AB_330744
Signalling Pathway	Mouse anti-pan-RAS	1:1,000	Merck Millipore, RRID:AB_2121151
Signalling Pathway	Mouse anti-Vinculin	1:1,000	Sigma-Aldrich, RRID:AB_477629
Secondary antibodies	Alexa488 goat anti-rabbit	1:1,000	Thermo Fisher Scientific, RRID:AB_143165
Secondary antibodies	Alexa555 donkey anti-mouse	1:1,000	Thermo Fisher Scientific, RRID:AB_2536180
Secondary antibodies	HPR donkey anti-rabbit	1:8,000	Sigma Aldrich, RRID:AB_2722659
Secondary antibodies	HPR donkey anti-mouse	1:8,000	Sigma Aldrich, RRID:AB_772210
Nuclear stain	Hoechst33342	8.1 μ M	Thermo Fisher Scientific, # H3570
Site-specific nuclease			
Nuclease information	Hifi SpCas9	IDT SpCas9 Hi-Fi v.3	
Delivery method	Nucleofection	4D Amaxa Nucleofector system (Lonza, program CA-137), and P3 Primary Cell 4D-Nucleofector X Kit (Lonza)	

Selection/enrichment strategy	N/A	N/A
Primers and Oligonucleotides used in this study		
	Target	Forward/Reverse primer (5'-3')
Genotyping	PCR specific for KRAS exon 2	GATACACGTCTGCAGTCAACT/ TGTATCAAAGAATGGTCCTGCAC
gRNA oligonucleotide/crRNA sequence	KRAS exon 2	CTTGTGGTAGTTGGAGCTGG
Genomic target sequence	Including PAM and other sequences likely to affect UCN activity	GRCh37 chr12:25398281-25398303
Bioinformatic gRNA on- and -off-target binding prediction tool used, specific sequence/outputs link(s)	CRISPOR	http://37.187.154.234/crispor.py?batchId=BPeF9sWfy4NLQjNCu9vU
Primers for top off-target mutagenesis predicted site sequencing (for all CRISPR/Cas9, ZFN and TALENs)	OT1 - F&R OT2 - F&R OT3 - F&R OT4 - F&R OT5 - F&R	GGTTTAGATGAAGCTGGGCC/ AGCTGTATCGTCAAGACTT TCTGCACCCACATGATAACCT/ AAAACAAAAGCCACCCCTCC GTACCATCTCTCCCACCCAG/ GAGTGGCAGGTGGGAAATTC TTGAGGGCTGAATCCAAGGT/ AAGCTTGCTGAGACAACCTG CAGGCAGGAGATGAGGAACA/ CATGAAGATCCGCACAGAGG
ODNs/plasmids/RNAs molecules used as templates for HDR-mediated site-directed mutagenesis.	no modifications	IDT-HDR ATTATTTTA TTATAAGGCC TGCTGAAAAT GACTGAATAT AAACTTGTGG TAGTCGGTGC AGTTGGCGTA GGCAAGAGTG CCTTGACGAT ACAGCTAATT CAGAATCATT TTGTGGACGA

7 General discussion

Although RASopathies affect a limited group of patients, the numbers may be underestimated due to the difficulty of diagnosis. Therefore, intensive research to identify and elucidate additional disease-causing mutations and the corresponding individual pathomechanisms will be of great benefit to the RASopathy- and the cardiovascular field. At the start of this work, there was a growing understanding of the molecular mechanism behind dominant LZTR1 variants in NS patients, but few studies of recessive variants. Using our expertise in somatic tissue reprogramming, iPSC culture, cardiac differentiation and CRISPR/Cas9 editing, we reprogrammed skin biopsies from a recessive LZTR1 patient diagnosed with NS and early-onset HCM into patient-specific iPSCs. The main aim here was to model the disease using iPSC-CMs to understand the cardiac pathology induced by the *LZTR1*^{L580P} mutation. In addition, we generated isogenic control lines by correcting the disease-causing mutations using CRISPR/Cas9 editing. In two additional studies, we generated iPSC lines to study the NS-associated mutation *MRAS*^{G23V} and a cancer-associated mutation *KRAS*^{G12V}. Our aim was to validate whether MRAS-mutant iPSC-CMs recapitulate the phenotype of an NS patient with a severe form of HCM²³ and to further investigate the role of MRAS in cardiac pathology. This is of particular interest, as MRAS was identified as one of the major interaction partners of LZTR1, with significant impact on cardiomyocytes. Furthermore, we generated a *KRAS*^{G12V} iPSC line since this mutation has previously been reported to cause immense hyperactivation of the RAS/MAPK pathway in cancer cells. With this iPSC line, we aimed to study the cardiac effect of continuous RAS/MAPK hyperactivation over time and to compare it to the signalling activity levels in NS patients.

7.1 Noonan syndrome – focus on LZTR1

Increased RAS/MAPK signalling is one of the major causes for RASopathies and further clinically related disorders affecting development and growth. The knowledge gained over the last five years has further shed light on previously unknown disease-causing variants such as the existence of recessive Noonan syndrome, new disease-associated genes, and the underlying pathological signalling network.³² Although mutations within 11 prominent genes (*PTPN11*, *KRAS*, *SOS1*, *RAF1*, *SHOC2*, *NRAS*, *CBL*, *BRAF*, *MAP2K1*, *RIT1* and *RASA2*) may account for 80% of all NS cases, around 20% of cases remain unresolved.¹²³ Following hypothesis-free genome-wide sequencing approaches, new disease-causing genes were identified: *SOS2* known to be closely involved in RAS/MAPK signalling, one *de novo* mutation in *PPPC1B*¹²⁴ and further variants in *LZTR1*, a gene previously not known to be directly associated with the RAS/MAPK-signalling pathway.¹²³

Until then, *LZTR1* had only been described as a tumor suppressor gene belonging to the BTB Kelch superfamily. *LZTR1* has also been implicated in apoptosis, and - as it is the case for the BTB Kelch family, in ubiquitination as an adaptor protein that delivers substrates to CUL3 ligases.^{38,125} In terms of subcellular localization, studies suggest that *LZTR1* is associated with the Golgi apparatus.³⁸ A few years later, further insights into the functional role of *LZTR1*, also in the context of NS, were published. Studies showed a strong association between mutated *LZTR1* and cancer predisposition or developmental disorders like NS. Furthermore, it was shown that homozygous loss of *Lztr1* was embryonically lethal whereas a heterozygous variant induced a NS-like phenotype in mice including hypertrophy.⁴⁴ Still, open questions remain about the potential interaction partners of *LZTR1* which were predicted to be *KRAS*, *NRAS*, *HRAS*, *MRAS* or *RIT1*, depending on the studied cell- or tissue type. Besides these RAS GTPases, *EGFR* and *AXL* were recently identified as potential new *LZTR1* substrates.^{39,42,44,126} Moreover, the exact localization of *LZTR1* is still under debate, with some studies showing its association with the Golgi apparatus, while others claimed a co-localization with recycling endosomes or lysosomes.^{38,40,126} As many of the above-mentioned information about *LZTR1* were identified using overexpression experiments in HEK293T cells, HeLa cells, or mice, it is highly relevant to study the pathogenic effect of *LZTR1* in a humanized model to particularly capture potential differences in protein structure, localization, and function. In particular, the development of specific symptoms as HCM as a consequence of the pathogenic effect of elevated RAS activity, cannot be evaluated in artificial cellular overexpression systems. To date, all detected missense variants in *LZTR1* associated with NS were inherited in a dominant manner and clustered in the N-terminal domain of the protein, the so-called Kelch domain. Later in 2018, the first biallelic variant was identified. It is responsible for the development of a recessive form of NS in 12 families.³⁴ On the basis of the studies of Motta et al., the different pathological effects of dominant versus recessive *LZTR1* mutations were clarified. They

performed a functional and biochemical characterization of the dominant NS mutations. They showed that they do not specifically affect the stability, localization or binding of LZTR1 to CUL3. In fact, in contrast to missense mutations found in recessive NS, overexpression of dominant variants led to an increase in MAPK activity upon stimulation. In addition, dominant mutations were predominantly located on the surface of the Kelch motif, which is essential for proper substrate binding. In summary, dominant *LZTR1* mutations prevent substrate binding and subsequently impair substrate ubiquitination and degradation, leading to hyperactive signalling activity.⁴⁰ Since little is known about recessive LZTR1 variants, part of this thesis focused on uncovering the pathological role of a recessive *LZTR1*^{L580P} variant, both at the molecular level and in cardiac physiology.

7.2 Recessive LZTR1 mutation and its role in cardiac pathology

In contrast to dominant mutations, recessive *LZTR1* mutations are distributed throughout the protein, making it more difficult to determine the functional defect, which is highly dependent on the affected protein domain.⁴⁰ Both autosomal dominant, as well as autosomal recessive variants, are present with a broad clinical spectrum, ultimately resulting in different disease phenotypes. Therefore, the main goal of the study was to investigate the underlying molecular and functional mechanisms that cause the cardiac phenotype in a recessive *LZTR1* patient.

In this work, we obtained skin fibroblasts from a patient who was diagnosed with NS carrying a recessive mutation within the *LZTR1* gene (p.L580P). The patient presented with early-onset HCM and typical NS facial features. This particular variant has not been described before. After reprogramming the skin fibroblasts, we obtained patient-derived iPSCs and differentiated them into functional ventricular-like cardiomyocytes. We combined *in vitro* disease modelling and CRISPR/Cas9 application to investigate the cellular and functional properties of patient-derived and CRISPR-corrected iPSC-CMs.

First, we designed a target-site specific crRNA using the bioinformatics tool CRISPOR¹²⁷ and a repair template containing the desired corrected variant. After successful gene correction by introducing the above-mentioned compounds in addition to the Cas9 protein into patient's iPSC via nucleofection, all cell lines including patient-, and the new heterozygously- and homozygously- corrected iPSCs (*LZTR1*^{L580P}, *LZTR1*^{corr-het}, *LZTR1*^{corr-hom}) were characterized. All cell lines expressed pluripotency markers (OCT3/4, NANOG, TRA-1-60) as confirmed by immunocytochemistry and flow cytometry analysis. It is noteworthy that the karyotype showed an increased level homozygosity due to the consanguinity of the patient's parents. The next step was the differentiation of WT-, patient- and heterozygous/homozygous corrected iPSC into ventricular-like cardiomyocytes using the differentiation protocol published by Kleinsorge et al.⁴⁹ and the subsequent analysis of their functional and molecular properties. Initially, proteomic analysis was conducted with all four lines differentiated

into cardiomyocytes, fixed at day 60 after the start of differentiation, to identify potential common or distinct disease signatures. A significant accumulation of RAS proteins was observed, in particular MRAS and RIT1, and to a lesser extent KRAS, HRAS, or NRAS, although all of these proteins were robustly expressed in iPSC-CM. This result is consistent with the findings of Castel et al. who suggested that RIT1 is the most prominent interaction partners of LZTR1.⁴³ In addition, in homozygous *Lztr1* knockout mice, RIT1 protein levels were elevated in different organs including the heart compared to HRAS, KRAS or NRAS.⁹⁹ In contrast, other studies showed selective binding of KRAS, HRAS or NRAS proteins.^{39,42,44} Consistent with the published data related to the truncating *LZTR1* variant, our data suggests that RAS GTPase MRAS is a crucial LZTR1 substrate with a very high affinity to LZTR1 compared to other RAS proteins, indicating a key role of MRAS in driving the NS-associated cardiac defects.⁴⁵ There may also be cell- and tissue-specific differences that have an impact on the substrate selectivity of LZTR1. Another interesting candidate that showed higher protein levels in the patient compared to WT-or CRISPR-corrected cells was HSPA2. HSPA2 is so far not known to be a close interaction partner of LZTR1 but it displayed a higher abundance in LZTR1 deficient cells in our previous LZTR1 study⁴⁵, as well as in a RAF1 NS iPSC-CM study⁴⁶, and in iPSC-CMs derived from Fabry disease patients suffering from a lysosomal storage disorder along with HCM and arrhythmias.¹⁰⁰ Interestingly, increased HSPA2 protein levels were identified in HCM tissue and also proven as a suitable marker to distinguish HCM from non-HCM hearts.^{101,102} HSPA2 is known to belong to the group of chaperones that mediate the disaggregation of misfolded proteins or refolding as well as protein degradation via ubiquitination or autophagy.¹⁰¹ We hypothesized that elevated HSPA2 protein levels might be a cardio protective response of hypertrophic iPSC-CMs to compensate for accumulated RAS proteins and the protein polymers induced by *LZTR1*^{L580P}. HSPA2 in this case is supposed to regulate the quality control mechanism for protein degradation.¹⁰¹ In general, the proteomic study revealed pathophysiological changes in protein levels of those who are involved in muscle contraction, metabolism and extracellular matrix composition, all of which are known being affected in hypertrophic hearts.¹⁰⁷

Further cellular phenotyping showed increased cell diameter indicating recapitulation of cardiac hypertrophy. In line with a normalization of the proteomic profiles in CRISPR corrected iPSC-CMs, the cellular enlargement was reverted upon gene correction via CRISPR/Cas9. Another important parameter is sarcomere and myofibril organization which is often used in cardiac disease models to evaluate the cardiac defects. Whereas others could observe myofibrillar disarray in RAF1-patient derived cells^{46,108}, we and others did not see any effect of mutated LZTR1-, BRAF-or PTPN11 on the sarcomeric apparatus^{45,89,90}, confirming that genotypic differences might influence the manifestation of the phenotype.

As we aimed to model the patient's phenotype coming along with HCM and stress-induced arrhythmias, we used established protocols to generate more mature three-dimensional cardiac tissues based on EHM, having the potential to more faithfully recapitulate those symptoms.⁵² Once generated and cultured, these tissues were subjected to optical measurements. These measurements provided further insight into the functional properties of WT and patient iPSC-CMs in a more physiological environment. Analyzing the following parameters: spontaneous beat frequency, beat-to-beat variability, force of contraction, contraction, and relaxation times, no significant phenotypical differences could be detected in the *LZTR1*^{L580P} patient tissues compared to *LZTR1*^{WT}- and CRISPR-corrected tissues. Slight differences in beat frequency, contraction and relaxation times could be observed, however, all patient-derived cell lines, including the CRISPR-corrected ones exhibited higher rates compared to WT, suggesting that these differences can be attributed to cell line-specific differences independent of the *LZTR1* variant. Interestingly, we did not detect arrhythmias in the patient EHM tissues.

Variants within the BTB-BACK domains are thought to induce protein mislocalization and/or impaired CUL3 binding, as well as inappropriate protein dimerization, compared to dominant missense variants, which mainly affect substrate binding affinity. According to the literature mutations within the BTB-BACK domain (*LZTR1*^{V456G}, *LZTR1*^{R466Q}, *LZTR1*^{P520L}, *LZTR1*^{R688C}) cause subcellular mislocalization resulting in a diffuse cytosolic distribution.^{42,44} Similar observations could be made in truncating *LZTR1* variants.⁴⁵ Overexpression of *LZTR1*^{L580P} in WT iPSC-CM not only led to mislocalization, but to an additional protein polymerization, which has not been observed before. However, as expected, substrate binding was unaffected as both MRAS and CUL3 were still able to bind to *LZTR1*^{L580P}. To test whether this was a mutation-specific effect, we overexpressed several BACK1 mutations, some of uncertain significance, in close proximity to the L580P mutation. The phenotype was only observed with the L580P mutation, suggesting a specific dysfunction within the protein structure attributed to the particular localization of L580P in the BACK1 domain. Interestingly, dual-overexpression of WT and mutant *LZTR1* rescued the protein polymerization, suggesting that polymerization only occurs when the mutation is homozygously present. Consistent with this, SPOP proteins, which also act as an adaptor protein for CUL3 (by having just one BTB-BACK domain), were able to form high-order linear oligomers via their BACK domain. In addition, these proteins were present in membrane-less spots, which have been proposed to be hotspots for ubiquitination.¹¹⁰ During the preparation time of this thesis, another interesting study about SPOP proteins and their potential oligomerization properties was published in the context of various cancer types including prostate and endometrial cancer. The authors claim that newly considered mutations in SPOP induced a structural change that leads to an oligomerization, finally resulting in an increased half-time of the protein and elevated ubiquitination

activity.¹²⁸ This might explain why mutated *LZTR1* arranges in the observed polymer confirmation as a compensatory mechanism to cope with accumulated RAS proteins.

Based on the generated data, our proposed model is that LZTR1 dimers cluster in speckles to process the ubiquitination of defined RAS proteins. The role of the different LZTR1 domains is still under debate. Castel et al. claim that dimerization is processed via the BTB1 and BACK1 domain, whereas Steklov et al. demonstrated impaired dimerization upon variants within the BACK 2 domain.^{43,44} Based on our studies, we observed a dimerization in *LZTR1*^{WT} via the BACK2-BACK2 domain that was changed upon the L580P variant inducing a second dimerization site within the BACK1 domain. These observations could be confirmed via *in silico* modelling data. We could further detect monomer as well as trimer formations for other variants and WT, but exclusively in lower-ranked prediction models. When LZTR1 is present as a polymer due to the homozygous mutation, ubiquitination cannot be properly processed due to mislocalization and aberrant protein structure. This leads to the accumulation of active RAS proteins. Consequently, higher abundancies of active MRAS and RIT1 ultimately induce the severe disease phenotype. In addition to the novel insights about LZTR1 dysfunction in NS, we could prove the potential of iPSCs to model human disease and to uncover a novel single variant-dependent molecular pathomechanism for NS related to a recessive *LZTR1* variant. Additionally, the successful application of CRISPR/Cas9 gene correction might be a promising therapeutic strategy in the future, as the correction of only one allele was sufficient to revert the patient's phenotype.

7.3 MRAS-just one LZTR1 interaction partner or is it one of the key players in cardiac hypertrophy?

To evaluate whether MRAS is one out of many RAS GTPases targeted by LZTR1 for degradation, or whether MRAS is a key player in driving the cardiac hypertrophy in NS, we introduced the activating mutation *MRAS*^{G23V}, into an established WT iPSC line. Higgins et al. uncovered this *de novo* variant within the *MRAS* gene upon whole exome sequencing of a 15-year-old NS patient. The mutation was disease-causing and led to the development of a severe form of early-onset HCM. Within this study, they could demonstrate that this mutation affects the GTP-binding site and effector interaction regions of the MRAS protein. As a result, they demonstrated a 40-fold increase in MRAS activation and increased RAS/MAPK activity.²³ In a follow-up study, they examined the pathological effect of *MRAS*^{G23V} in patient-derived iPSC-CMs. They could show that iPSC-CMs were significantly enlarged compared to control cells and exhibited pathological alterations concerning gene expression and signalling comparable to known cardiac hypertrophy characteristics. Both studies confirmed the monogenetic pathogenicity of *MRAS*^{G23V} that could be recapitulated by using patient-derived iPSC-CMs.

Based on these results and the fact that MRAS seemed to be one of the key players in LZTR1-affected hypertrophic iPSC-CMs, we were interested to study its role in cardiac pathology. To do so, we used, CRISPR/Cas9 ribonucleoprotein in combination with a single-stranded oligonucleotide harboring the desired mutation and introduced both into WT iPSCs by nucleofection. Post-transfection single-cell colonies were screened for the desired mutation via Sanger sequencing. Only heterozygous clones carrying the mutation were identified. Screening of multiple clones did not reveal any homozygous clones, which could be due to low editing efficiency or it might indicate that clones with a homozygous mutation did not survive. In line with this, according to the literature, no homozygous *MRAS*^{G23V} mutations have been found as they could be potentially embryonic lethal. As the variant in the case report was present in a heterozygous manner, the heterozygous *MRAS*^{G23V} iPSCs were expanded, and upon proving its pluripotency via immunocytochemistry, flow cytometry, and embryoid body formation, we differentiated them into functional ventricular-like cardiomyocytes. Western blot showed equal expression of MRAS proteins compared to control iPSC-CMs. To prove equal MRAS expression on transcript level compared to control cells, we designed a primer targeting exon 2. Surprisingly, upon Reverse-Transcriptase-PCR (RT-PCR) using complementary DNA (cDNA) of WT and edited iPSC-CMs, we detected the expression of two isoforms. A long isoform including exon 2 and a shorter isoform where exon 2 is missing. As the disease-causing mutation was present in exon 2, the mutation's effect might vary between tissues and highly depend on the expression levels of the different transcripts. Future experiments will involve the examination of MRAS activity, and global proteomics analysis to check if the introduction of the pathogenic *MRAS* mutation is sufficient to cause the disease phenotype *in vitro*

7.4 *KRAS*^{G12V}-induced effect on RAS/MAPK signalling

As Noonan syndrome and other RASopathies are based on a RAS/MAPK hyperactivation, we aimed to generate a iPSC line presented with a continuously hyperactive RAS/MAPK signalling to study its effect on cardiac physiology. *De novo* germline mutation within the *KRAS* gene were identified in five Noonan syndrome patients: V14I, T58I, and D153V. Investigations of recombinant proteins K-Ras V12I and T58I showed a defective GTP hydrolysis and GTPases response, thereby inducing a hypersensitivity to growth factors and consequently an overall dysregulated signal transduction.¹²⁹ As we intended to induce a more severe signalling activation that could also serve as a 'positive control' in comparison to NS patient-derived iPSC lines, we decided to use a cancer-associated *KRAS* variant in codon 12, namely *KRAS* p.G12V. Activating *KRAS* codon 12 mutations are known to cause a strong upregulation of RAS/MAPK signalling, increased tumor growth and low survival compared to the milder NS-associated *KRAS* germline mutations. Generally, *KRAS* is one of the most frequently mutated genes and is

causative for 80% of pancreatic and around 30% of colorectal, cholangial and lung adenocarcinomas.¹³⁰ Upon CRISPR/Cas9 editing, we screened for *KRAS*^{G12V}-positive iPSC clones and could only detect heterozygous introduced SNV mutations. In general, homozygous *KRAS* mutations are present, but less frequent than heterozygous ones. Studies have also shown that the balance between WT and mutant *KRAS* can fundamentally alter its function on RAS/MAPK activity and promote more aggressive tumor growth.^{131,132} Before investigating the mutation's effect on signalling activity and cell physiology, the newly generated iPSC line was characterized and checked for its pluripotency, karyotype, and genotypic status before and after the editing process. No changes before and after the editing could be observed. Preliminary data supported our hypothesis that the *KRAS*^{G12V} mutation induces increased RAS/MAPK activity under basal conditions, and to a much greater extent when cells are stimulated. The results were consistent with the report by Rivard et al. showing increased ERK1/2 activity in the cytoplasm of *KRAS*^{G12V} or *BRAF*^{V600E} intestinal epithelial crypt cells.¹³³ Furthermore, we showed that *KRAS*^{G12V} iPSCs have slightly increased proliferation rates compared to WT cells. Considering the literature, there are controversial results regarding the effect of *KRAS*^{G12V} on proliferation, but this may be highly dependent on the cell type and whether the mutation affects proliferation or cell migration rates.^{25,134} In addition, it is known that mutations in codons 12, 13, and 61 promote RAS to act as an oncoprotein.¹³⁵ This is due to an impaired GTPase activity of mutated RAS protein, keeping these in an active GTP-bound state.¹³⁶ Therefore, we are confident that we will be able to study the effect of constitutively active RAS on the physiology of iPSC-CMs and in the development of HCM and beyond, using this cell line as a suitable positive control.

8 Conclusion & Outlook

In general, preclinical testing of future personalized therapeutic interventions for NS is currently the main goal of ongoing research, as treatment options are still very limited. In this work, we were able to uncover a novel mechanism behind a recessive *LZTR1* missense variant by studying NS patient-derived iPSC and the corresponding genetically corrected isogenic controls. We were able to show that a homozygous L580P mutation causes *LZTR1* polymerization, resulting in impaired ubiquitination and lack of degradation of active RAS proteins. This ultimately leads to cellular and molecular changes such as RAS/MAPK hyperactivation, resulting in NS associated with manifestation of HCM. In addition, a series of NS patient-derived iPSCs (Figure 18) was characterized and two genetically modified cell lines by introducing *KRAS*^{G12V} and *MRAS*^{G23V} mutations were introduced into WT iPSCs to establish a platform for future genotype-phenotype correlation studies *in vitro*. Subsequently, all generated iPSC lines will be differentiated into iPSC-CMs or any other disease-relevant cell type of interest to study the effect of the mutations on signalling activity and cellular physiology. Each of these NS cell lines with different disease-causing mutations, and- based on the patients' clinical data, different degrees of manifested cardiac defects, make a suitable platform to study disease progression, particularly in the heart. The overall aim is to identify unique disease signatures in these patients to potentially cluster them into groups that respond differently to certain treatments/drug applications. In addition, the knowledge gained could facilitate the identification of novel pharmacological treatments based on individual genotypes, either targeting RAS/MAPK directly or other closely interacting pathways based on cross-activation. The use of iPSCs as a model is not only valuable because it can replace immortalized cell lines, but it could also reduce the number of animals needed to test multiple compounds. By using the iPSC platform based on different genetic backgrounds of multiple NS patients for preclinical drug screening or testing of CRISPR/Cas9 gene therapy approaches, we aim to generate clinically relevant data in the future. Our overall goal is to translate the knowledge gained from our iPSC platform into clinical application for the treatment of NS and, in particular, NS-associated HCM.

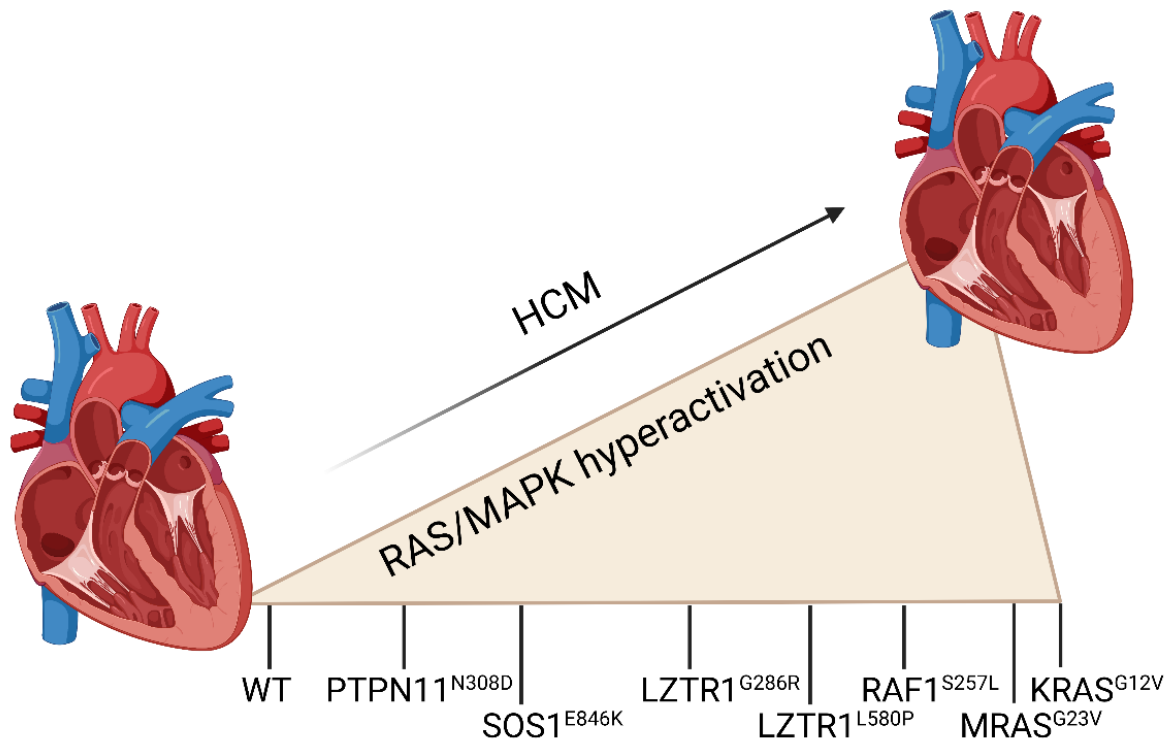


Figure 18: Genotype-phenotype correlation of Noonan syndrome patients.

Proposed correlation between the underlying gene mutations in NS patients, RAS/MAPK hyperactivity and the manifestation of HCM. Within this study LZTR1 p.L580P, KRAS p.G12V and MRAS p.G23V were further studied. Remaining patient-derived iPSCs were characterized and already used for gene correction via CRISPR/Cas9. (unpublished)

9 References

1. Gelb BD, Yohe ME, Wolf C, Andelfinger G. New perspectives on treatment opportunities in RASopathies. *American Journal of Medical Genetics Part C: Seminars in Medical Genetics*. 2022;190:541–560. doi: 10.1002/ajmg.c.32024
2. Linglart L, Gelb BD. Congenital heart defects in Noonan syndrome: Diagnosis, management, and treatment. *American Journal of Medical Genetics Part C: Seminars in Medical Genetics*. 2020;184:73–80. doi: 10.1002/ajmg.c.31765
3. Wilkinson JD, Lowe AM, Salbert BA, Sleeper LA, Colan SD, Cox GF, Towbin JA, Connuck DM, Messere JE, Lipshultz SE. Outcomes in children with Noonan syndrome and hypertrophic cardiomyopathy: a study from the Pediatric Cardiomyopathy Registry. *Am Heart J*. 2012;164:442–448. doi: 10.1016/j.ahj.2012.04.018
4. Hickey EJ, Mehta R, Elmi M, Asoh K, McCrindle BW, Williams WG, Manlihot C, Benson L. Survival implications: hypertrophic cardiomyopathy in Noonan syndrome. *Congenital Heart Disease*. 2011;6:41–47. doi: 10.1111/j.1747-0803.2010.00465.x
5. Östman-Smith I. Beta-Blockers in Pediatric Hypertrophic Cardiomyopathies. *Reviews on Recent Clinical Trials*. 2014;9:82–85. doi: 10.2174/1574887109666140908125158
6. McCallen LM, Ameduri RK, Denfield SW, Dodd DA, Everitt MD, Johnson JN, Lee TM, Lin AE, Lohr JL, May LJ, Pierpont ME, Stevenson DA, Chatfield KC. Cardiac transplantation in children with Noonan syndrome. *Pediatr Transplant*. 2019;23:e13535. doi: 10.1111/petr.13535
7. Noonan JA. Hypertelorism with Turner phenotype. A new syndrome with associated congenital heart disease. *Am J Dis Child*. 1968;116:373–380. doi: 10.1001/archpedi.1968.02100020377005
8. Mendez HM, Opitz JM. Noonan syndrome: a review. *Am J Med Genet*. 1985;21:493–506. doi: 10.1002/ajmg.1320210312
9. Gelb BD, Roberts AE, Tartaglia M. Cardiomyopathies in Noonan syndrome and the other RASopathies. *Prog Pediatr Cardiol*. 2015;39:13–19. doi: 10.1016/j.ppedcard.2015.01.002
10. Roberts AE, Allanson JE, Tartaglia M, Gelb BD. Noonan syndrome. *Lancet*. 2013;381:333–342. doi: 10.1016/S0140-6736(12)61023-X
11. Binder G, Grathwol S, Loeper K von, Blumenstock G, Kaulitz R, Freiberg C, Webel M, Lissewski C, Zenker M, Paul T. Health and quality of life in adults with Noonan syndrome. *J Pediatr*. 2012;161:501-505.e1. doi: 10.1016/j.jpeds.2012.02.043
12. Norrish G, Field E, Mcleod K, Ilina M, Stuart G, Bhole V, Uzun O, Brown E, Daubeney PEF, Lota A, Linter K, Mathur S, Bharucha T, Kok KL, Adwani S, Jones CB, Reinhardt Z, Kaski JP. Clinical presentation and survival of childhood hypertrophic cardiomyopathy: a retrospective study in United Kingdom. *Eur Heart J*. 2019;40:986–993. doi: 10.1093/eurheartj/ehy798
13. Aoki Y, Niihori T, Inoue S, Matsubara Y. Recent advances in RASopathies. *J Hum Genet*. 2016;61:33–39. doi: 10.1038/jhg.2015.114

14. Calcagni G, Adorisio R, Martinelli S, Grutter G, Baban A, Versacci P, Digilio MC, Drago F, Gelb BD, Tartaglia M, Marino B. Clinical Presentation and Natural History of Hypertrophic Cardiomyopathy in RASopathies. *Heart Fail Clin*. 2018;14:225–235. doi: 10.1016/j.hfc.2017.12.005
15. Cerrato F, Pacileo G, Limongelli G, Gagliardi MG, Santoro G, Digilio MC, Di Salvo G, Ardorisio R, Miele T, Calabrò R. A standard echocardiographic and tissue Doppler study of morphological and functional findings in children with hypertrophic cardiomyopathy compared to those with left ventricular hypertrophy in the setting of Noonan and LEOPARD syndromes. *Cardiol Young*. 2008;18:575–580. doi: 10.1017/S104795110800320X
16. Kaltenecker E, Schleihauf J, Meierhofer C, Shehu N, Mkrtchyan N, Hager A, Kühn A, Cleuziou J, Klingel K, Seidel H, Zenker M, Ewert P, Hessling G, Wolf CM. Long-term outcomes of childhood onset Noonan compared to sarcomere hypertrophic cardiomyopathy. *Cardiovasc Diagn Ther*. 2019;9:S299-S309. doi: 10.21037/cdt.2019.05.01
17. Lioncino M, Monda E, Verrillo F, Moscarella E, Calcagni G, Drago F, Marino B, Digilio MC, Putotto C, Calabrò P, Russo MG, Roberts AE, Gelb BD, Tartaglia M, Limongelli G. Hypertrophic Cardiomyopathy in RASopathies: Diagnosis, Clinical Characteristics, Prognostic Implications, and Management. *Heart Fail Clin*. 2022;18:19–29. doi: 10.1016/j.hfc.2021.07.004
18. Aoki Y, Niihori T, Banjo T, Okamoto N, Mizuno S, Kurosawa K, Ogata T, Takada F, Yano M, Ando T, Hoshika T, Barnett C, Ohashi H, Kawame H, Hasegawa T, Okutani T, Nagashima T, Hasegawa S, Funayama R, Nagashima T, Nakayama K, Inoue S, Watanabe Y, Ogura T, Matsubara Y. Gain-of-function mutations in RIT1 cause Noonan syndrome, a RAS/MAPK pathway syndrome. *American journal of human genetics*. 2013;93:173–180. doi: 10.1016/j.ajhg.2013.05.021
19. Tartaglia M, Gelb BD, Zenker M. Noonan syndrome and clinically related disorders. *Best practice & research. Clinical endocrinology & metabolism*. 2011;25:161–179. doi: 10.1016/j.beem.2010.09.002
20. Aoki Y, Matsubara Y. Ras/MAPK syndromes and childhood hemato-oncological diseases. *International journal of hematology*. 2013;97:30–36. doi: 10.1007/s12185-012-1239-y
21. Rauen KA. The RASopathies. *Annual review of genomics and human genetics*. 2013;14:355–369. doi: 10.1146/annurev-genom-091212-153523
22. Capri Y, Flex E, Krumbach OHF, Carpentieri G, Cecchetti S, Lißewski C, Rezaei Adariani S, Schanze D, Brinkmann J, Piard J, Pantaleoni F, Lepri FR, Goh ES-Y, Chong K, Stieglitz E, Meyer J, Kuechler A, Bramswig NC, Sacharow S, Strullu M, Vial Y, Vignal C, Kensah G, Cuturilo G, Kazemineh Jasemi NS, Dvorsky R, Monaghan KG, Vincent LM, Cavé H, Verloes A, Ahmadian MR, Tartaglia M, Zenker M. Activating Mutations of RRAS2 Are a Rare Cause of Noonan Syndrome. *American journal of human genetics*. 2019;104:1223–1232. doi: 10.1016/j.ajhg.2019.04.013
23. Higgins EM, Bos JM, Mason-Suares H, Tester DJ, Ackerman JP, MacRae CA, Sol-Church K, Gripp KW, Urrutia R, Ackerman MJ. Elucidation of MRAS-mediated Noonan syndrome with cardiac hypertrophy. *JCI Insight*. 2017;2:e91225. doi: 10.1172/jci.insight.91225
24. Piotrowski A, Xie J, Liu YF, Poplawski AB, Gomes AR, Madanecki P, Fu C, Crowley MR, Crossman DK, Armstrong L, Babovic-Vuksanovic D, Bergner A, Blakeley JO, Blumenthal AL, Daniels MS, Feit H, Gardner K, Hurst S, Kobelka C, Lee C, Nagy R, Rauen KA, Slopis JM, Suwannarat P, Westman JA, Zanko A, Korf BR, Messiaen LM. Germline loss-of-function mutations in LZTR1 predispose to an

- inherited disorder of multiple schwannomas. *Nature genetics*. 2014;46:182–187. doi: 10.1038/ng.2855
25. Motta M, Pannone L, Pantaleoni F, Bocchinfuso G, Radio FC, Cecchetti S, Ciolfi A, Di Rocco M, Elting MW, Brilstra EH, Boni S, Mazzanti L, Tamburrino F, Walsh L, Payne K, Fernández-Jaén A, Ganapathi M, Chung WK, Grange DK, Dave-Wala A, Reshmi SC, Bartholomew DW, Mouhlahs D, Carpentieri G, Bruselles A, Pizzi S, Bellacchio E, Picci-Sparascio F, Liśewski C, Brinkmann J, Waclaw RR, Waisfisz Q, van Gassen K, Wentzensen IM, Morrow MM, Álvarez S, Martínez-García M, Luca A de, Memo L, Zampino G, Rossi C, Seri M, Gelb BD, Zenker M, Dallapiccola B, Stella L, Prada CE, Martinelli S, Flex E, Tartaglia M. Enhanced MAPK1 Function Causes a Neurodevelopmental Disorder within the RASopathy Clinical Spectrum. *American journal of human genetics*. 2020;107:499–513. doi: 10.1016/j.ajhg.2020.06.018
 26. Tartaglia M, Pennacchio LA, Zhao C, Yadav KK, Fodale V, Sarkozy A, Pandit B, Oishi K, Martinelli S, Schackwitz W, Ustaszewska A, Martin J, Bristow J, Carta C, Lepri F, Neri C, Vasta I, Gibson K, Curry CJ, Siguero JPL, Digilio MC, Zampino G, Dallapiccola B, Bar-Sagi D, Gelb BD. Gain-of-function SOS1 mutations cause a distinctive form of Noonan syndrome. *Nature genetics*. 2007;39:75–79. doi: 10.1038/ng1939
 27. Tartaglia M, Kalidas K, Shaw A, Song X, Musat DL, van der Burgt I, Brunner HG, Bertola DR, Crosby A, Ion A, Kucherlapati RS, Jeffery S, Patton MA, Gelb BD. PTPN11 mutations in Noonan syndrome: molecular spectrum, genotype-phenotype correlation, and phenotypic heterogeneity. *American journal of human genetics*. 2002;70:1555–1563. doi: 10.1086/340847
 28. Lepri F, Luca A de, Stella L, Rossi C, Baldassarre G, Pantaleoni F, Cordeddu V, Williams BJ, Dentici ML, Caputo V, Venanzi S, Bonaguro M, Kavamura I, Faienza MF, Pilotta A, Stanzial F, Faravelli F, Gabrielli O, Marino B, Neri G, Silengo MC, Ferrero GB, Torrente I, Selicorni A, Mazzanti L, Digilio MC, Zampino G, Dallapiccola B, Gelb BD, Tartaglia M. SOS1 mutations in Noonan syndrome: molecular spectrum, structural insights on pathogenic effects, and genotype-phenotype correlations. *Human mutation*. 2011;32:760–772. doi: 10.1002/humu.21492
 29. Cordeddu V, Yin JC, Gunnarsson C, Virtanen C, Drunat S, Lepri F, Luca A de, Rossi C, Ciolfi A, Pugh TJ, Bruselles A, Priest JR, Pennacchio LA, Lu Z, Danesh A, Quevedo R, Hamid A, Martinelli S, Pantaleoni F, Gnazzo M, Daniele P, Lisowski C, Bocchinfuso G, Stella L, Odent S, Philip N, Faivre L, Vlckova M, Seemanova E, Digilio C, Zenker M, Zampino G, Verloes A, Dallapiccola B, Roberts AE, Cavé H, Gelb BD, Neel BG, Tartaglia M. Activating Mutations Affecting the Dbl Homology Domain of SOS2 Cause Noonan Syndrome. *Human mutation*. 2015;36:1080–1087. doi: 10.1002/humu.22834
 30. Pandit B, Sarkozy A, Pennacchio LA, Carta C, Oishi K, Martinelli S, Pogna EA, Schackwitz W, Ustaszewska A, Landstrom A, Bos JM, Ommen SR, Esposito G, Lepri F, Faul C, Mundel P, López Siguero JP, Tenconi R, Selicorni A, Rossi C, Mazzanti L, Torrente I, Marino B, Digilio MC, Zampino G, Ackerman MJ, Dallapiccola B, Tartaglia M, Gelb BD. Gain-of-function RAF1 mutations cause Noonan and LEOPARD syndromes with hypertrophic cardiomyopathy. *Nature genetics*. 2007;39:1007–1012. doi: 10.1038/ng2073
 31. Yaoita M, Niihori T, Mizuno S, Okamoto N, Hayashi S, Watanabe A, Yokozawa M, Suzumura H, Nakahara A, Nakano Y, Hokosaki T, Ohmori A, Sawada H, Migita O, Mima A, Lapunzina P, Santos-Simarro F, García-Miñaúr S, Ogata T, Kawame H, Kurosawa K, Ohashi H, Inoue S, Matsubara Y,

- Kure S, Aoki Y. Spectrum of mutations and genotype-phenotype analysis in Noonan syndrome patients with RIT1 mutations. *Human genetics*. 2016;135:209–222. doi: 10.1007/s00439-015-1627-5
32. Tartaglia M, Aoki Y, Gelb BD. The molecular genetics of RASopathies: An update on novel disease genes and new disorders. *American Journal of Medical Genetics Part C: Seminars in Medical Genetics*. 2022;190:425–439. doi: 10.1002/ajmg.c.32012
33. Evans R, O'Neill M, Pritzel A, Antropova N, Senior A, Green T, Židek A, Bates R, Blackwell S, Yim J, Ronneberger O, Bodenstern S, Zielinski M, Bridgland A, Potapenko A, Cowie A, Tunyasuvunakool K, Jain R, Clancy E, Kohli P, Jumper J, Hassabis D. *Protein complex prediction with AlphaFold-Multimer*, 2021
34. Johnston JJ, van der Smagt JJ, Rosenfeld JA, Pagnamenta AT, Alswaid A, Baker EH, Blair E, Borck G, Brinkmann J, Craigen W, Dung VC, Emrick L, Everman DB, van Gassen KL, Gulsuner S, Harr MH, Jain M, Kuechler A, Leppig KA, McDonald-McGinn DM, Can NTB, Peleg A, Roeder ER, Rogers RC, Sagi-Dain L, Sapp JC, Schäffer AA, Schanze D, Stewart H, Taylor JC, Verbeek NE, Walkiewicz MA, Zackai EH, Zweier C, Zenker M, Lee B, Biesecker LG. Autosomal recessive Noonan syndrome associated with biallelic LZTR1 variants. *Genet Med*. 2018;20:1175–1185. doi: 10.1038/gim.2017.249
35. Pagnamenta AT, Kaisaki PJ, Bennett F, Burkitt-Wright E, Martin HC, Ferla MP, Taylor JM, Gompertz L, Lahiri N, Tatton-Brown K, Newbury-Ecob R, Henderson A, Joss S, Weber A, Carmichael J, Turnpenny PD, McKee S, Forzano F, Ashraf T, Bradbury K, Shears D, Kini U, Burca A de, Blair E, Taylor JC, Stewart H. Delineation of dominant and recessive forms of LZTR1-associated Noonan syndrome. *Clin Genet*. 2019;95:693–703. doi: 10.1111/cge.13533
36. Umeki I, Niihori T, Abe T, Kanno S-I, Okamoto N, Mizuno S, Kurosawa K, Nagasaki K, Yoshida M, Ohashi H, Inoue S, Matsubara Y, Fujiwara I, Kure S, Aoki Y. Delineation of LZTR1 mutation-positive patients with Noonan syndrome and identification of LZTR1 binding to RAF1-PPP1CB complexes. *Human genetics*. 2019;138:21–35. doi: 10.1007/s00439-018-1951-7
37. Frattini V, Trifonov V, Chan JM, Castano A, Lia M, Abate F, Keir ST, Ji AX, Zoppoli P, Niola F, Danussi C, Dolgalev I, Porrati P, Pellegatta S, Heguy A, Gupta G, Pisapia DJ, Canoll P, Bruce JN, McLendon RE, Yan H, Aldape K, Finocchiaro G, Mikkelsen T, Privé GG, Bigner DD, Lasorella A, Rabadan R, Iavarone A. The integrated landscape of driver genomic alterations in glioblastoma. *Nature genetics*. 2013;45:1141–1149. doi: 10.1038/ng.2734
38. Nacak TG, Leptien K, Fellner D, Augustin HG, Kroll J. The BTB-kelch protein LZTR-1 is a novel Golgi protein that is degraded upon induction of apoptosis. *J Biol Chem*. 2006;281:5065–5071. doi: 10.1074/jbc.M509073200
39. Abe T, Umeki I, Kanno S-I, Inoue S, Niihori T, Aoki Y. LZTR1 facilitates polyubiquitination and degradation of RAS-GTPases. *Cell Death Differ*. 2020;27:1023–1035. doi: 10.1038/s41418-019-0395-5
40. Motta M, Fidan M, Bellacchio E, Pantaleoni F, Schneider-Heieck K, Coppola S, Borck G, Salviati L, Zenker M, Cirstea IC, Tartaglia M. Dominant Noonan syndrome-causing LZTR1 mutations specifically affect the Kelch domain substrate-recognition surface and enhance RAS-MAPK signaling. *Human molecular genetics*. 2019;28:1007–1022. doi: 10.1093/hmg/ddy412

41. Sewduth RN, Pandolfi S, Steklov M, Sheryazdanova A, Zhao P, Criem N, Baietti MF, Lechat B, Quarck R, Impens F, Sablina AA. The Noonan Syndrome Gene *Lztr1* Controls Cardiovascular Function by Regulating Vesicular Trafficking. *Circulation research*. 2020;126:1379–1393. doi: 10.1161/CIRCRESAHA.119.315730
42. Bigenzahn JW, Collu GM, Kartnig F, Pieraks M, Vladimer GI, Heinz LX, Sedlyarov V, Schischlik F, Fauster A, Rebsamen M, Parapatics K, Blomen VA, Müller AC, Winter GE, Kralovics R, Brummelkamp TR, Mlodzik M, Superti-Furga G. LZTR1 is a regulator of RAS ubiquitination and signaling. *Science*. 2018;362:1171–1177. doi: 10.1126/science.aap8210
43. Castel P, Cheng A, Cuevas-Navarro A, Everman DB, Papageorge AG, Simanshu DK, Tankka A, Galeas J, Urisman A, McCormick F. RIT1 oncoproteins escape LZTR1-mediated proteolysis. *Science*. 2019;363:1226–1230. doi: 10.1126/science.aav1444
44. Steklov M, Pandolfi S, Baietti MF, Batiuk A, Carai P, Najm P, Zhang M, Jang H, Renzi F, Cai Y, Abbasi Asbagh L, Pastor T, Troyer M de, Simicek M, Radaelli E, Brems H, Legius E, Tavernier J, Gevaert K, Impens F, Messiaen L, Nussinov R, Heymans S, Eyckerman S, Sablina AA. Mutations in LZTR1 drive human disease by dysregulating RAS ubiquitination. *Science*. 2018;362:1177–1182. doi: 10.1126/science.aap7607
45. Hanses U, Kleinsorge M, Roos L, Yigit G, Li Y, Barbarics B, El-Battrawy I, Lan H, Tiburcy M, Hindmarsh R, Lenz C, Salinas G, Diecke S, Müller C, Adham I, Altmüller J, Nürnberg P, Paul T, Zimmermann W-H, Hasenfuss G, Wollnik B, Cyganek L. Intronic CRISPR Repair in a Preclinical Model of Noonan Syndrome-Associated Cardiomyopathy. *Circulation*. 2020;142:1059–1076. doi: 10.1161/CIRCULATIONAHA.119.044794
46. Jaffré F, Miller CL, Schänzer A, Evans T, Roberts AE, Hahn A, Kontaridis MI. Inducible Pluripotent Stem Cell-Derived Cardiomyocytes Reveal Aberrant Extracellular Regulated Kinase 5 and Mitogen-Activated Protein Kinase Kinase 1/2 Signaling Concomitantly Promote Hypertrophic Cardiomyopathy in RAF1-Associated Noonan Syndrome. *Circulation*. 2019;140:207–224. doi: 10.1161/CIRCULATIONAHA.118.037227
47. Takahashi K, Tanabe K, Ohnuki M, Narita M, Ichisaka T, Tomoda K, Yamanaka S. Induction of pluripotent stem cells from adult human fibroblasts by defined factors. *Cell*. 2007;131:861–872. doi: 10.1016/j.cell.2007.11.019
48. Robinton DA, Daley GQ. The promise of induced pluripotent stem cells in research and therapy. *Nature*. 2012;481:295–305. doi: 10.1038/nature10761
49. Kleinsorge M, Cyganek L. Subtype-Directed Differentiation of Human iPSCs into Atrial and Ventricular Cardiomyocytes. *STAR Protoc*. 2020;1:100026. doi: 10.1016/j.xpro.2020.100026
50. Zhang H, Tian L, Shen M, Tu C, Wu H, Gu M, Paik DT, Wu JC. Generation of Quiescent Cardiac Fibroblasts From Human Induced Pluripotent Stem Cells for In Vitro Modeling of Cardiac Fibrosis. *Circulation research*. 2019;125:552–566. doi: 10.1161/CIRCRESAHA.119.315491
51. Cyganek L, Tiburcy M, Sekeres K, Gerstenberg K, Bohnenberger H, Lenz C, Henze S, Stauske M, Salinas G, Zimmermann W-H, Hasenfuss G, Guan K. Deep phenotyping of human induced pluripotent stem cell-derived atrial and ventricular cardiomyocytes. *JCI Insight*. 2018;3. doi: 10.1172/jci.insight.99941

52. Tiburcy M, Hudson JE, Balfanz P, Schlick S, Meyer T, Chang Liao M-L, Levent E, Raad F, Zeidler S, Wingender E, Riegler J, Wang M, Gold JD, Kehat I, Wettwer E, Ravens U, Dierickx P, van Laake LW, Goumans MJ, Khadjeh S, Toischer K, Hasenfuss G, Couture LA, Unger A, Linke WA, Araki T, Neel B, Keller G, Gepstein L, Wu JC, Zimmermann W-H. Defined Engineered Human Myocardium With Advanced Maturation for Applications in Heart Failure Modeling and Repair. *Circulation*. 2017;135:1832–1847. doi: 10.1161/CIRCULATIONAHA.116.024145
53. Higgins EM, Bos JM, Dotzler SM, John Kim CS, Ackerman MJ. MRAS Variants Cause Cardiomyocyte Hypertrophy in Patient-Specific Induced Pluripotent Stem Cell-Derived Cardiomyocytes: Additional Evidence for MRAS as a Definitive Noonan Syndrome-Susceptibility Gene. *Circ Genom Precis Med*. 2019;12:e002648. doi: 10.1161/CIRCGEN.119.002648
54. Sayed N, Liu C, Wu JC. Translation of Human-Induced Pluripotent Stem Cells: From Clinical Trial in a Dish to Precision Medicine. *Journal of the American College of Cardiology*. 2016;67:2161–2176. doi: 10.1016/j.jacc.2016.01.083
55. Sharma A, McKeithan WL, Serrano R, Kitani T, Burridge PW, Del Álamo JC, Mercola M, Wu JC. Use of human induced pluripotent stem cell-derived cardiomyocytes to assess drug cardiotoxicity. *Nat Protoc*. 2018;13:3018–3041. doi: 10.1038/s41596-018-0076-8
56. Wolf CM, Zenker M, Burkitt-Wright E, Edouard T, García-Miñaur S, Lebl J, Shaikh G, Tartaglia M, Verloes A, Östman-Smith I. Management of cardiac aspects in children with Noonan syndrome - results from a European clinical practice survey among paediatric cardiologists. *European journal of medical genetics*. 2022;65:104372. doi: 10.1016/j.ejmg.2021.104372
57. Roden DM, McLeod HL, Relling MV, Williams MS, Mensah GA, Peterson JF, van Driest SL. Pharmacogenomics. *Lancet*. 2019;394:521–532. doi: 10.1016/S0140-6736(19)31276-0
58. Leoni C, Blandino R, Delogu AB, Rosa G de, Onesimo R, Verusio V, Marino MV, Lanza GA, Rigante D, Tartaglia M, Zampino G. Genotype-cardiac phenotype correlations in a large single-center cohort of patients affected by RASopathies: Clinical implications and literature review. *Am J Med Genet A*. 2022;188:431–445. doi: 10.1002/ajmg.a.62529
59. Zenker M, Buheitel G, Rauch R, Koenig R, Bosse K, Kress W, Tietze H-U, Doerr H-G, Hofbeck M, Singer H, Reis A, Rauch A. Genotype-phenotype correlations in Noonan syndrome. *J Pediatr*. 2004;144:368–374. doi: 10.1016/j.jpeds.2003.11.032
60. Razzaque MA, Nishizawa T, Komoike Y, Yagi H, Furutani M, Amo R, Kamisago M, Momma K, Katayama H, Nakagawa M, Fujiwara Y, Matsushima M, Mizuno K, Tokuyama M, Hirota H, Muneuchi J, Higashinakagawa T, Matsuoka R. Germline gain-of-function mutations in RAF1 cause Noonan syndrome. *Nature genetics*. 2007;39:1013–1017. doi: 10.1038/ng2078
61. Davies H, Bignell GR, Cox C, Stephens P, Edkins S, Clegg S, Teague J, Woffendin H, Garnett MJ, Bottomley W, Davis N, Dicks E, Ewing R, Floyd Y, Gray K, Hall S, Hawes R, Hughes J, Kosmidou V, Menzies A, Mould C, Parker A, Stevens C, Watt S, Hooper S, Wilson R, Jayatilake H, Gusterson BA, Cooper C, Shipley J, Hargrave D, Pritchard-Jones K, Maitland N, Chenevix-Trench G, Riggins GJ, Bigner DD, Palmieri G, Cossu A, Flanagan A, Nicholson A, Ho JWC, Leung SY, Yuen ST, Weber BL, Seigler HF, Darrow TL, Paterson H, Marais R, Marshall CJ, Wooster R, Stratton MR, Futreal PA. Mutations of the BRAF gene in human cancer. *Nature*. 2002;417:949–954. doi: 10.1038/nature00766

62. Prior IA, Hood FE, Hartley JL. The Frequency of Ras Mutations in Cancer. *Cancer research*. 2020;80:2969–2974. doi: 10.1158/0008-5472.CAN-19-3682
63. Moore AR, Rosenberg SC, McCormick F, Malek S. RAS-targeted therapies: is the undruggable drugged? *Nat Rev Drug Discov*. 2020;19:533–552. doi: 10.1038/s41573-020-0068-6
64. Zhao Y, Adjei AA. The clinical development of MEK inhibitors. *Nat Rev Clin Oncol*. 2014;11:385–400. doi: 10.1038/nrclinonc.2014.83
65. Blumenschein GR, Smit EF, Planchard D, Kim D-W, Cadranet J, Pas T de, Dunphy F, Udud K, Ahn M-J, Hanna NH, Kim J-H, Mazieres J, Kim S-W, Baas P, Rappold E, Redhu S, Puski A, Wu FS, Jänne PA. A randomized phase II study of the MEK1/MEK2 inhibitor trametinib (GSK1120212) compared with docetaxel in KRAS-mutant advanced non-small-cell lung cancer (NSCLC)†. *Annals of oncology : official journal of the European Society for Medical Oncology*. 2015;26:894–901. doi: 10.1093/annonc/mdv072
66. Cleary JM, Wang V, Heist RS, Kopetz ES, Mitchell EP, Zwiebel JA, Kapner KS, Chen HX, Li S, Gray RJ, McShane LM, Rubinstein LV, Patton DR, Meric-Bernstam F, Dillmon MS, Williams PM, Hamilton SR, Conley BA, Aguirre AJ, O'Dwyer PJ, Harris LN, Arteaga CL, Chen AP, Flaherty KT. Differential Outcomes in Codon 12/13 and Codon 61 NRAS-Mutated Cancers in the Phase II NCI-MATCH Trial of Binimetinib in Patients with NRAS-Mutated Tumors. *Clin Cancer Res*. 2021;27:2996–3004. doi: 10.1158/1078-0432.CCR-21-0066
67. Dummer R, Schadendorf D, Ascierto PA, Arance A, Dutriaux C, Di Giacomo AM, Rutkowski P, Del Vecchio M, Gutzmer R, Mandala M, Thomas L, Demidov L, Garbe C, Hogg D, Liszky G, Queirolo P, Wasserman E, Ford J, Weill M, Sirulnik LA, Jehl V, Bozón V, Long GV, Flaherty K. Binimetinib versus dacarbazine in patients with advanced NRAS-mutant melanoma (NEMO): a multicentre, open-label, randomised, phase 3 trial. *The Lancet. Oncology*. 2017;18:435–445. doi: 10.1016/S1470-2045(17)30180-8
68. Kenney C, Kunst T, Webb S, Christina D, Arrowood C, Steinberg SM, Mettu NB, Kim EJ, Rudloff U. Phase II study of selumetinib, an orally active inhibitor of MEK1 and MEK2 kinases, in KRASG12R-mutant pancreatic ductal adenocarcinoma. *Investigational new drugs*. 2021;39:821–828. doi: 10.1007/s10637-020-01044-8
69. Chen P-C, Wakimoto H, Conner D, Araki T, Yuan T, Roberts A, Seidman CE, Bronson R, Neel BG, Seidman JG, Kucherlapati R. Activation of multiple signaling pathways causes developmental defects in mice with a Noonan syndrome–associated Sos1 mutation. *J Clin Invest*. 2010;120:4353–4365. doi: 10.1172/JCI43910
70. Hernández-Porras I, Fabbiano S, Schuhmacher AJ, Aicher A, Cañamero M, Cámara JA, Cussó L, Desco M, Heeschen C, Mulero F, Bustelo XR, Guerra C, Barbacid M. K-RasV14I recapitulates Noonan syndrome in mice. *Proc Natl Acad Sci U S A*. 2014;111:16395–16400. doi: 10.1073/pnas.1418126111
71. Bonetti M, Paardekooper Overman J, Tessadori F, Noël E, Bakkers J, Hertog J den. Noonan and LEOPARD syndrome Shp2 variants induce heart displacement defects in zebrafish. *Development*. 2014;141:1961–1970. doi: 10.1242/dev.106310
72. Runtuwene V, van Eekelen M, Overvoorde J, Rehmann H, Yntema HG, Nillesen WM, van Haeringen A, van der Burgt I, Burgering B, Hertog J den. Noonan syndrome gain-of-function

- mutations in NRAS cause zebrafish gastrulation defects. *Dis Model Mech*. 2011;4:393–399. doi: 10.1242/dmm.007112
73. Andelfinger G, Marquis C, Raboisson M-J, Théoret Y, Waldmüller S, Wiegand G, Gelb BD, Zenker M, Delrue M-A, Hofbeck M. Hypertrophic Cardiomyopathy in Noonan Syndrome Treated by MEK-Inhibition. *Journal of the American College of Cardiology*. 2019;73:2237–2239. doi: 10.1016/j.jacc.2019.01.066
74. Casey D, Demko S, Sinha A, Mishra-Kalyani PS, Shen Y-L, Khasar S, Goheer MA, Helms WS, Pan L, Xu Y, Fan J, Leong R, Liu J, Yang Y, Windsor K, Ou M, Stephens O, Oh B, Reaman GH, Nair A, Shord SS, Bhatnagar V, Daniels SR, Sickafuse S, Goldberg KB, Theoret MR, Pazdur R, Singh H. FDA Approval Summary: Selumetinib for Plexiform Neurofibroma. *Clin Cancer Res*. 2021;27:4142–4146. doi: 10.1158/1078-0432.CCR-20-5032
75. Hahn A, Lauriol J, Thul J, Behnke-Hall K, Logeswaran T, Schänzer A, Böğürücü N, Garvalov BK, Zenker M, Gelb BD, Gerlach S von, Kandolf R, Kontaridis MI, Schranz D. Rapidly progressive hypertrophic cardiomyopathy in an infant with Noonan syndrome with multiple lentigines: palliative treatment with a rapamycin analog. *Am J Med Genet A*. 2015;167A:744–751. doi: 10.1002/ajmg.a.36982
76. Molkenstein JD. Calcineurin-NFAT signaling regulates the cardiac hypertrophic response in coordination with the MAPKs. *Cardiovasc Res*. 2004;63:467–475. doi: 10.1016/j.cardiores.2004.01.021
77. Mendoza MC, Er EE, Blenis J. The Ras-ERK and PI3K-mTOR pathways: cross-talk and compensation. *Trends Biochem Sci*. 2011;36:320–328. doi: 10.1016/j.tibs.2011.03.006
78. Norris JL, Baldwin AS. Oncogenic Ras enhances NF-kappaB transcriptional activity through Raf-dependent and Raf-independent mitogen-activated protein kinase signaling pathways. *J Biol Chem*. 1999;274:13841–13846. doi: 10.1074/jbc.274.20.13841
79. van Allen EM, Wagle N, Sucker A, Treacy DJ, Johannessen CM, Goetz EM, Place CS, Taylor-Weiner A, Whittaker S, Kryukov GV, Hodis E, Rosenberg M, McKenna A, Cibulskis K, Farlow D, Zimmer L, Hillen U, Gutzmer R, Goldinger SM, Ugurel S, Gogas HJ, Egberts F, Berking C, Trefzer U, Loquai C, Weide B, Hassel JC, Gabriel SB, Carter SL, Getz G, Garraway LA, Schadendorf D. The genetic landscape of clinical resistance to RAF inhibition in metastatic melanoma. *Cancer Discov*. 2014;4:94–109. doi: 10.1158/2159-8290.CD-13-0617
80. Weisner J, Landel I, Reintjes C, Uhlenbrock N, Trajkovic-Arsic M, Dienstbier N, Hardick J, Ladigan S, Lindemann M, Smith S, Quambusch L, Scheinpflug R, Depta L, Gontla R, Unger A, Müller H, Baumann M, Schultz-Fademrecht C, Günther G, Maghnoij A, Müller MP, Pohl M, Teschendorf C, Wolters H, Viebahn R, Tannapfel A, Uhl W, Hengstler JG, Hahn SA, Siveke JT, Rauh D. Preclinical Efficacy of Covalent-Allosteric AKT Inhibitor Borussertib in Combination with Trametinib in KRAS-Mutant Pancreatic and Colorectal Cancer. *Cancer research*. 2019;79:2367–2378. doi: 10.1158/0008-5472.CAN-18-2861
81. Terns MP. CRISPR-Based Technologies: Impact of RNA-Targeting Systems. *Mol Cell*. 2018;72:404–412. doi: 10.1016/j.molcel.2018.09.018
82. Ran FA, Hsu PD, Wright J, Agarwala V, Scott DA, Zhang F. Genome engineering using the CRISPR-Cas9 system. *Nat Protoc*. 2013;8:2281–2308. doi: 10.1038/nprot.2013.143

83. Chen F, Pruett-Miller SM, Huang Y, Gjoka M, Duda K, Taunton J, Collingwood TN, Frodin M, Davis GD. High-frequency genome editing using ssDNA oligonucleotides with zinc-finger nucleases. *Nature methods*. 2011;8:753–755. doi: 10.1038/nmeth.1653
84. Maeder ML, Stefanidakis M, Wilson CJ, Baral R, Barrera LA, Bounoutas GS, Bumcrot D, Chao H, Ciulla DM, DaSilva JA, Dass A, Dhanapal V, Fennell TJ, Friedland AE, Giannoukos G, Gloskowski SW, Glucksmann A, Gotta GM, Jayaram H, Haskett SJ, Hopkins B, Horng JE, Joshi S, Marco E, Mepani R, Reyon D, Ta T, Tabbaa DG, Samuelsson SJ, Shen S, Skor MN, Stetkiewicz P, Wang T, Yudkoff C, Myer VE, Albright CF, Jiang H. Development of a gene-editing approach to restore vision loss in Leber congenital amaurosis type 10. *Nature medicine*. 2019;25:229–233. doi: 10.1038/s41591-018-0327-9
85. Gillmore JD, Gane E, Taubel J, Kao J, Fontana M, Maitland ML, Seitzer J, O'Connell D, Walsh KR, Wood K, Phillips J, Xu Y, Amaral A, Boyd AP, Cehelsky JE, McKee MD, Schiermeier A, Harari O, Murphy A, Kyratsous CA, Zambrowicz B, Soltys R, Gutstein DE, Leonard J, Sepp-Lorenzino L, Lebowitz D. CRISPR-Cas9 In Vivo Gene Editing for Transthyretin Amyloidosis. *The New England journal of medicine*. 2021;385:493–502. doi: 10.1056/NEJMoa2107454
86. Amoasii L, Hildyard JCW, Li H, Sanchez-Ortiz E, Mireault A, Caballero D, Harron R, Stathopoulou T-R, Massey C, Shelton JM, Bassel-Duby R, Piercy RJ, Olson EN. Gene editing restores dystrophin expression in a canine model of Duchenne muscular dystrophy. *Science*. 2018;362:86–91. doi: 10.1126/science.aau1549
87. Aoki Y, Niihori T, Inoue S, Matsubara Y. Recent advances in RASopathies. *J Hum Genet*. 2016;61:33–39. doi: 10.1038/jhg.2015.114
88. van Mil A, Balk GM, Neef K, Buikema JW, Asselbergs FW, Wu SM, Doevendans PA, Sluijter JPG. Modelling inherited cardiac disease using human induced pluripotent stem cell-derived cardiomyocytes: progress, pitfalls, and potential. *Cardiovasc Res*. 2018;114:1828–1842. doi: 10.1093/cvr/cvy208
89. Meier AB, Raj Murthi S, Rawat H, Toepfer CN, Santamaria G, Schmid M, Mastantuono E, Schwarzmayr T, Berutti R, Cleuziou J, Ewert P, Görlach A, Klingel K, Laugwitz K-L, Seidman CE, Seidman JG, Moretti A, Wolf CM. Cell cycle defects underlie childhood-onset cardiomyopathy associated with Noonan syndrome. *iScience*. 2022;25:103596. doi: 10.1016/j.isci.2021.103596
90. Josowitz R, Mulero-Navarro S, Rodriguez NA, Falce C, Cohen N, Ullian EM, Weiss LA, Rauen KA, Sobie EA, Gelb BD. Autonomous and Non-autonomous Defects Underlie Hypertrophic Cardiomyopathy in BRAF-Mutant hiPSC-Derived Cardiomyocytes. *Stem cell reports*. 2016;7:355–369. doi: 10.1016/j.stemcr.2016.07.018
91. Lemcke H, Skorska A, Lang CI, Johann L, David R. Quantitative Evaluation of the Sarcomere Network of Human hiPSC-Derived Cardiomyocytes Using Single-Molecule Localization Microscopy. *International Journal of Molecular Sciences*. 2020;21:2819. doi: 10.3390/ijms21082819
92. Mosqueira D, Mannhardt I, Bhagwan JR, Lis-Slimak K, Katili P, Scott E, Hassan M, Prondzynski M, Harmer SC, Tinker A, Smith JGW, Carrier L, Williams PM, Gaffney D, Eschenhagen T, Hansen A, Denning C. CRISPR/Cas9 editing in human pluripotent stem cell-cardiomyocytes highlights

- arrhythmias, hypocontractility, and energy depletion as potential therapeutic targets for hypertrophic cardiomyopathy. *Eur Heart J*. 2018;39:3879–3892. doi: 10.1093/eurheartj/ehy249
93. Levin MD, Saitta SC, Gripp KW, Wenger TL, Ganesh J, Kalish JM, Epstein MR, Smith R, Czosek RJ, Ware SM, Goldenberg P, Myers A, Chatfield KC, Gillespie MJ, Zackai EH, Lin AE. Nonreentrant atrial tachycardia occurs independently of hypertrophic cardiomyopathy in RASopathy patients. *Am J Med Genet A*. 2018;176:1711–1722. doi: 10.1002/ajmg.a.38854
 94. Maron BJ, Desai MY, Nishimura RA, Spirito P, Rakowski H, Towbin JA, Rowin EJ, Maron MS, Sherrid MV. Diagnosis and Evaluation of Hypertrophic Cardiomyopathy: JACC State-of-the-Art Review. *Journal of the American College of Cardiology*. 2022;79:372–389. doi: 10.1016/j.jacc.2021.12.002
 95. Tiburcy M, Meyer T, Liaw NY, Zimmermann W-H. Generation of Engineered Human Myocardium in a Multi-well Format. *STAR Protoc*. 2020;1:100032. doi: 10.1016/j.xpro.2020.100032
 96. NSEuroNet.com. <https://nseuro.net.com/php/>. Accessed December 29, 2022
 97. Canning P, Cooper CDO, Krojer T, Murray JW, Pike ACW, Chaikuad A, Keates T, Thangaratnarajah C, Hojzan V, Marsden BD, Gileadi O, Knapp S, Delft F von, Bullock AN. Structural basis for Cul3 protein assembly with the BTB-Kelch family of E3 ubiquitin ligases. *J Biol Chem*. 2013;288:7803–7814. doi: 10.1074/jbc.M112.437996
 98. Mirdita M, Schütze K, Moriwaki Y, Heo L, Ovchinnikov S, Steinegger M. ColabFold: making protein folding accessible to all. *Nat Methods*. 2022;19:679–682. doi: 10.1038/s41592-022-01488-1
 99. Cuevas-Navarro A, Rodriguez-Muñoz L, Grego-Bessa J, Cheng A, Rauhen KA, Urisman A, McCormick F, Jimenez G, Castel P. Cross-species analysis of LZTR1 loss-of-function mutants demonstrates dependency to RIT1 orthologs. *Elife*. 2022;11. doi: 10.7554/eLife.76495
 100. Birket MJ, Raibaud S, Lettieri M, Adamson AD, Letang V, Cervello P, Redon N, Ret G, Viale S, Wang B, Biton B, Guillemot J-C, Mikol V, Leonard JP, Hanley NA, Orsini C, Itier J-M. A Human Stem Cell Model of Fabry Disease Implicates LIMP-2 Accumulation in Cardiomyocyte Pathology. *Stem cell reports*. 2019;13:380–393. doi: 10.1016/j.stemcr.2019.07.004
 101. Dorsch LM, Schuldt M, dos Remedios CG, Schinkel AFL, Jong PL de, Michels M, Kuster DWD, Brundel BJJM, van der Velden J. Protein Quality Control Activation and Microtubule Remodeling in Hypertrophic Cardiomyopathy. *Cells*. 2019;8. doi: 10.3390/cells8070741
 102. Pei J, Schuldt M, Nagyova E, Gu Z, El Bouhaddani S, Yiangou L, Jansen M, Calis JJA, Dorsch LM, Blok CS, van den Dungen NAM, Lansu N, Boukens BJ, Efimov IR, Michels M, Verhaar MC, Weger R de, Vink A, van Steenbeek FG, Baas AF, Davis RP, Uh HW, Kuster DWD, Cheng C, Mokry M, van der Velden J, Asselbergs FW, Harakalova M. Multi-omics integration identifies key upstream regulators of pathomechanisms in hypertrophic cardiomyopathy due to truncating MYBPC3 mutations. *Clin Epigenetics*. 2021;13:61. doi: 10.1186/s13148-021-01043-3
 103. Kirkegaard T, Gray J, Priestman DA, Wallom K-L, Atkins J, Olsen OD, Klein A, Drndarski S, Petersen NHT, Ingemann L, Smith DA, Morris L, Bornæs C, Jørgensen SH, Williams I, Hinsby A, Arenz C, Begley D, Jäättelä M, Platt FM. Heat shock protein-based therapy as a potential candidate for treating the sphingolipidoses. *Sci Transl Med*. 2016;8:355ra118. doi: 10.1126/scitranslmed.aad9823

104. Kim Y-K, Suarez J, Hu Y, McDonough PM, Boer C, Dix DJ, Dillmann WH. Deletion of the inducible 70-kDa heat shock protein genes in mice impairs cardiac contractile function and calcium handling associated with hypertrophy. *Circulation*. 2006;113:2589–2597. doi: 10.1161/CIRCULATIONAHA.105.598409
105. Ranek MJ, Stachowski MJ, Kirk JA, Willis MS. The role of heat shock proteins and co-chaperones in heart failure. *Philos Trans R Soc Lond B Biol Sci*. 2018;373. doi: 10.1098/rstb.2016.0530
106. Fernández-Fernández MR, Gragera M, Ochoa-Ibarrola L, Quintana-Gallardo L, Valpuesta JM. Hsp70 - a master regulator in protein degradation. *FEBS Letters*. 2017;591:2648–2660. doi: 10.1002/1873-3468.12751
107. Nakamura M, Sadoshima J. Mechanisms of physiological and pathological cardiac hypertrophy. *Nature reviews. Cardiology*. 2018;15:387–407. doi: 10.1038/s41569-018-0007-y
108. Nakhaei-Rad S, Bazgir F, Dahlmann J, Busley AV, Buchholzer M, Haghghi F, Schänzer A, Hahn A, Kötter S, Schanze D, Anand R, Funk F, Borchardt A, Kronenbitter AV, Scheller J, Piekorz RP, Reichert AS, Volleth M, Wolf MJ, Cirstea IC, Gelb BD, Tartaglia M, Schmitt J, Krüger M, Kutschka I, Cyganek L, Zenker M, Kensah G, Ahmadian MR. *Alteration of myocardial structure and function in RAF1-associated Noonan syndrome: Insights from cardiac disease modeling based on patient-derived iPSCs, 2022*
109. Wang Y, Zhang J, Zhang P, Zhao Z, Huang Q, Yun D, Chen J, Chen H, Wang C, Lu D. LZTR1 inactivation promotes MAPK/ ERK pathway activation in glioblastoma by stabilizing oncoprotein RIT1. *bioRxiv*. 2020:2020.03.14.989954. doi: 10.1101/2020.03.14.989954
110. Marzahn MR, Marada S, Lee J, Nourse A, Kenrick S, Zhao H, Ben-Nissan G, Kolaitis R-M, Peters JL, Pounds S, Errington WJ, Privé GG, Taylor JP, Sharon M, Schuck P, Ogden SK, Mittag T. Higher-order oligomerization promotes localization of SPOP to liquid nuclear speckles. *EMBO J*. 2016;35:1254–1275. doi: 10.15252/embj.201593169
111. Karbassi E, Fenix A, Marchiano S, Muraoka N, Nakamura K, Yang X, Murry CE. Cardiomyocyte maturation: advances in knowledge and implications for regenerative medicine. *Nature reviews. Cardiology*. 2020;17:341–359. doi: 10.1038/s41569-019-0331-x
112. Guo Y, Pu WT. Cardiomyocyte Maturation: New Phase in Development. *Circulation research*. 2020;126:1086–1106. doi: 10.1161/CIRCRESAHA.119.315862
113. Rössler U, Hennig AF, Stelzer N, Bose S, Kopp J, Søre K, Cyganek L, Zifarelli G, Ali S, Hagen M von der, Strässler ET, Hahn G, Pusch M, Stauber T, Izsvák Z, Gossen M, Stachelscheid H, Kornak U. Efficient generation of osteoclasts from human induced pluripotent stem cells and functional investigations of lethal CLCN7-related osteopetrosis. *J Bone Miner Res*. 2021;36:1621–1635. doi: 10.1002/jbmr.4322
114. Yousefi R, Fornasiero EF, Cyganek L, Montoya J, Jakobs S, Rizzoli SO, Rehling P, Pacheu-Grau D. Monitoring mitochondrial translation in living cells. *EMBO Rep*. 2021;22:e51635. doi: 10.15252/embr.202051635
115. Haeussler M, Schöning K, Eckert H, Eschstruth A, Mianné J, Renaud J-B, Schneider-Maunoury S, Shkumatava A, Teboul L, Kent J, Joly J-S, Concordet J-P. Evaluation of off-target and on-target

- scoring algorithms and integration into the guide RNA selection tool CRISPOR. *Genome Biol.* 2016;17:148. doi: 10.1186/s13059-016-1012-2
116. Zech ATL, Prondzynski M, Singh SR, Pietsch N, Orthey E, Alizoti E, Busch J, Madsen A, Behrens CS, Meyer-Jens M, Mearini G, Lemoine MD, Krämer E, Mosqueira D, Viridi S, Indenbirken D, Depke M, Salazar MG, Völker U, Braren I, Pu WT, Eschenhagen T, Hammer E, Schlossarek S, Carrier L. ACTN2 Mutant Causes Proteopathy in Human iPSC-Derived Cardiomyocytes. *Cells.* 2022;11:2745. doi: 10.3390/cells11172745
117. Suomi T, Elo LL. Enhanced differential expression statistics for data-independent acquisition proteomics. *Sci Rep.* 2017;7:5869. doi: 10.1038/s41598-017-05949-y
118. Seyednasrollah F, Rantanen K, Jaakkola P, Elo LL. ROTS: reproducible RNA-seq biomarker detector-prognostic markers for clear cell renal cell cancer. *Nucleic acids research.* 2016;44:e1. doi: 10.1093/nar/gkv806
119. Pasqualin C, Gannier F, Yu A, Malécot CO, Bredeloux P, Maupoil V. SarcOptiM for ImageJ: high-frequency online sarcomere length computing on stimulated cardiomyocytes. *Am J Physiol Cell Physiol.* 2016;311:C277-83. doi: 10.1152/ajpcell.00094.2016
120. Young LC, Hartig N, Del Boned Río I, Sari S, Ringham-Terry B, Wainwright JR, Jones GG, McCormick F, Rodriguez-Viciano P. SHOC2-MRAS-PP1 complex positively regulates RAF activity and contributes to Noonan syndrome pathogenesis. *Proc Natl Acad Sci U S A.* 2018;115:E10576-E10585. doi: 10.1073/pnas.1720352115
121. Brandt R, Sell T, Lüthen M, Uhlitz F, Klinger B, Riemer P, Giesecke-Thiel C, Schulze S, El-Shimy IA, Kunkel D, Fauler B, Mielke T, Mages N, Herrmann BG, Sers C, Blüthgen N, Morkel M. Cell type-dependent differential activation of ERK by oncogenic KRAS in colon cancer and intestinal epithelium. *Nat Commun.* 2019;10:2919. doi: 10.1038/s41467-019-10954-y
122. Huang L, Guo Z, Wang F, Fu L. KRAS mutation: from undruggable to druggable in cancer. *Signal Transduct Target Ther.* 2021;6:386. doi: 10.1038/s41392-021-00780-4
123. Yamamoto GL, Agueno M, Gos M, Hung C, Pilch J, Fahiminiya S, Abramowicz A, Cristian I, Buscarilli M, Naslavsky MS, Malaquias AC, Zatz M, Bodamer O, Majewski J, Jorge AAL, Pereira AC, Kim CA, Passos-Bueno MR, Bertola DR. Rare variants in SOS2 and LZTR1 are associated with Noonan syndrome. *J Med Genet.* 2015;52:413–421. doi: 10.1136/jmedgenet-2015-103018
124. Gripp KW, Aldinger KA, Bennett JT, Baker L, Tusi J, Powell-Hamilton N, Stabley D, Sol-Church K, Timms AE, Dobyns WB. A novel rasopathy caused by recurrent de novo missense mutations in PPP1CB closely resembles Noonan syndrome with loose anagen hair. *Am J Med Genet A.* 2016;170:2237–2247. doi: 10.1002/ajmg.a.37781
125. Pintard L, Willis JH, Willems A, Johnson J-LF, Srayko M, Kurz T, Glaser S, Mains PE, Tyers M, Bowerman B, Peter M. The BTB protein MEL-26 is a substrate-specific adaptor of the CUL-3 ubiquitin-ligase. *Nature.* 2003;425:311–316. doi: 10.1038/nature01959
126. Ko A, Hasanain M, Oh YT, D'Angelo F, Sommer D, Frangaj B, Tran S, Bielle F, Pollo B, Paterra R, Mokhtari K, Soni RK, Peyre M, Eoli M, Papi L, Kalamarides M, Sanson M, Iavarone A, Lasorella A. LZTR1 Mutation Mediates Oncogenesis through Stabilization of EGFR and AXL. *Cancer Discov.* 2023;13:702–723. doi: 10.1158/2159-8290.CD-22-0376

127. Concordet J-P, Haeussler M. CRISPOR: intuitive guide selection for CRISPR/Cas9 genome editing experiments and screens. *Nucleic acids research*. 2018;46:W242-W245. doi: 10.1093/nar/gky354
128. Cuneo MJ, O'Flynn BG, Lo Y-H, Sabri N, Mittag T. Higher-order SPOP assembly reveals a basis for cancer mutant dysregulation. *Mol Cell*. 2023;83:731-745.e4. doi: 10.1016/j.molcel.2022.12.033
129. Schubbert S, Zenker M, Rowe SL, Böll S, Klein C, Bollag G, van der Burgt I, Musante L, Kalscheuer V, Wehner L-E, Nguyen H, West B, Zhang KYJ, Sistermans E, Rauch A, Niemeyer CM, Shannon K, Kratz CP. Germline KRAS mutations cause Noonan syndrome. *Nature genetics*. 2006;38:331-336. doi: 10.1038/ng1748
130. Buday L, Downward J. Many faces of Ras activation. *Biochimica et biophysica acta*. 2008;1786:178-187. doi: 10.1016/j.bbcan.2008.05.001
131. Burgess MR, Hwang E, Mroue R, Bielski CM, Wandler AM, Huang BJ, Firestone AJ, Young A, LaCap JA, Crocker L, Asthana S, Davis EM, Xu J, Akagi K, Le Beau MM, Li Q, Haley B, Stokoe D, Sampath D, Taylor BS, Evangelista M, Shannon K. KRAS Allelic Imbalance Enhances Fitness and Modulates MAP Kinase Dependence in Cancer. *Cell*. 2017;168:817-829.e15. doi: 10.1016/j.cell.2017.01.020
132. Zhang Z, Wang Y, Vikis HG, Johnson L, Liu G, Li J, Anderson MW, Sills RC, Hong HL, Devereux TR, Jacks T, Guan KL, You M. Wildtype Kras2 can inhibit lung carcinogenesis in mice. *Nature genetics*. 2001;29:25-33. doi: 10.1038/ng721
133. Cagnol S, Rivard N. Oncogenic KRAS and BRAF activation of the MEK/ERK signaling pathway promotes expression of dual-specificity phosphatase 4 (DUSP4/MKP2) resulting in nuclear ERK1/2 inhibition. *Oncogene*. 2013;32:564-576. doi: 10.1038/onc.2012.88
134. Fatrai S, van Gosliga D, Han L, Daenen SMGJ, Vellenga E, Schuringa JJ. KRAS(G12V) enhances proliferation and initiates myelomonocytic differentiation in human stem/progenitor cells via intrinsic and extrinsic pathways. *J Biol Chem*. 2011;286:6061-6070. doi: 10.1074/jbc.M110.201848
135. Adari H, Lowy DR, Willumsen BM, Der CJ, McCormick F. Guanosine triphosphatase activating protein (GAP) interacts with the p21 ras effector binding domain. *Science*. 1988;240:518-521. doi: 10.1126/science.2833817
136. Edin ML, Juliano RL. Raf-1 serine 338 phosphorylation plays a key role in adhesion-dependent activation of extracellular signal-regulated kinase by epidermal growth factor. *Molecular and cellular biology*. 2005;25:4466-4475. doi: 10.1128/MCB.25.11.4466-4475.2005